

University of Windsor

## Scholarship at UWindor

---

Electronic Theses and Dissertations

Theses, Dissertations, and Major Papers

---

2008

### Study of self excited induction generators with aluminium and copper rotors taking skin effect into account

Khurshid Hafiz  
*University of Windsor*

Follow this and additional works at: <https://scholar.uwindsor.ca/etd>

---

#### Recommended Citation

Hafiz, Khurshid, "Study of self excited induction generators with aluminium and copper rotors taking skin effect into account" (2008). *Electronic Theses and Dissertations*. 8210.  
<https://scholar.uwindsor.ca/etd/8210>

This online database contains the full-text of PhD dissertations and Masters' theses of University of Windsor students from 1954 forward. These documents are made available for personal study and research purposes only, in accordance with the Canadian Copyright Act and the Creative Commons license—CC BY-NC-ND (Attribution, Non-Commercial, No Derivative Works). Under this license, works must always be attributed to the copyright holder (original author), cannot be used for any commercial purposes, and may not be altered. Any other use would require the permission of the copyright holder. Students may inquire about withdrawing their dissertation and/or thesis from this database. For additional inquiries, please contact the repository administrator via email ([scholarship@uwindsor.ca](mailto:scholarship@uwindsor.ca)) or by telephone at 519-253-3000ext. 3208.

**STUDY OF SELF EXCITED INDUCTION GENERATORS  
WITH ALUMINIUM AND COPPER ROTORS  
TAKING SKIN EFFECT INTO ACCOUNT**

by

**Khurshid Hafiz**

A Thesis  
Submitted to the Faculty of Graduate Studies  
through the Department of Electrical and Computer Engineering  
in Partial Fulfillment of the Requirements for the  
Degree of Master of Applied Science at the  
University of Windsor

Windsor, Ontario, Canada

2008

© 2008 Khurshid Hafiz



Library and  
Archives Canada

Bibliothèque et  
Archives Canada

Published Heritage  
Branch

Direction du  
Patrimoine de l'édition

395 Wellington Street  
Ottawa ON K1A 0N4  
Canada

395, rue Wellington  
Ottawa ON K1A 0N4  
Canada

*Your file    Votre référence*  
*ISBN: 978-0-494-47069-5*  
*Our file    Notre référence*  
*ISBN: 978-0-494-47069-5*

**NOTICE:**

The author has granted a non-exclusive license allowing Library and Archives Canada to reproduce, publish, archive, preserve, conserve, communicate to the public by telecommunication or on the Internet, loan, distribute and sell theses worldwide, for commercial or non-commercial purposes, in microform, paper, electronic and/or any other formats.

The author retains copyright ownership and moral rights in this thesis. Neither the thesis nor substantial extracts from it may be printed or otherwise reproduced without the author's permission.

**AVIS:**

L'auteur a accordé une licence non exclusive permettant à la Bibliothèque et Archives Canada de reproduire, publier, archiver, sauvegarder, conserver, transmettre au public par télécommunication ou par l'Internet, prêter, distribuer et vendre des thèses partout dans le monde, à des fins commerciales ou autres, sur support microforme, papier, électronique et/ou autres formats.

L'auteur conserve la propriété du droit d'auteur et des droits moraux qui protègent cette thèse. Ni la thèse ni des extraits substantiels de celle-ci ne doivent être imprimés ou autrement reproduits sans son autorisation.

---

In compliance with the Canadian Privacy Act some supporting forms may have been removed from this thesis.

Conformément à la loi canadienne sur la protection de la vie privée, quelques formulaires secondaires ont été enlevés de cette thèse.

While these forms may be included in the document page count, their removal does not represent any loss of content from the thesis.

Bien que ces formulaires aient inclus dans la pagination, il n'y aura aucun contenu manquant.

  
**Canada**

## **Authors Declaration of Originality**

I hereby certify that I am the sole author of this thesis and that no part of this thesis has been published or submitted for publication.

I certify that, to the best of my knowledge, my thesis does not infringe upon anyone's copyright nor violate any proprietary rights and that any ideas, techniques, quotations, or any other material from the work of other people included in my thesis, published or otherwise, are fully acknowledged in accordance with the standard referencing practices. Furthermore, to the extent that I have included copyrighted material that surpasses the bounds of fair dealing within the meaning of the Canada Copyright Act, I certify that I have obtained a written permission from the copyright owner(s) to include such material(s) in my thesis and have included copies of such copyright clearances to my appendix.

I declare that this is a true copy of my thesis, including any final revisions, as approved by my thesis committee and the Graduate Studies office, and that this thesis has not been submitted for a higher degree to any other University or Institution.

## ABSTRACT

This thesis covers the dynamic modeling and analysis of self-excited induction generators (SEIG) used in wind turbine applications. The process of self excitation or build-up of terminal voltage of an induction generator is explained as a physical process and also mathematically using higher order differential equations.

A complete system model in d-q axis stationary reference frame has been formulated that consists of several non-linear differential equations. The non-linear variation of the magnetizing inductance with stator current of the induction machine has been taken into account in this model. Moreover this mathematical model takes skin effect into consideration. The rotor parameters determined from standard induction machine tests are modified by taking the rotor bar geometry, the material of the rotor bars and the frequency of the induced emf into account.

The developed model has been used to analyze the performance of two industrial type 7.5 hp induction machines, one with an aluminium-rotor, the other with copper-rotor. A comparative performance analysis of these aluminum-rotor and copper-rotor SEIGs, considering saturation and skin effect has been carried out both theoretically and experimentally, and presented in the thesis.

## **DEDICATION**

This thesis is dedicated to my wonderful parents, who have nurtured me to be the person I am today. My father, a teacher himself, inspired me toward science and mathematics; my mother taught me that it is never too late to learn. They have been a source of encouragement and inspiration to me throughout my life.

And to my wife and children, who offered me unconditional love and support and had to bear with me throughout the course of this program.

## ACKNOWLEDGEMENTS

With the remembrance of His name, all praises are due to God Almighty, Who blessed me with the worldly comfort, guided me with the knowledge and provided me with the strength to pursue the Master's program in this University.

It was indeed a delightful experience to work with my thesis supervisor Dr. Narayan Chandra Kar who impressed me with the aura of warm companionship and encouragement and for believing in my abilities. He is a dynamic advisor and always available, physically, on the phone or the e-mail. On every occasion we met he took the time to discuss about anything from research, recent exams, aspirations, to life's many joys and disappointments. His guidance took me through the ups and downs of my research with ease. This thesis would indeed appear disarrayed had it not been for his meticulous review, corrections, sage advice, and insightful criticisms. He is indeed a rare breed of educators, with a great sense of humour, professional ethics and technical expertise. It has been a rewarding experience to work under his guidance.

I would like to express gratitude to my other thesis committee members, Dr. Arunita Jaekel and Dr. Kemal Tepe. I have interacted with both of them not only as a part of this thesis but also in their teaching capacity. Dr. Jaekel has been my instructor during my undergrad studies in Computer Science. Her valuable suggestions and constructive advice have indeed enriched this thesis. Dr. Tepe has also been my teaching mentor during my graduate studies. Not only had I the opportunity to take one of his courses, we had interactions on other subjects as well. He offered some helpful comments that were useful in making this thesis worthwhile. My sincere thanks to both of them for taking the time to participate in the seminars, review the draft copies and provide useful criticisms.

This research would indeed be deficient without the support of Mr. Frank Cicchello and Mr. Don Tersigni. To them I owe a debt of gratitude for all their assistance. Thanks are also due to Mr. Steve Budinsky in the Technical Support Center for his help.

Lastly I wish to express my sincere appreciation to my fellow graduate students in Electrical Machines and Drives Research Lab specially Gaurav and Mariam. Their wonderful companionship and support made this research work a pleasant experience.

You all have made it a memorable time of my life.

## TABLE OF CONTENTS

AUTHORS DECLARATION OF ORIGINALITY	iii
ABSTRACT	iv
DEDICATION	v
ACKNOWLEDGEMENTS	vi
LIST OF TABLES	x
LIST OF FIGURES	xi
LIST OF SYMBOLS	xv
CHAPTER	
1.0 INTRODUCTION	
1.1 Background	1
1.2 Thesis Organization	3
1.3 Literature Review	4
1.3.1 Transient analysis of SEIG	5
1.3.2 Steady-state analysis of SEIG	5
1.3.3 Aluminium and copper-rotor induction machines	6
1.4 Analysis of SEIG Considering Skin Effect	8
1.4.1 Research objective	9
1.4.2 Scope of research	9
1.5 Bibliography	10
2.0 THEORY OF SELF EXCITATION OF INDUCTION GENERATORS	
2.1 Process of Self Excitation and Voltage Build-up	15
2.2 Relationship between Capacitor Value, Rotor Speed and Generated Voltage	19
2.3 Conditions for Self Excitation of an Induction Generator	21
2.4 Bibliography	23



3.0	DYNAMIC MODELLING OF SELF EXCITED INDUCTION GENERATORS	
3.1	Introduction	25
3.2	Development of the Mathematical Model of Induction Machines	26
3.2.1	Loop impedance model	28
3.2.2	Node admittance model	29
3.2.3	Model using d-q reference frame	31
3.3	Approach to Skin Effect Modelling	35
3.4	Bibliography	40
4.0	DETERMINATION OF ALUMINIUM-ROTOR AND COPPER-ROTOR INDUCTION MACHINE PARAMETERS	
4.1	Introduction	42
4.2	DC Resistance Test	42
4.3	Open Circuit Test	43
4.4	Short Circuit Test	44
4.5	Saturation Characteristics	47
4.6	Bibliography	50
5.0	NUMERICAL AND EXPERIMENTAL INVESTIGATION OF SEIG WITH ALUMINIUM-ROTOR AND COPPER-ROTOR	
5.1	Physical Features of Aluminium-rotor and Copper-rotor SEIGs	51
5.2	Voltage Build-up under Open Circuit Conditions ignoring Skin Effect	55
5.3	Simulation and Experimental Results Considering Skin Effect	61
5.3.1	Experimental Set-up	62
5.3.2	Open Circuit Condition	63
5.3.3	SEIG with Resistive Load	76
5.3.4	SEIG with <i>RL</i> Load	81
5.4	Voltage Regulation of SEIGs	85
5.5	Copper Losses in a Self Excited Induction Generator	90

5.6	Bibliography	95
6.0	CONCLUSION	97
	LIST OF CONTRIBUTIONS	100
APPENDIX A	Matlab Program to Calculate the Equivalent Circuit Parameters of an Induction Machine	101
APPENDIX B	Auxiliary Power Unit for Truck Idling Reduction	102
VITA AUCTORIS		115

## **LIST OF TABLES**

Table I	Name Plate Data and other Features of the Induction Machine	46
Table II	Equivalent Circuit Parameters of the Induction Machines	47
Table III	Physical Properties of Aluminium and Copper	52
Table IV	Voltage Build-up Characteristics of the Induction Machines	76
Table V	Voltage Regulation of the Induction Generators	90

## LIST OF FIGURES

Fig. 1.1	Trend in the price of aluminium and copper in world market	7
Fig. 2.1	An <i>RLC</i> circuit with a charged capacitor	16
Fig. 2.2	Transient voltage across capacitor when <i>R</i> is positive	16
Fig. 2.3	Transient voltage across capacitor when <i>R</i> is zero.	17
Fig. 2.4	Transient voltage across capacitor when <i>R</i> is negative.	18
Fig. 2.5	V-I characteristics of an induction machine and excitation capacitor	20
Fig. 3.1	Per-phase model of an induction machine connected to excitation capacitor and load.	27
Fig. 3.2	Per-phase model of an induction machine in terms of base frequency.	28
Fig. 3.3	Per-phase model of an induction machine for loop analysis.	29
Fig. 3.4	Per-phase model of an induction machine for nodal analysis.	30
Fig. 3.5	Modified per-phase model of an induction machine.	31
Fig. 3.6	Equivalent circuit of an SEIG.	32
Fig. 3.7	Influence of skin effect on the flux and current distribution in the rotor bars.	36
Fig. 3.8	Dimensions of a rectangular rotor bar.	38
Fig. 3.9	Variation of rotor resistance coefficient and inductance coefficient with stator frequency	39
Fig. 4.1	Per-phase equivalent circuit of an induction machine.	42
Fig. 4.2	Per-phase equivalent circuit of an induction machine at no load.	43
Fig. 4.3	Modified per-phase equivalent circuit of an induction machine at no load.	44
Fig. 4.4	Per-phase equivalent circuit of an induction machine at blocked rotor condition.	45

Fig. 4.5	Measured saturation characteristics of aluminium-rotor induction machine for two voltage configurations.	48
Fig. 4.6	Measured saturation characteristics of copper-rotor induction machine for two voltage configurations.	49
Fig. 4.7	Magnetizing reactance of the induction machines	49
Fig. 5.1	Stators and rotors of the two 7.5 hp induction machines used in the investigations.	53
Fig. 5.2	Torque-Speed characteristics of the induction machines	54
Fig. 5.3	Saturation characteristics of 7.5 hp SEIGs	55
Fig. 5.4	Magnetizing reactance of 7.5 hp aluminium-rotor SEIG	57
Fig. 5.5	Magnetizing inductance of 7.5 hp copper-rotor SEIG	57
Fig. 5.6	Stator voltage build-up process of the aluminium-rotor SEIG under no load condition	58
Fig. 5.7	Stator current build-up process of the aluminium-rotor SEIG under no load condition	59
Fig. 5.8	Stator voltage and current build up process of the aluminium-rotor SEIG under no load condition	59
Fig. 5.9	Stator voltage build-up process of the copper-rotor SEIG under no load condition	60
Fig. 5.10	Stator current build-up process of the copper-rotor SEIG under no load condition	60
Fig. 5.11	Stator voltage and current build up process of the copper-rotor SEIG under no load condition	61
Fig. 5.12	Flowchart to calculate stator voltages and currents taking skin effect into account.	62
Fig. 5.13	Schematic diagram of the experimental set-up of the SEIG	63
Fig. 5.14	Experimental set-up of the SEIG	64
Fig. 5.15	Experimental set-up of the three-phase capacitor bank	64
Fig. 5.16	Experimental set-up of the three-phase <i>RL</i> load	65

Fig. 5.17	Variation of frequency with rotor speed for the aluminium-rotor SEIG.	66
Fig. 5.18	Stator voltage of phase 'a' build-up process under no load condition for aluminum-rotor SEIG ignoring and considering skin effect.	66
Fig. 5.19	Experimental results of stator voltage and current build-up for aluminum-rotor SEIG using Tektronix oscilloscope.	67
Fig. 5.20	Experimental results of stator voltage build-up for aluminum-rotor SEIG using Fluke Power Quality Analyzer.	67
Fig. 5.21	Stator voltage build-up process under no load condition for copper-rotor SEIG ignoring and considering skin effect.	68
Fig. 5.22	Experimental results of stator voltage and current build-up for copper-rotor SEIG using Tektronix oscilloscope.	68
Fig. 5.23	Experimental results of stator voltage build-up for copper-rotor SEIG using Fluke Power Quality Analyzer.	69
Fig. 5.24	Calculated real and reactive power under no load conditions for aluminium-rotor SEIG.	70
Fig. 5.25	Measured real and reactive power under no load condition or aluminium-rotor SEIG.	71
Fig. 5.26	Calculated real and reactive power under no load condition for copper-rotor SEIG.	72
Fig. 5.27	Measured real and reactive power under no load conditions for copper-rotor SEIG	73
Fig. 5.28	Measured voltage wave shapes of the three phases of SEIGs	74
Fig. 5.29	Measured Total Harmonic Distortion	75
Fig. 5.30	Calculated real and reactive power for aluminium-rotor SEIG under Resistive load condition.	77
Fig. 5.31	Measured real and reactive power under resistive load condition for aluminium-rotor SEIG	78
Fig. 5.32	Calculated real and reactive power for copper-rotor SEIG under Resistive load condition.	79

Fig. 5.33	Measured real and reactive power under resistive load condition for copper-rotor SEIG.	80
Fig.5 34	Simulated real and reactive power for aluminum-rotor SEIG under <i>RL</i> load.	82
Fig.5 35	Measured real and reactive power for aluminum-rotor SEIG under <i>RL</i> load.	83
Fig. 5.36	Simulated real and reactive power for copper-rotor SEIG under <i>RL</i> load.	84
Fig. 5.37	Measured real and reactive power for copper-rotor SEIG under <i>RL</i> load.	85
Fig. 5.38	Voltage regulation of aluminium SEIG with <i>R</i> load	87
Fig. 5.39	Voltage regulation of copper SEIG with <i>R</i> load	88
Fig. 5.40	Voltage regulation of the SEIGs with <i>RL</i> load	89
Fig. 5.41	Calculated power delivered at stator terminals for <i>R</i> load	90
Fig. 5.42	Calculated stator copper loss for <i>R</i> load	91
Fig. 5.43	Calculated rotor copper loss for <i>R</i> load	91
Fig. 5.44	Calculated power delivered at stator terminals for <i>RL</i> load	92
Fig. 5.45	Calculated stator copper loss for <i>RL</i> load	93
Fig. 5.46	Calculated rotor copper loss for <i>R</i> load.	93
Fig. 5.47.	Calculated rotor copper loss for aluminium-rotor and copper-rotor SEIGs under <i>RL</i> load for $C= 160\mu\text{F}$ .	94

## LIST OF SYMBOLS

$a$	:	Per-unit frequency
$b$	:	Per-unit speed
	:	Rotor speed/speed corresponding to base frequency
$h_r$	:	Height of rotor slot
$b_r$	:	Width of rotor bar
$b_s$	:	Width of rotor slot
$\mu_o$	:	Permeability of free space
$\sigma$	:	Conductivity of bar
$f$	:	Frequency of induced current
$s$	:	Slip of rotor
$v_{ds}, v_{qs}$	:	d- and q- axis stator voltages
$v_{dr}, v_{qr}$	:	d- and q- axis rotor voltages
$i_{ds}, i_{qs}$	:	d- and q- axis stator currents
$i_{dr}, i_{qr}$	:	d- and q- axis rotor currents
$\lambda_{ds}, \lambda_{qs}$	:	d- and q- axis stator flux linkages
$\lambda_{dr}, \lambda_{qr}$	:	d- and q- axis rotor flux linkages
$R_s, R_r$	:	Stator and rotor resistances
$L_{ls}, L_{lr}$	:	Stator and rotor leakage inductances
$L_m, i_m$	:	Magnetization inductance and current
$R_l, L_l$	:	Load resistance and inductance
$\omega, \omega_r$	:	Base and rotor speeds
$i_{cd}, i_{cq}$	:	d- and q- axis capacitor currents
$i_{ld}, i_{lq}$	:	d- and q- axis load currents
$i_{dm}, i_{qm}$	:	d- and q- axis magnetizing currents
$C$	:	Parallel excitation capacitance per phase
$E$	:	Air gap voltage per phase
$Y$	:	Conductance per phase
$I_s$	:	Stator current per phase
$R_s$	:	Stator resistance per phase



$R_r$	:	Rotor resistance per phase referred to the stator
$R_c$	:	Core loss resistance per phase
$R_l$	:	Load resistance per phase
$V_a, V_b, V_c$	:	Stator/Load voltage per phase
$I_a, I_b, I_c$	:	Stator currents
$L_{ls}$	:	Stator leakage reactance per phase
$L_{lr}$	:	Rotor leakage reactance per phase referred to the stator
$X_c$	:	Parallel excitation capacitive reactance per phase
$X_l$	:	Load reactance per phase
$X_m$	:	Magnetizing reactance per phase
$Y_l$	:	Load admittance per phase
$Z_l$	:	Load impedance per phase
$N_s$	:	Synchronous or base speed
$N_r$	:	Speed of rotor

# **1 INTRODUCTION**

## **1.1 Background**

With the progress of human civilization the use of electrical energy has increased many folds. In fact, a world without electricity is now unimaginable. As the demand for electrical energy increased, the number of generating stations has also multiplied in order to meet the ever growing energy demand. At present most of the electricity generated comes from conventional thermal, hydro or nuclear power plants. Thermal power stations use fossil fuels in the form of coal, oil and natural gas. These types of fuels have a finite reserve. Moreover, fossil fuels release green house gases and are a major cause of pollution. The rate of depletion of conventional energy sources has increased many folds and consequently, the environmental conditions have also degraded. This situation has unleashed a pursuit for an alternative energy source. With the concern about the limited supply of fossil fuels and environmental issues, more and more attention is now being given to renewable energy. The growth of suitable isolated power generators driven by wind, small hydro-power, biogas, etc. has recently gained great importance and popularity.

Energy from wind has been used since the dawn of civilization in the form of sailing vessels and wind-mills for grinding grain. Extracting electricity from wind is a relatively new and challenging technology. The use of wind power is gaining momentum worldwide. In Canada the wind power is growing at a remarkable pace as a potential energy source. The total installed generating capacity has increased from a trivial 19 MW in 1994 to 444 MW in 2004. Generally two types of generators find use in wind power plants – the synchronous generators and the induction generators. About 85% of the wind generators are induction type [1]. Since wind energy is renewable, virtually clean and free from pollutants, it is gaining recognition as a viable source of alternate and renewable energy. Induction generators have been the subject of research since early 1930s and still receive considerable attention.

Induction machines have been used in the electrical industry since more than six decades. This is due to the fact that induction machines are rugged, simple in construction, easy to maintain and reliable. Besides being used as drives in industries, the induction

machine has been widely used as induction generators in wind energy application. Wind power generation as it stands today is dominated by induction generators, of both squirrel cage and wound rotor type.

Other uses of induction generators are in small hydro and bio-gas. In the field of renewable energy which is environmentally clean and safe, the wind electrical generating system is the most cost effective of all [2]. Apart from the advantages of the induction machine mentioned above, the induction generator is brushless and does not require separate dc source for excitation. Moreover, it has an inherent protection against short circuit because the voltage collapses when there is a short circuit at its terminals [3]. The induction generator's ability to generate power at varying speed facilitates its application in various modes such as self-excited stand-alone (isolated) system, in parallel with synchronous generator to supplement local load, and in grid-connected mode [4].

The interesting features of these types of asynchronous generators are that they are actually designed as electric motors. The key component of the squirrel cage induction generator is the cage rotor. The rotor consists of a number of copper or aluminium bars which are connected at each end by end rings of similar material. As mentioned earlier, the wind power generation is dominated by both squirrel-cage and wound-rotor induction machines. In the domain of self-excited induction generators (SEIGs), aluminium-rotor cages play a significant role. This is because most induction machines of different horsepower range and sizes are made with die-cast aluminium-rotor cages. Largely because of ease of manufacturing, and being cheaper than copper, aluminium has been the common conductor material for the squirrel cage of the induction machine for long. However, recent innovations in material engineering have brought forth copper-cage rotor induction machines with promising results.

The electrical conductivity of copper is almost 60% higher than that of aluminium, so an SEIG with copper rotor would have lower  $I^2R$  losses, if copper were substituted for aluminium in the squirrel cage bars. This in turn would reduce Joule heating losses and lower the operating temperatures of both the rotor and the stator. However SEIGs with copper rotor are yet to penetrate the area dominated by aluminium-rotor SEIGs. It would be of significance to evaluate and compare their performance with the aluminium equivalent.

## 1.2 Thesis Organization

Development of mathematical models, experimental investigations and comparison of results are the main theme of this thesis. This thesis has been organised into six chapters. The first chapter starts with a brief introduction on induction machines and its applications. The use of SEIG in renewable energy systems is explained. A brief survey of various scholarly articles related to induction generators is presented here.

The physical process of self-excitation is explained in the second chapter. With the help of a series *RLC* circuit, and assuming there is some residual charge in the capacitor, the build up of voltage across the capacitor is explained taking into account the magnitude and sign of the series resistance. It is shown mathematically that if the sign of the resistance is negative, then the transient in the circuit increases indefinitely. On this basis the voltage build up in an SEIG is illustrated in details.

Models of induction generators that have been derived are given in details in chapter three. These models include the machine models based on d-q reference frame principles. The frequency of the terminal voltage of a stand-alone induction generator is influenced by rotor speed, magnitude of the excitation capacitance and load. In wind turbines, variations in turbine speed and load are common phenomena. These variations affect the stator frequency of an SEIG, which in turn influence the magnitude of the machine impedances. Consequently, the ac current in the rotor has the tendency to concentrate near the outer part or “skin” of a conductor. This phenomenon is known as skin effect. Due to skin effect, the effective cross-section of the rotor conductor is reduced. Depending on the material of the rotor conductor bars, this will have an impact on the dynamic behaviour of the machine. The mathematical models developed are further enhanced by taking skin effect and rotor material into account and described in depth.

In chapter four, the determination of induction machine parameters from laboratory tests has been described. Here no load, blocked rotor, dc resistance tests are illustrated. Also, the measurement of saturation characteristics and calculation of magnetising characteristics are explained.

The fifth chapter deals with the numerical analysis of the SEIG with aluminium rotor and copper rotor using the developed models. Simulations are carried out on developed model considering and ignoring skin effect. A comparison of the physical properties,

electrical parameters and simulation results for both types of SEIGs are demonstrated in this chapter. Experimental results for both the aluminium- and copper-rotor SEIGs are also presented

In the last chapter a summary of the work that has been carried out, discussions and conclusions are given.

### **1.3 Literature Review**

The phenomenon of self-excitation in induction machines has been known for more than 70 years. In this section research carried out previously in the area of self-excited induction generators using squirrel cage rotors, especially in the field of wind power application is reviewed. The areas of interest in this field are:

- Modelling
- Determination of minimum capacitance required for excitation
- Voltage build-up
- Steady-state analysis of isolated induction generators
- Steady-state analysis of generators connected to the grid
- Parallel operation of induction generators
- Voltage regulation and control
- Transient analysis.

Induction generators can be classified on the basis of rotor construction. They can be wound-rotor or squirrel-cage type. Wound-rotor induction generators are generally used as Doubly-Fed Induction Generators (DFIG) while squirrel-cage rotors are used as grid connected or isolated type induction generators. Depending on the type of prime-movers and their control mechanism induction generators can also be classified as [5]:

- Constant Speed Constant Frequency
- Variable Speed Constant Frequency
- Variable Speed Variable Frequency

For variable speed corresponding to the changing speed of the prime mover, SEIG can be conveniently used for loads which are essentially frequency insensitive. This scheme is gaining importance for stand-alone wind power applications.

### **1.3.1 Transient analysis of SEIG**

Using the  $d-q$  reference frame model of a three phase induction generator, the transient performance can be studied. For transient analysis, the  $d-q$  reference frame model of the SEIG, based on generalized machine theory, has been used [6]–[11]. The conventional three phase  $a-b-c$  reference frames of the machine are transformed into two reference frames,  $d$  and  $q$  and all the analysis are carried out using rotor, stationary or synchronous reference frame [12]–[13]. The results are then transformed back to the actual  $a-b-c$  reference frames. If the time varying terms in the  $d-q$  axis model are ignored, the equations then represent only the steady-state conditions [14]. Most of the transient studies of induction generators are related to voltage build-up due to self-excitation and load or speed perturbation. Symmetrical component concepts have been used to analyze unbalanced systems using positive and negative sequence equivalent circuits [15]. Study of long-shunt and short-shunt configurations on dynamic performance of an isolated SEIG, and the analysis of SEIG feeding an induction motor has been done by other authors [5] using  $d-q$  frames of reference.

### **1.3.2 Steady-state analysis of SEIG**

In the steady-state analysis, per phase equivalent circuit of the SEIG has been developed from the classical model of an induction machine. The main feature that distinguishes an induction machine from other electrical machines is that, like the transformer, the secondary currents are created totally by magnetic induction. In the analysis of an isolated system consisting of an induction generator, excitation capacitor and load, both the terminal voltage and frequency are unknown and have to be computed for a given speed, capacitance and load impedance. Usually there are four unknowns,

reactance of the excitation capacitor  $X_c$ , magnetizing reactance  $X_m$ , per unit frequency  $a$ , and per unit speed  $b$ . Early articles on this subject emphasised on evaluating the value of the minimum capacitance required for self-excitation. Two different methods of solution have been used namely, the loop impedance method [16]-[19] and the nodal admittance method [20]-[22]. Both these methods used the classical model of the induction machine. In the loop impedance method, for a given load and speed, two non-linear simultaneous equations in per unit frequency,  $a$  and magnetizing reactance,  $X_m$  are obtained by equating the real and imaginary terms of the complex loop impedances respectively to zero. The generator performance can then be evaluated by solving these equations. An alternative method of solution using the steady-state equivalent circuit is by considering the nodal admittance method described in [20]-[22].

By means of loop impedance or nodal admittance method technique, equations are obtained and then separated into its real and imaginary parts to solve for the per unit frequency  $a$  and then for capacitive reactance  $X_c$  or magnetizing reactance,  $X_m$ . Chan [20] has proposed an iterative technique by assuming some initial value of  $a$ . The second technique proposed by Chan [23] is based on the nodal admittance method. Here the symbolic programming using Maxima (software of MACSYMA) is employed for the derivation and solution of the high-order polynomial. Other authors have used Newton-Raphson method to solve for the unknowns [24]. Harrington [25] and Malik et al [19] have shown that the minimum capacitance requirement of an SEIG is inversely proportional to the speed and maximum saturated magnetizing reactance. Calculation to predict both minimum and maximum values of capacitance required for self-excitation based on eigenvalues and eigenvalue sensitivity analyses has also been reported in [26] and [27]. Harrington [25] has proposed a method based on the analysis of the complex impedance matrix of the induction generator when loaded with a general inductive load.

### **1.3.3 Aluminium- and copper-rotor induction machines**

Aluminium is strong and lightweight that has many applications. The principal uses are in transportation, packaging, electrical industry and construction. Most induction

machines of different horsepower range and sizes are made with die-cast aluminium-rotor cages. Aluminum die-cast rotors have been manufactured since the 1930s [28].

Like aluminium, copper is used in nearly every major industry of the world: transportation, engineering, machinery and equipment, electrical, building, automotive and computer. The related die-cast aluminium-rotor technology is mature, easy and less expensive in terms of manufacturing and material costs as compared to its copper counterpart. Because of this, aluminium-rotor induction machines are still the popular choice of the manufacturers. Moreover, as can be seen from Fig. 1.1, the trend in price in the world market is higher in case of copper [29] as compared to aluminium. Due to significant demand of copper worldwide, the base metal has outpaced all of the other base metals like gold, silver, platinum, and aluminium by a significant margin over the last five years.

Since the electrical conductivity of copper is nearly 60% higher than that of aluminum, the  $I^2R$  losses in the rotor can be expected to be substantially lower if copper were substituted for aluminium as conductive material of the squirrel cage structure [30].

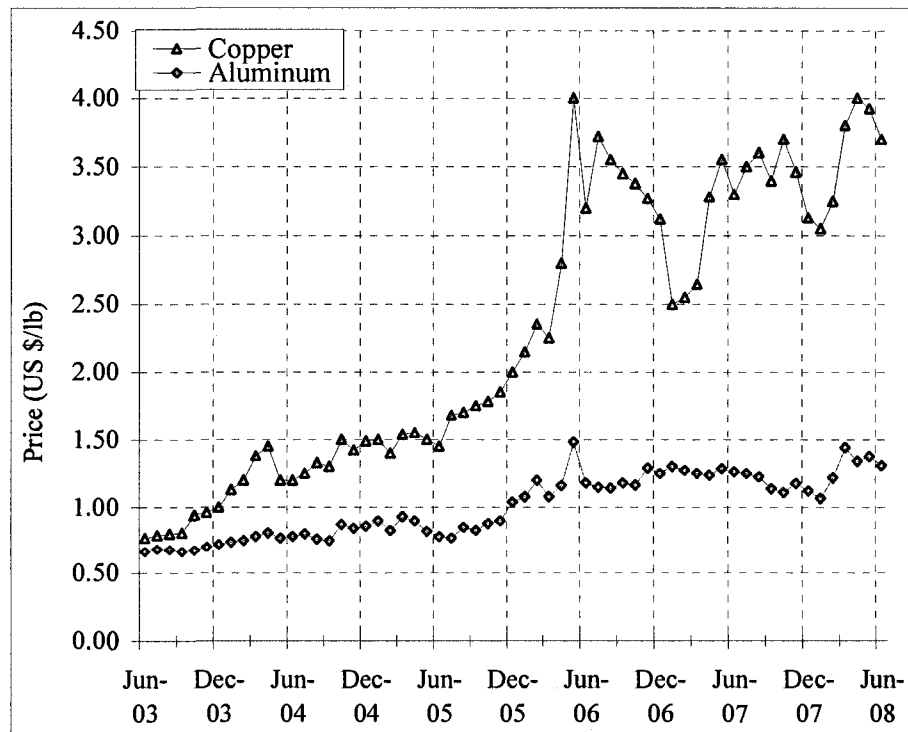


Fig. 1.1. Trend in the price of aluminium and copper in the world market.



Motor modeling by several manufacturers has shown that motors with copper rotors would have overall loss reductions of 15 to 20%. Data presented in [31]-[33], show that in addition to reduced rotor losses and improvement in overall electrical energy efficiency, an important derivative benefit is the reduced motor operating temperature which leads to longer motor life and reduced maintenance costs in high duty cycle motors.

At present four types of rotor construction exist:

- Aluminum die cast
- Fabricated aluminum bar
- Copper die cast
- Fabricated copper bar.

Design, material and production techniques are evolving on AC induction motors leading to improved efficiencies over older designs [34]. About 250,000 units with die cast copper-rotors are currently in use. The efficiency of these motors improves on average of 3% compared to rotor with aluminium. This 3% improvement corresponds to a global annual electricity savings of 108 Twh based on an annual electricity consumption of 15,000 Twh of which 3,600 Twh is used by motor systems.

#### **1.4 Analysis of SEIG Considering Skin Effect - Research Goal**

The analysis of the performance of induction machines due of variation of frequency has been reported by several authors [35]–[38]. The frequency of the stator voltage is dependent on rotor speed, magnitude of the excitation capacitance and load [39]. The variation of stator frequency has a profound effect on the rotor parameters. This in turn influences the performance of the machine. As a consequence the classical equations describing the induction machine are not accurate, since the influence of skin effect on the rotor parameters are not taken into account. The rotor parameters can be modified using the resistance and reactance coefficient by considering rotor dimensions, rotor bar material and frequency [40]-[42].

### **1.4.1 Research objective**

The main objective of this research is to explore the influence of the degree of saturation and skin effect on the transient performance of an SEIG. Investigations on the induction generators are performed where either saturation of the main flux [43] or skin effect [38] were considered and the machines studied were either wound rotor or aluminium bar squirrel-cage rotor type. However performance analysis of a squirrel-cage rotor SEIG considering both saturation and skin effect has not yet been carried out. Studies on the performance of copper cage induction machines working as motors have been reported in [30] and [44]–[45]. In this research a new method of representing the magnetic saturation based on data obtained from experiments carried out in the laboratory has been proposed. A model considering skin effect to determine the transient performance of an SEIG is developed and presented in this thesis.

### **1.4.2 Scope of research**

A model of an SEIG with aluminium cage rotor by considering both saturation and skin effect in the d-q axis reference frame has been developed [46]. The model is based on the following assumptions:

- Core loss has been neglected
- Harmonics in voltages and currents has not been considered
- Speed of the prime mover is considered to be constant

This model has been used to analyze the performance of an SEIG with copper substituted for aluminium in the rotor bars [47]. In order to verify the accuracy of the proposed model, numerical and experimental investigations have been carried out on two industrial grade 7.5 hp aluminium-rotor and copper-rotor SEIGs. A comparative performance analysis of these two machines considering saturation as well as skin effect has been conducted. Effects of resistive load and  $RL$  load on the performance of the machines have also been looked into. The results obtained from numerical analysis and laboratory investigations are presented here.

## 1.5 Bibliography

- [1] S.N. Bhadra, D. Kastha and S. Banerjee, *Wind Electrical Systems*, Oxford University Press, 2005.
- [2] A. Kishore, R.C. Prashad and B.M. Karan, "Matlab Simulink Based DQ Modeling and Dynamic Characteristics of Three Phase Self Excited Induction Generator," *Progress in Electromagnetics Research Symposium 2006*, Cambridge, USA, pp. 312-316, Mar. 2006.
- [3] D. Seyoum, C. Grantham, F. Rahman and M. Nagrial, "An Insight into the Dynamics of Loaded and Free Running Isolated Self Excited Induction Generators," *IEE Conference on Power Electronics, Machines and Drives*, Publication No. 487, pp. 580-585, Apr. 2002.
- [4] G.K. Singh, "Self-Excited Induction Generator Research - a Survey," *Electric Power Systems Research*, Elsevier B.V. pp. 107-114, 2004.
- [5] R.C. Bansal, "Three Phase Self Excited Induction Generator: An overview," *IEEE Transaction on Energy Conversion*, Vol.20, No. 2, pp. 292-299, Jun. 2005.
- [6] P.C. Krause and C.H. Thomas, "Simulation of Symmetrical Induction Machinery," *IEEE Transaction on Power Apparatus and Systems*, Vol. PAS-84, No. 11, pp. 1038-1053, Nov. 1965.
- [7] L. Wang and C.H. Lee, "Dynamic Analysis of Parallel Operated Self-Excited Induction Generators feeding an Induction Motor Load," *IEEE Transaction on Energy Conversion*, Vol. 14, No. 3, pp. 479-486, Sep. 1999.
- [8] R.H. Nelson, T.A. Lipo and P.C. Krause, "Stability Analysis of a Symmetrical Induction Machine," *IEEE Transaction on Power Apparatus and Systems*, Vol. 88, pp. 1710-1717, Nov 1969.
- [9] E. Levi, "Application of the Current State Space Model in Analyses of Saturated Induction Machines," *Electric Power Research*, pp. 203-216. 1994.
- [10] R. Djamila and R. Toufik, "An Approach for the Modeling of an Autonomous Induction Generator Taking into Account the Saturation Effect," *International Journal of Emerging Electric Power Systems*, Vol. 4 No. 1, pp. 391-415, 2005.

- [11] J.J. Narrayway, "Eigenvalues of the State Matrix for an Induction Machine", *Journal of Franklin Institute*, pp. 75-78, Jul. 1975.
- [12] P.C. Krause, *Analysis of Electric Machinery and Drive Systems*, 2<sup>nd</sup> Edition, IEEE Press, 2002.
- [13] O.I. Okoro, "Matlab Simulation of Induction Machine with Saturable Leakage and Magnetizing Inductances", *The Pacific Journal of Science and Technology*, Vol. 5, No. 1, pp. 5-15, Apr. 2003.
- [14] D. Seyoum, "The Dynamic Analysis and Control of a Self-Excited Induction Generator Driven by a Wind Turbine," Ph. D. Dissertation, The University of New South Wales, Australia, 1999.
- [15] S S Murthy and S. Acharya, "Matlab Based Steady State Analysis of Self Excited Induction Generator," *The Fifth International Conference on Power Electronics and Drive Systems*, Vol. 1, pp. 749-753, Nov. 2003.
- [16] S.S. Murthy, O.P. Malik and A.K. Tandon, "Analysis of Self-Excited Induction Generators," *Proceedings of IEE*, Vol. 129, Part C, No. 6, pp. 260-265, Nov. 1982.
- [17] N.H. Malik and S.E. Haque, "Steady State Analysis and Performance of an Isolated Self-Excited Induction Generator," *IEEE Transaction on Energy Conversion*, Vol. EC-1, No. 3, pp.134-139, Sept. 1986.
- [18] T.F. Chan, "Steady State Analysis of Self Excited Induction Generators," *IEEE Transactions on Energy Conversion*, Vol.9, No. 2, pp. 288-296, Jun. 1994.
- [19] N.H. Malik and A.A. Mazi, "Capacitance Requirements for Isolated Self Excited Induction Generators," *IEEE Transaction on Energy Conversion*, Vol. EC-2, No. 1, pp. 62-68, Mar. 1987.
- [20] T.F. Chan, "Analysis of Self-Excited Induction Generators Using an Iterative Method," *IEEE Transactions on Energy Conversion*, Vol. 10, No. 3, pp. 502-507 Sept. 1995.
- [21] A.M. Eltamaly, "New Formula to Determine the Minimum Capacitance Required for Self-Excited Induction Generator," *IEEE 33<sup>rd</sup> Annual Power Electronics Specialists Conference*, Vol. 1, pp. 106-110, Jun. 2002.

- [22] S. U Alghuwainem, "Steady-State Analysis of an Isolated Self-Excited Induction Generator supplying an Induction Motor Load," *IEEE Transaction on Energy Conversion*, Vol. 14, Issue 3, pp. 718-723, Sept. 1999.
- [23] T.F. Chan, "Capacitance Requirements of Self-Excited Induction Generators," *IEEE Transactions on Energy Conversion*, Vol. 8, No. 2, pp. 304-311, Jun. 1993.
- [24] S.S. Murthy and A.J.P. Pinto, "A Generalized Dynamic and Steady State Analysis of Self Excited Induction Generator (SEIG) Based on Matlab," *Proceedings of the Eighth International Conference on Electrical Machines and Systems*, Vol. 3, pp. 1933-1938, Sep. 2005.
- [25] R.J. Harrington and F.M.M. Bassiouny, "New Approach to Determine the Critical Capacitance for Self-Excited Induction Generators," *IEEE Transactions on Energy Conversion*, Vol. 13, No. 3, pp. 244-249, Sep. 1998.
- [26] L. Wang and C.H. Lee, "A Novel Analysis on the Performance of an Isolated Self-Excited Induction Generator," *IEEE Transactions on Energy Conversion*, Vol. 12, No. 2, pp. 109-117, Jun. 1997.
- [27] L. Wang and J.Y. Su, "Determination of Minimum and Maximum Capacitance of an Isolated SEIG using Eigenvalue Sensitivity Approach," *Proceedings of International Conference on Power System Technology*, Vol.1, pp. 610-614, Aug. 1998.
- [28] W.R. Finley, M.M. Hodowanec, "Selection of Copper vs. Aluminum Rotors for Induction Motors," *IEEE Transaction on Industry Applications*, Vol. 37, No. 6, pp. 1563-1573, Nov.- Dec. 2001.
- [29] <http://www.infomine.com> accessed on June 15th, 2008.
- [30] D.T. Peters, J.G. Cowie, E.F. Brush Jr., and D.J. Van Son, "Copper in the Squirrel Cage for Improved Motor Performance," *Proceedings of the IEEE International Electric Machines and Drives Conference*, Vol. 2, pp. 1265 – 1271, 2003.
- [31] J.G. Cowie, D.T. Peters and D.T. Brender, "Die-Cast Copper Rotors for Improved Motor Performance," *Record of the 2003 Annual Pulp and Paper Industry Technical Conference*, pp. 42-49, Jun. 2003.
- [32] D.T. Peters, J.G. Cowie, E.F. Brush, Jr., M. Doppelbauer and R. Kimmich, "Performance of Motors with Die-cast Copper Rotors in Industrial and

- Agricultural Pumping Applications,” *IEEE International Conference on Electric Machines and Drives*, pp. 987-992, May 2005.
- [33] R. Kimmich, M. Doppelbauer, J.L. Kirtley, D.T. Peters, J.G. Cowie, E.F. Brush, Jr., “Performance Characteristics of Drive Motors Optimized for Die-Cast Copper Cages,” *4<sup>th</sup> International Conference on Energy Efficiency in Motor Driven Systems*, pp. 1-8, Sep. 2005.
- [34] J. Malinowski, J. McComick and K. Dunn, “Advances in Construction Techniques of AC Induction Motors Preparation for Super-Premium Efficiency Levels,” *IEEE Transactions on Industry Applications*, Vol. 40, No. 6, Nov.-Dec. 2004.
- [35] J. Langheim, “Modeling of Rotor Bars with Skin Effect for Dynamic Simulation of Induction Machines,” *Conference Record of the 1989 IEEE Industry Application Society Annual Meeting*, Vol. 1, pp. 38-44, 1989.
- [36] H. Kabbaj, X Roboam, Y. Lefevre and J. Faucher, “Skin Effect Characterization in a Squirrel Cage Induction Machine,” *Proceedings of the IEEE International Symposium on Industrial Electronics*, Vol. 2, pp. 532-536, 1997.
- [37] N. Erdogan, T. Assaf, R. Grisel and M. Aubourg, “An Accurate 3-phase Induction Machine Model Including Skin Effect and Saturations for Transient Studies,” *Sixth International Conference on Electrical Machines and Systems*, pp. 646-649, 2003.
- [38] O.I. Okoro, “Transient State Modeling of Asynchronous Generator with Skin Effect,” *The Pacific Journal of Science and Technology*, Vol. 5, No. 2, pp. 63-71, 2004.
- [39] Y.N. Anagreh and I.M. Al-Refae, “Teaching the Self Excited Generator Using Matlab,” *International Journal of Electrical Engineering Education*, Vol. 40, No. 1, pp. 55-65, 2003.
- [40] M. Kostenko and L. Piotrovsky, *Electrical Machines, Alternating Current Machines*, Vol. 2, Translated from Russian by A. Chernukhin, Mir Publishers, 1972.
- [41] P.L. Alger, *Induction Machines Their Behavior and Uses*, Gordon and Breach Science Publishers, New York, 1970.

- [42] R.H. Engelmann and W.H. Middendorf, *Handbook of Electric Motors*, Marcel Dekker Inc., New York, 1995.
- [43] L. Wang and J.Y. Su, "Dynamic Performances of an Isolated Self- Excited Induction Generator under Various Loading Conditions," *IEEE Transactions on Energy Conversion*, Vol. 14, No. 1, pp. 93-100, 1999.
- [44] J.L. Kirtley Jr., J.G. Cowie, E.F. Brush Jr., D.T. Peters and R. Kimmich, "Improving Induction Motor Efficiency with Die-Cast Copper Rotor Cages," *Proceedings of the IEEE Power Engineering Society General Meeting*, pp. 1- 6, 2007.
- [45] A. Boglietti, A. Cavagnino, L. Ferraris and M. Lazzari, "Energetic Considerations about the Use of Cast Copper Squirrel Cage Induction Motors," *Proceedings of 33rd Annual Conference of the IEEE Industrial Electronics Society*, pp. 157-162, 2007.
- [46] K. Hafiz, G. Nanda and N.C. Kar, "Skin Effect Modeling of Self Excited Induction Generator in Wind Power Application," *Canadian Conference on Electrical and Computer Engineering*, May, 2008.
- [47] —, "Comparative Performance Analysis of Aluminum-Rotor and Copper-Rotor SEIG Considering Skin Effect," *International Conference on Electrical Machines*, Sep. 2008.

## 2 THEORY OF SELF-EXCITATION OF INDUCTION GENERATORS

### 2.1 Process of Self-Excitation and Voltage Build-up

The phenomenon of self-excitation in induction machines has been known and studied for over 70 years [1]. When an induction machine is connected to an ac source, a component of its stator current is used to build up the air gap magnetic flux whether the machine works as a motor, brake or a generator [2]. If the machine operates as a generator, reactive energy is required to build up the magnetic flux. This energy can be provided from a grid from where the reactive power is drawn. In an isolated mode, this excitation can be provided by an external capacitor of appropriate value. In other words, to build up the voltage across the generator terminals, some means of excitation is required [3]. To achieve a given voltage level, in an isolated mode, the external capacitors must supply the required magnetizing current.

An induction generator without any external source, using capacitors can self-excite if there is a remnant magnetic flux in the machine core [4]–[5] or residual charge across the capacitor terminals. The residual magnetism in the field circuit produces a small voltage. That voltage produces a small capacitive current flow. This boosts up the voltage which further increases the capacitive current until the voltage reaches the steady-state value. Thus a three phase induction machine can be made to work as a self-excited induction generator provided the capacitance connected across the stator terminals have sufficient charge to provide necessary initial magnetizing current [6]–[9]. In such a case, this phenomenon is known as capacitor self-excitation, and the induction machine is called Self-Excited Induction Generator (SEIG).

The phenomenon of self-excitation can be explained by a series  $RLC$  circuit as shown in Fig. 2.1. When the switch  $S$  is closed, the differential equation representing the system is given by

$$Ri + L \frac{di}{dt} + \frac{1}{C} \int i dt + V_c(0) = 0 \quad (2.1)$$

where  $V_c(0)$  is the residual charge in the capacitor.

Grantham et. al. [1] has explained that a transient solution to an  $RLC$  circuit similar to



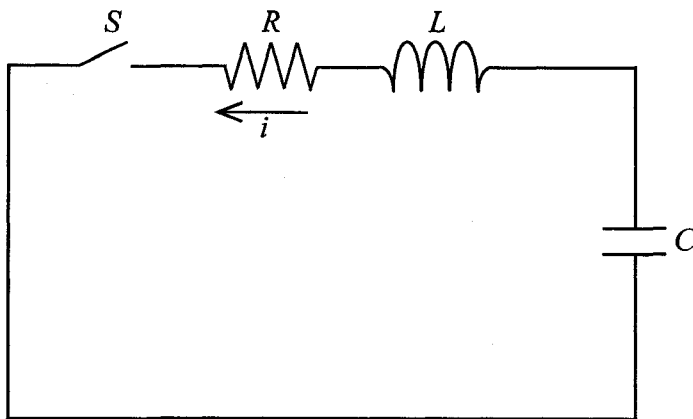


Fig. 2.1. An  $RLC$  circuit with a charged capacitor.

the one shown in Fig 2.1 is of the form  $Ke^{pt}$  where  $K$  is a constant and  $p$  is one of the roots of the polynomial and  $t$  the time. The roots  $p$  of the characteristic equation are given by

$$p = -\frac{R}{2L} \pm \sqrt{\left(\frac{R}{2L}\right)^2 - \frac{1}{LC}} \quad (2.2)$$

In general the root  $p$  is complex, the real part represents the rate of decay or rise of the transient while the imaginary part represents the frequency of oscillation. In most cases the real part of  $p$  is negative (since  $R$  is positive), indicating that the transient is decaying in nature as seen in Fig 2.2.

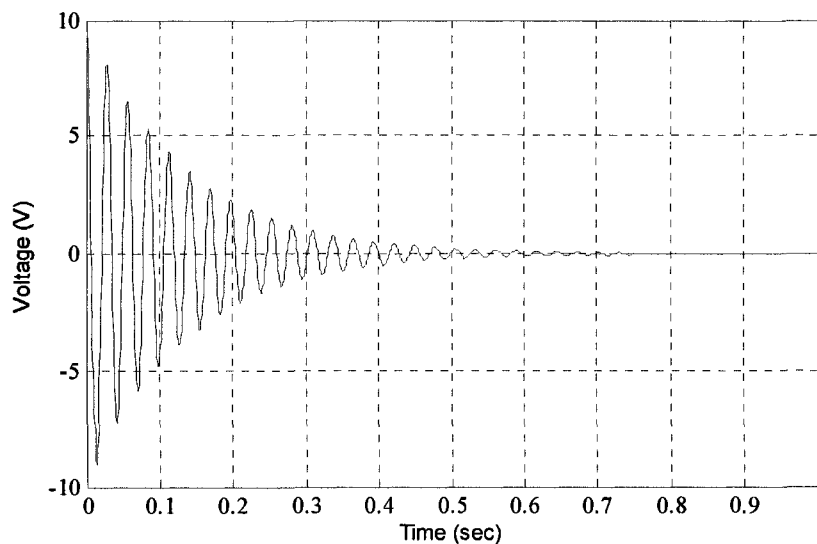


Fig. 2.2. Transient voltage across capacitor when  $R$  is positive.

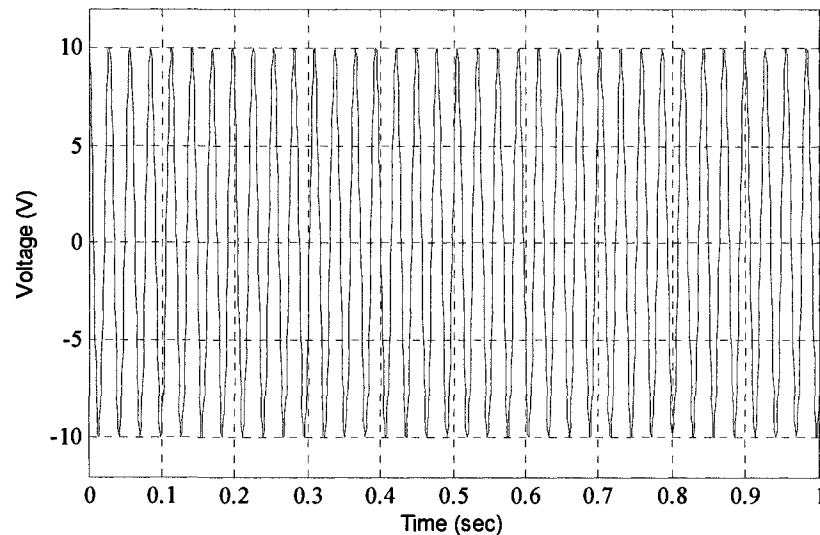
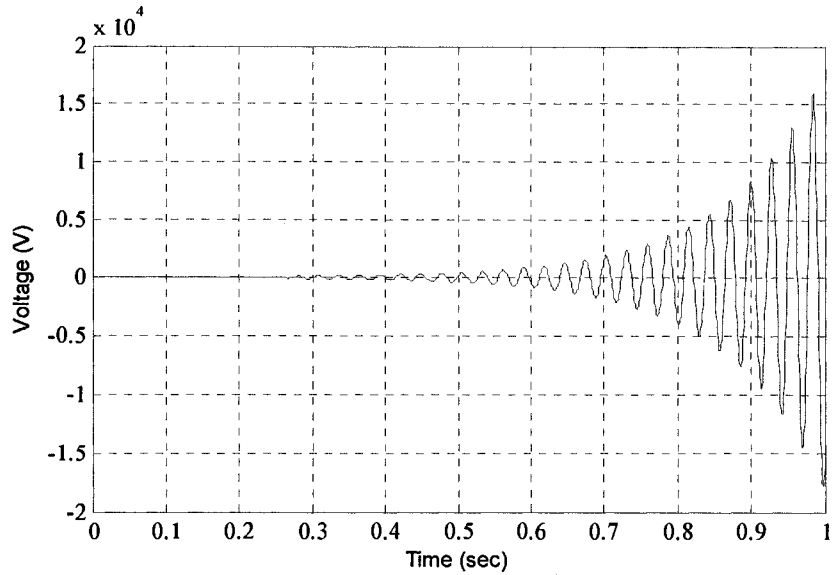


Fig. 2.3. Transient voltage across capacitor when  $R$  is zero.

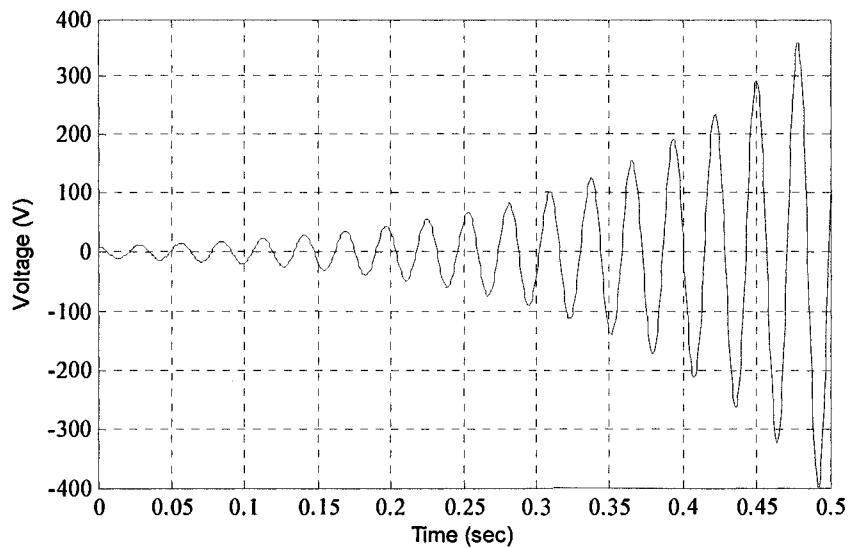
In passive circuits like this RLC circuit the real part is negative and thus the transient will finally decay to zero.

On the other hand, if the real part is zero ( $R$  is zero), the circuit is resonant and the transient neither decays or increases as seen in Fig. 2.3. However if the value is positive (i.e.  $R$  is negative), it means that the transient would increase to infinity with time as shown in Fig. 2.3(a) and Fig. 2.3(b). As the flow of current in a circuit will cause power to be dissipated in the circuit resistance, an increasing current dissipates increasing power. Transients which grow in magnitude, in the manner described, are very rare. This implies that for the value of the real part of the root to be positive, the circuit resistance  $R$  must be negative. Since real positive resistance is a sign of a power sink, negative resistance indicates a power source. In other words, in this circumstance some external energy source must be available to supply the real power [10].

This example of a very unusual transient is the distinctive feature of the self-excited induction generator. The process of terminal voltage build up continues in the manner described, until the magnetic circuit of the machine saturates causing the voltage to stabilize. In terms of the transient solution considered above, the effect of this saturation is to modify the magnetization reactance  $X_m$  so that the real part of the root  $p$  becomes zero; the transient then neither increases nor decreases and becomes a steady-state quantity giving continuous self-excitation.



(a)



(b)

Fig. 2.4. Transient voltage across capacitor when  $R$  is negative.  
 (a) Time = 1 sec. (b) Time = 0.5 sec.

In an induction machine with a capacitor connected across its terminals, if the effect of its small stator resistance  $R_s$  and stator leakage inductance  $L_{ls}$  is neglected, the equivalent circuit for no load excitation takes the form of a parallel  $LC$  circuit, where  $L$  represents the inductance of the induction motor and  $C$  the excitation capacitor. Such a circuit can be excited at a given frequency with the least amount of energy when the currents in the inductor and capacitor are equal. Thus if an induction machine is driven by a prime mover, and if the capacitor is charged, that capacitor provides the exciting current

required by the induction generator to produce a magnetic flux. The magnetic flux in the induction generator charges the capacitor to increase the terminal voltage. An increase in the capacitor voltage boosts up the excitation current to the generator to increase the flux which in turn increases the terminal voltage. In this way the voltage and current build up continues until the magnetizing inductance decreases to its saturated value and an equilibrium point is attained. The process will continue until steady-state is reached as described above.

## 2.2 Relationship between Capacitor Value, Rotor Speed and Generated Voltage

In order to estimate the level of saturation and the mutual inductance term at a particular operating condition, the representation of the magnetization curve of the induction generator under that condition is required. The magnetizing characteristic of an induction machine is nonlinear. In the absence of saturation of the iron this line should ideally be straight. But due to saturation the line becomes bent inward beyond a certain excitation current. This curve represents characteristic at a particular rotor speed. If the magnetizing characteristic is obtained at a higher rotor speed, a steeper curve will be obtained as shown in Fig. 2.5. This figure shows the relationship between the size of the excitation capacitance, the rotor speed and generated voltage. Here the top curve represents the magnetizing characteristic at a higher rotor speed.

As the reactive current produced by a capacitor is directly proportional to the voltage applied to it, the locus of the voltage and current relationship is a straight line. It can be seen from Fig. 2.5 that for certain value of capacitance there is a single point where the inductor and capacitor currents are equal. This is the intersection point of the magnetizing curve and the linear capacitor volt-ampere characteristic at the particular rotor speed at no load. At this point the voltage and current will oscillate at a certain peak value and frequency. Once self-excitation has been initiated, the open circuit voltage to which the machine will self-excite can be calculated (i.e.  $V_{21}$ ). If the capacitance is increased (from  $C_1$  to  $C_2$ ) a higher voltage,  $V_{22}$  will be generated as the slope of the capacitive reactance will be lower with increasing value of  $C$ . At a higher rotor speed,  $\omega_2$  a higher voltage,  $V_{11}$

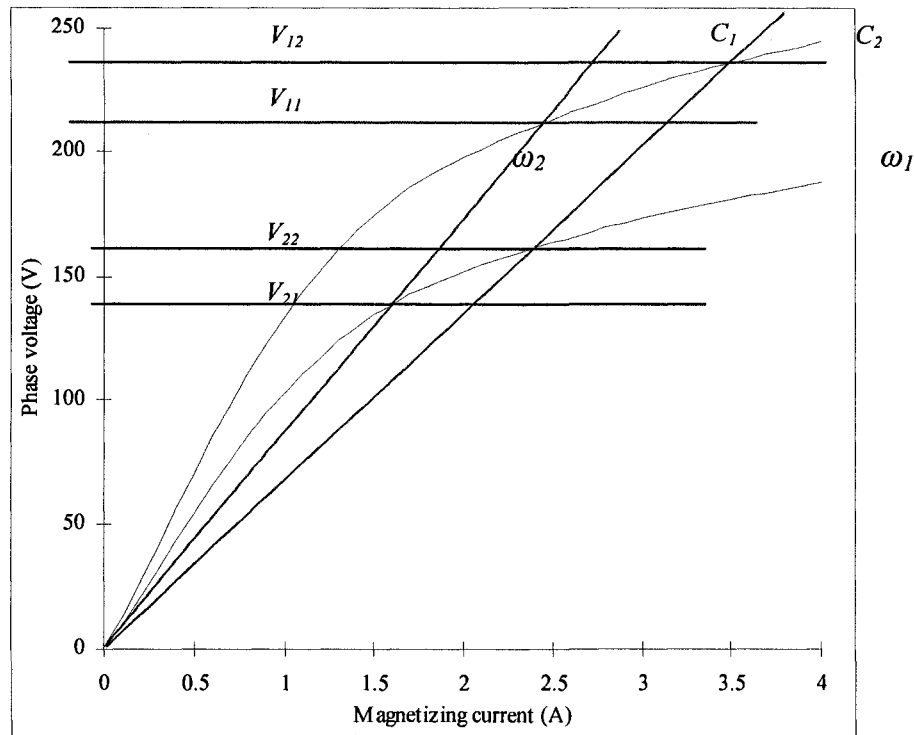


Fig. 2.5. V-I characteristics of an induction machine (shown in black) and excitation capacitor (shown in red)  $\omega_1 > \omega_2$ ,  $C_1 < C_2$ .

can also be generated since the capacitor load line will now intersect the upper magnetizing curve of the generator at  $V_{12}$ .

At low magnetizing current where the magnetizing curve is practically linear, the intersection with the capacitor line is not well defined. This will result in poor flux stability and voltage regulation in this region. This is the minimum value of capacitance beyond which the machine will not maintain or build up excitation at all. Any value of capacitor lower than the minimum will result in loss of excitation if the machine is already generating or will not be able to initiate self-excitation if the machine is starting.

The relationship between the capacitor, rotor speed and generated voltage can be summed up as follows:

- Increasing rotor speed increases the stator terminal voltage
- Increasing the capacitance increases the stator terminal voltage
- The minimum capacitance required for voltage build-up varies inversely with the rotor speed
- The frequency of the terminal voltage varies directly as the rotor speed

### 2.3 Conditions for Self-Excitation of an Induction Generator

As seen in the previous section, that for the transient voltage to build up and sustain, the real part of the roots of the characteristic equation should be positive. That means it is necessary that some external energy source should be available to the rotor to supply the losses associated with the stator current. There must also be an initial charge on the capacitor or residual magnetism in the rotor iron to initiate the voltage and current to build up. As explained earlier, when the machine is driven by an external prime-mover, the remnant flux in the rotating rotor induces a small voltage in stator windings, which carries a leading current if suitable terminal capacitors are connected [11]. The reactive energy to excite the induction generator thus oscillates between the electric field of the capacitors and magnetic field of the machine [2]. This assists the core flux and causes an avalanche effect due to the differential voltage equal to the difference between induced voltage and capacitor voltage. The voltage rise thus continues till saturation sets in and steady state is reached. Saturation of the magnetic circuit is the main requisite for the stabilization of the voltage. As can be seen from Fig. 2.5, for a certain value of the excitation capacitor the slope of the V-I line will be such that it intersects the magnetic saturation curve at a point. This point of intersection will be the steady-state terminal voltage ( $V_{11}$ ,  $V_{12}$ ,  $V_{21}$  and  $V_{22}$ ) and excitation current. If saturation is absent, the curve will essentially be a straight line and the two lines will not intersect. Consequently there will be no excitation.

The steady-state performance characteristics of an isolated self-excited induction generator are influenced by the magnitude of the excitation capacitor and rotor speed. The terminal capacitor must have its value within a certain range to sustain self-excitation. If the value of the excitation capacitor is outside this range, self-excitation will not be possible [12]-[14]. As explained above, the capacitor in such a machine must have a minimum value,  $C_{min}$  for self-excitation to take place. On the other hand in order to sustain operation, the terminal capacitor must also be below a certain maximum value  $C_{max}$  [13]. Both the minimum and maximum values are affected by the machine parameters, speed and load conditions.

In summary the following conditions must be satisfied for the induction generator to maintain self-excitation [2].

- The external power to the rotor shaft is equal to the copper losses in the machine and in the external stator resistance.
- The reactive power in the machine and load must be equal to the reactive power in the capacitors  $C$ , at a particular speed.
- Under no load condition, and a given rotor speed the machine will maintain self-excitation provided  $C_{min} < C < C_{max}$ .
- The equivalent circuit is in permanent resonance, i.e. the real and imaginary parts of the equivalent impedance are separately equal to zero.

## 2.4 Bibliography

- [1] C. Grantham, D. Sutanto, B. Mismail, "Steady-State and Transient Analysis of Self Excited Induction Generators," *IEE Proceedings on Electric Power Applications*, Vol. 136, Pt. E, No. 2, pp. 61-68, Mar. 1989.
- [2] Vlado Ostović, *Computer-aided Analysis of Electric Machines: a Mathematica Approach*, Hemel Hempstead, Herts, Prentice Hall International (UK), England 1994.
- [3] R.C. Bansal, "Three Phase Self-Excited Induction Generators: An Overview," *IEEE Transaction on Energy Conversion*, Vol. 20, No. 2, pp. 292-299, Jun. 2005.
- [4] O. Ojo, "Minimum Air Gap Flux Linkage Requirement for Self Excitation in Stand Alone Induction Generator," *IEEE Transaction on Energy Conversion*, Vol. 10, No. 3, pp. 484-491, Sep. 1995.
- [5] E. Levi, "Applications of Current State-Space Model in Analyses of Saturated Induction Machines," *Electric Power Systems Research*, pp. 203–216, 1994.
- [6] A. Kishore, R.C. Prashad and B.M. Karan, "Matlab Simulink Based DQ Modeling and Dynamic Characteristics of Three Phase Self Excited Induction Generator," *Progress in Electromagnetics Research Symposium 2006*, pp. 312-316, Mar. 2006.
- [7] C.F. Wagner, "Self-Excitation of Induction Motors with Series Capacitors," *AIEE Transactions*, Vol. 60, pp. 1241-1247, 1941.
- [8] S. J. Chapman, *Electrical Machinery Fundamentals*, 2<sup>nd</sup> edition. McGraw-Hill, New York, 1998.
- [9] E. Levi and Y.W. Liao, "An Experimental Investigation of Self-excitation in Capacitor Excited Induction Generators," *Electrical Power Research*, pp. 59-65, 2000.
- [10] D. Seyoum, "The Dynamic Analysis and Control of a Self-Excited Induction Generator driven by a Wind Turbine," Ph. D. Dissertation, The University of New South Wales, Australia, 1999.



- [11] S.S Murthy, "A Novel Self-Excited Self-Regulated Single Phase Induction Generator. Part-I: Basic System and Theory," *IEEE Transactions on Energy Conversion*, Vol. 8, No. 3, pp. 377-382, Sep. 1993.
- [12] N.H. Malik and A.H. Al-Bahrani, "Influence of the Terminal Capacitor on the Performance Characteristics of a Self Excited Induction Generator," *IEE Proceedings*, Vol. 137, Pt. C, No. 2, pp. 168-173, Mar.1990.
- [13] L. Wang and J.Y. Su, "Determination of Minimum and Maximum Capacitance of an Isolated SEIG using Eigenvalue Sensitivity Approach," *Proceedings of International Conference on Power System Technology*, Vol. 1 pp. 610-614, Aug. 1998.
- [14] M.B. Brennen M B and A. Abbondanti, "Static Exciters for Induction Generators," *IEEE Transaction on Industrial Applications*, Vol. 13(5), pp. 422-428, 1977.

### 3 DYNAMIC MODELLING OF SELF-EXCITED INDUCTION GENERATORS

#### 3.1 Introduction

Previous works on SEIG are mainly concerned with representing the machine by steady-state models and the dynamic models. The steady state model of an SEIG is developed as per-phase equivalent circuit. In this circuit the slip and angular frequency are expressed in per unit quantities. Previous authors have used either the loop impedance method [1]-[3] or the nodal admittance method [4]-[6] to analyze the machine performance. In the loop analysis technique the total loop impedance which includes the excitation capacitance, is equated to zero. In the nodal admittance method the overall admittance of the SEIG at a certain node is set to zero. These methods give an algebraic expression for magnetizing reactance in terms of generator frequency and other machine parameters and speed. For the determination of the operating frequency  $a$  and magnetizing reactance  $X_m$  the real and imaginary parts of the sum of admittances of the rotor, magnetizing and stator branches are separately equated to zero. In these approaches there are usually four unknowns, the magnetizing reactance  $X_m$ , the excitation capacitance  $X_c$ , per unit frequency  $a$  and per unit speed  $b$ . Assuming values of any two, the other two are found by iteration process [4] or numerical solution. In both the loop and nodal analysis a high order polynomial or a non-linear simultaneous equation is used where the general focus is to find the value of the capacitance required for self-excitation. Several researchers indicated that there is a minimum value of excitation capacitance to initiate self-excitation for a given speed and load condition [7], while some also exploited the maximum value of this capacitance [2], [5] beyond which excitation will not be maintained.

The d-q reference model using Park's transformation was proposed by Krause and Thomas [8]. This method was further extended by other authors [9]-[12] for dynamic analysis of induction machines. The non-linear differential equations that describe the dynamic performance of an induction machine in an arbitrary reference frame can be derived from the d-q equivalent circuits. To analyse the performance of an induction generator system, differential equations describing the excitation capacitance and load are also taken into account.

### 3.2 Development of the Mathematical Model of Induction Machines

Like a transformer the current in the secondary or the rotor circuit is created exclusively by magnetic induction. This makes it unique from other types of rotating machines where there is a requirement of dc supply or permanent magnet for the field. Depending on the configuration and condition of operation an induction machine can be made to work either as a motor or generator. In this chapter, modeling of a three phase induction generator is presented.

The mathematical model of a self-excited induction generator has been developed from the conventional model of an induction machine. When the stator of an induction machine is excited from a balanced three phase source, a synchronously revolving mmf or field in the air gap is created. This field rotates around the air gap at a synchronous speed  $N_s$  that can be calculated as

$$N_s = \frac{120f}{p} \quad (3.1)$$

where  $f$  is the frequency of the source and  $p$  is the number of poles. The slip  $s$  of the rotor with respect to the speed of the stator magnetic field, is defined as

$$s = \frac{N_s - N_r}{N_s} \quad (3.2)$$

where  $N_r$  is the rotational speed of the rotor. In terms of speed in radians per second,

$$s = \frac{\omega_b - \omega_r}{\omega_b} \quad (3.3)$$

where  $\omega_b$  is the synchronous or base speed in radians per second and  $\omega_r$  is the speed of the rotor.

Single-phase equivalent circuit of three-phase squirrel cage induction machine can be considered to be similar to a three phase transformer equivalent circuit with the secondary windings short-circuited. The circuit model is shown in Fig. 3.1. All reactance are referred to base frequency,  $\omega_b$  and the stator side. As shown in Fig. 3.1, the per phase

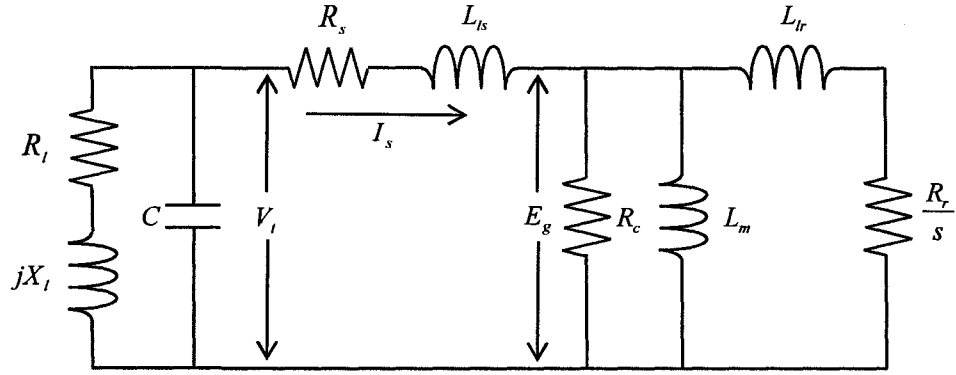


Fig. 3.1. Per phase model of an induction machine connected to excitation capacitor and load.

model of the induction machine is shown connected to an excitation capacitor  $C$  to feed the induction machine with reactive power and a load  $R_l + jX_l$ . The terminal voltage is  $V_t$  and the voltage across the mutual inductance is  $E_g$ . The stator and rotor circuits are linked by the mutual inductance  $L_m$ . The core loss which is due to hysteresis and eddy current losses are accounted for and shown by  $R_c$ . The no load current consists of the core loss component and magnetizing component.  $R_c$  is dependent on the flux in the core and frequency of excitation. Core loss is generally ignored in calculation, but core loss should be included in order to give more accurate prediction of the performance especially for efficiency calculations [9].

With reference to Fig. 3.1, the following voltage equation may be written

$$V_t = R_s I_s + j\omega_b L_{ls} I_s + E_g \quad (3.4)$$

which may be re-written as

$$V_t = R_s I_s + jaX_{ls} I_s + E_g \quad (3.5)$$

where  $a = \omega_r / \omega_b$  is the per unit frequency and  $\omega_b$  is the base frequency.

Dividing the equation by  $a$  yields

$$\frac{V_t}{a} = \frac{R_s I_s}{a} + jX_{ls} I_s + \frac{E_g}{a} \quad (3.6)$$

The per unit slip in 3.2 may also be expressed as

$$s = \frac{a - b}{a} \quad (3.7)$$

where

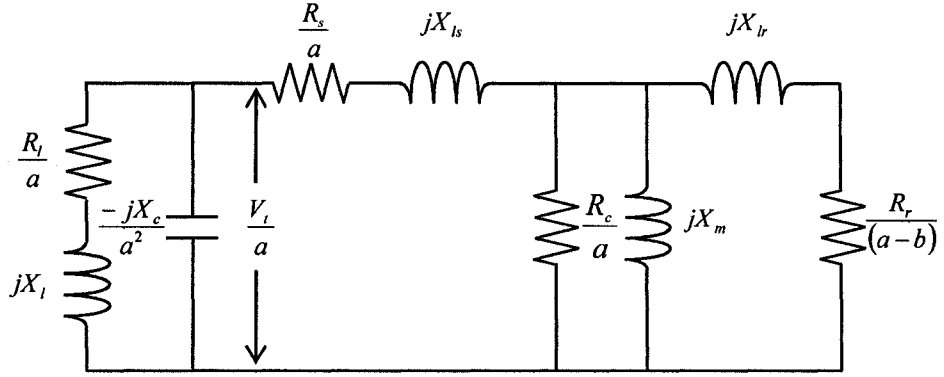


Fig. 3.2. Per phase model of an induction machine in terms of base frequency.

$$b = \frac{N_r}{N_b} \quad (3.8)$$

is the per unit speed . The equivalent circuit may now be re-drawn as Fig 3.2. This stator referred equivalent circuit in terms of base frequency is commonly used for predicting the performance of an SEIG.

### 3.2.1 Loop impedance model

The calculation of minimum capacitance has been presented by many researchers [6]. The loop equation in Fig. 3.3 may be written as

$$I_s Z_t = 0 \quad (3.9)$$

where  $I_s$  is the loop current in the loop 'abcd' and

$$Z_t = Z_{ab} + Z_{ac} + Z_{cd} \quad (3.10)$$

is the total loop impedance.

$$\frac{1}{Z_{ab}} = \frac{1}{\frac{R_l}{a} + jX_l} - j \frac{a^2}{X_c} \quad (3.11)$$

$$Z_{ac} = \frac{R_s}{a} + jX_{ls} \quad (3.12)$$

$$\frac{1}{Z_{cd}} = \frac{a}{R_c} + \frac{1}{jX_m} + \frac{1}{\frac{R_r}{(a-b)} + jX_{lr}} \quad (3.13)$$

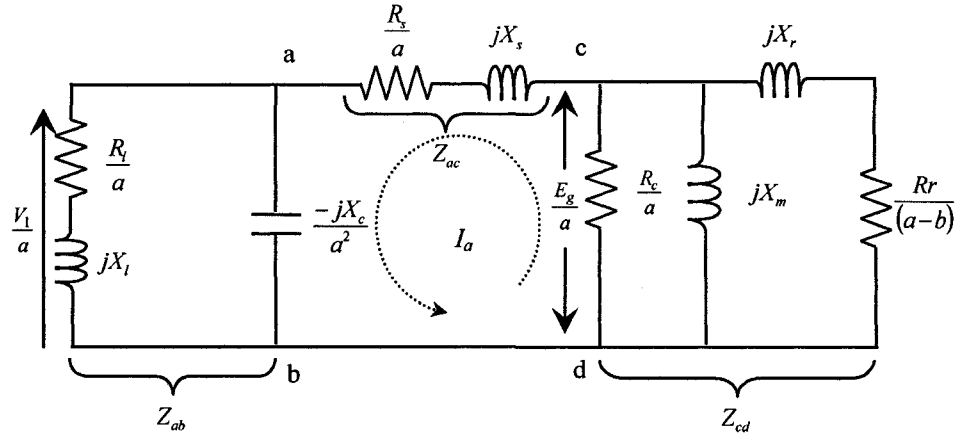


Fig. 3.3. Per phase model of an induction machine for loop analysis.

Since in steady state conditions  $I_s \neq 0$ , then  $Z_t = 0$ , therefore

$$\text{Real}(Z_t) = 0 \quad (3.14)$$

and

$$\text{Imag}(Z_t) = 0. \quad (3.15)$$

By equating real and imaginary components of  $Z_t$ , two non-linear equations in  $X_c$  and  $a$  can be set up. These equations are generally of high order polynomial and can be solved simultaneously for two unknowns. These two unknowns can be  $a$  and  $X_m$ , or  $a$  and  $X_c$ . Solving these two equations the value of  $X_m$ ,  $X_c$  and  $a$  can be calculated.

### 3.2.2 Nodal admittance model

The nodal admittance method is also used to determine the value of minimum capacitance and frequency. Based on the steady-state equivalent circuit model, and considering the circuit conductance a higher order polynomial in the per-unit frequency is obtained.

As can be seen from Fig. 3.4, the sum of the currents at node 'a' is

$$I_a + I_b + I_c = 0 \quad (3.16)$$

which can be written as

$$V_1(Y_t) = 0 \quad (3.17)$$

where  $V_l$  is the node voltage at 'a' and

$$Y_l = Y_l + Y_c + Y_{ad} \quad (3.18)$$

The admittance between point  $c$  and  $d$  in Fig. 3.4 may be written as

$$Y_{cd} = \frac{a}{R_c} + \frac{1}{jX_m} + \frac{1}{\frac{R_r}{(a-b)} + jX_{lr}} \quad (3.19)$$

$$Z_{cd} = \frac{1}{Y_{cd}} = R_{cd} + jX_{cd} \quad (3.20)$$

$$Y_l = \frac{aR_l}{(R_l^2 + a^2X_l^2)} - \frac{ja^2X_l^2}{(R_l^2 + a^2X_l^2)} \quad (3.21)$$

$$Y_c = \left[ -\frac{jX_c}{a^2} \right]^{-1} \quad (3.22)$$

$$Y_{ad} = \left[ \left( \frac{R_s}{a^2} + jX_{ls} \right) + (R_{cd} + jX_{cd}) \right]^{-1} \quad (3.23)$$

Therefore Fig. 3.4 may be re-drawn as Fig. 3.5, by replacing the equivalent impedance between  $c$  and  $d$  by  $R_{cd} + jX_{cd}$ .

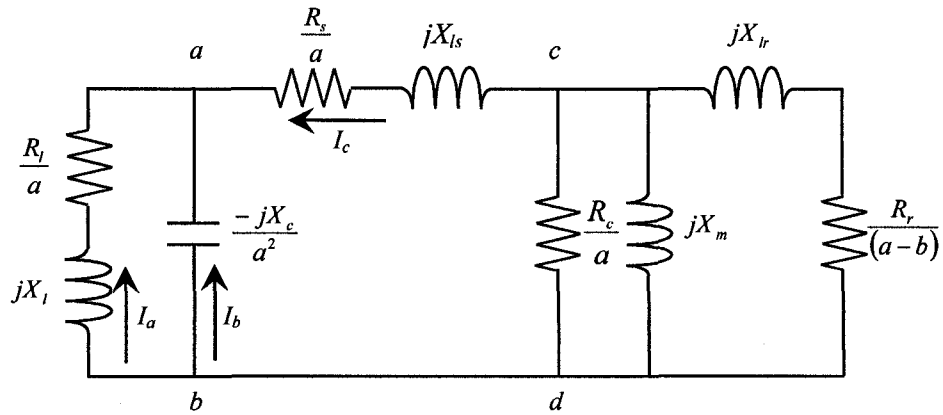


Fig.3.4. Per phase model of an induction machine for nodal analysis.

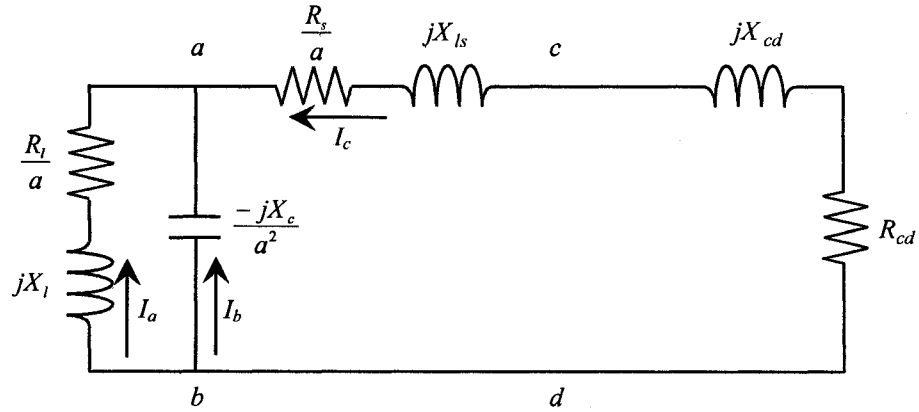


Fig. 3.5. Modified per phase model of an induction machine.

Since at steady state condition  $V_l \neq 0$ , then

$$Y_l = Y_l + Y_c + Y_{ad} = 0 \quad (3.24)$$

$$Y_l = \frac{1}{R} - \frac{1}{jX} = 0 \quad (3.25)$$

or

$$\text{Real}(Y_l) = 0 \quad (3.26)$$

and

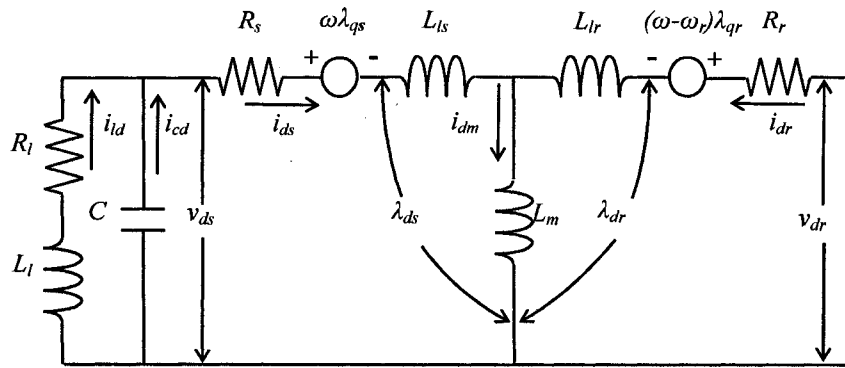
$$\text{Imag}(Y_l) = 0. \quad (3.27)$$

Equating real and imaginary parts of (3.24) separately to zero, the polynomial can be solved for real roots, which enables the value of  $a$  and  $C$ , to be calculated.

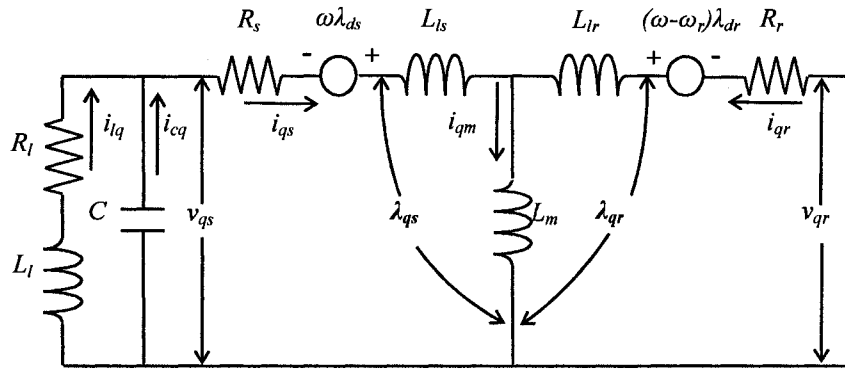
### 3.2.3 Model using d-q reference frame

The induction machine as presented in Fig. 3.6(a) and (b) can be modeled using d-q axis reference frame. These figures show the direct and quadrature axes representation of a squirrel-cage induction machine. It is the most commonly used transient state model in the d-q axis frames of reference [10]. This model of the induction machine offers a suitable way of modeling the machine and very much compliant for numerical solution. The advantage of the d-q axis model is that it is a powerful tool for analyzing the dynamic and steady state conditions, thus providing a complete solution for any dynamics. For steady-state analysis, the conventional model and the d-q reference are





(a)



(b)

Fig. 3.6. Equivalent circuit of an SEIG in d-q axes. (a) d-axis. (b) q-axis.

the same.

From the above figures the d-q axis stator and rotor voltages of an induction machine can be expressed in matrix notation as:

$$\begin{bmatrix} v_{qs} \\ v_{ds} \\ v_{qr} \\ v_{dr} \end{bmatrix} = \begin{bmatrix} R_s + pL_s & \omega L_s & pL_m & \omega L_m \\ -\omega L_s & R_s + pL_s & -\omega L_m & pL_m \\ pL_m & (\omega - \omega_r)L_m & R_r + pL_r & (\omega - \omega_r)L_r \\ -(\omega - \omega_r)L_m & pL_m & -(\omega - \omega_r)L_r & R_r + pL_r \end{bmatrix} \begin{bmatrix} i_{qs} \\ i_{ds} \\ i_{qr} \\ i_{dr} \end{bmatrix} \quad (3.28)$$

where  $p = \frac{d}{dt}$ ,  $\omega$  is the synchronous or base speed in radians per second and  $\omega_r$  is the speed of the rotor.

$$\begin{aligned} L_s &= L_{ls} + L_m \\ L_r &= L_{lr} + L_m \end{aligned} \quad (3.29)$$

$$\begin{aligned} \lambda_{qs} &= L_s i_{qs} + L_m i_{qr} \\ \lambda_{ds} &= L_s i_{ds} + L_m i_{dr} \\ \lambda_{qr} &= L_r i_{qr} + L_m i_{qs} \\ \lambda_{dr} &= L_r i_{dr} + L_m i_{ds} \end{aligned} \quad (3.30)$$

Equation 3.28 may be written as

$$[v_{dq}] = [RL_{dq}] [i_{dq}] + [L_{dq}] p[i_{dq}] \quad (3.31)$$

where

$$[v_{dq}] = [v_{qs} \ v_{ds} \ v_{qr} \ v_{dr}]^T \quad (3.32)$$

$$[i_{dq}] = [i_{qs} \ i_{ds} \ i_{qr} \ i_{dr}]^T \quad (3.33)$$

$$[RL_{dq}] = \begin{bmatrix} R_s & \omega(L_m + L_{ls}) & 0 & \omega L_m \\ -\omega(L_m + L_{ls}) & R_s & -\omega L_m & 0 \\ 0 & (\omega - \omega_r)L_m & R_r & (\omega - \omega_r)(L_m + L_{lr}) \\ -(\omega - \omega_r)L_m & 0 & -(\omega - \omega_r)(L_m + L_{lr}) & R_r \end{bmatrix} \quad (3.34)$$

$$[L_{dq}] = \begin{bmatrix} L_m + L_{ls} & 0 & L_m & 0 \\ 0 & L_m + L_{ls} & 0 & L_m \\ L_m & 0 & L_m + L_{lr} & 0 \\ 0 & L_m & 0 & L_m + L_{lr} \end{bmatrix} \quad (3.35)$$

Rearranging (3.31)

$$p[i_{dq}] = [L_{dq}]^{-1} [v_{dq}] - [L_{dq}]^{-1} [RL_{dq}] [i_{dq}] \quad (3.36)$$

Since the rotor is squirrel-cage one,  $v_{qr}$  and  $v_{dr}$  are both equal to zero.

The differential equations representing the capacitor circuit is given by

$$\begin{bmatrix} i_{cq} \\ i_{cd} \end{bmatrix} = C \begin{bmatrix} p & \omega \\ -\omega & p \end{bmatrix} \cdot \begin{bmatrix} v_{qs} \\ v_{ds} \end{bmatrix} \quad (3.37)$$

where the voltage across the capacitor is  $v_{qs}$  and  $v_{ds}$  and the currents are  $i_{cq}$  and  $i_{cd}$  respectively. Equation (3.37) can be re-arranged to give

$$p \begin{bmatrix} v_{qs} \\ v_{ds} \end{bmatrix} = \begin{bmatrix} 1/C & 0 \\ 0 & 1/C \end{bmatrix} \begin{bmatrix} i_{qs} \\ i_{ds} \end{bmatrix} + \begin{bmatrix} 0 & -\omega \\ \omega & 0 \end{bmatrix} \begin{bmatrix} v_{qs} \\ v_{ds} \end{bmatrix} \quad (3.38)$$

For open circuit conditions, (3.36) and (3.38) form the set of differential equations to represent the system.

For a resistive load connected across the terminals of the SEIG and noting that

$$i_{qs} = i_{cq} + i_{lq} \quad (3.39)$$

and

$$i_{ds} = i_{cd} + i_{ld} \quad (3.40)$$

the load currents may be expressed as

$$R_l \begin{bmatrix} i_{lq} \\ i_{ld} \end{bmatrix} = \begin{bmatrix} v_{qs} \\ v_{ds} \end{bmatrix} \quad (3.41)$$

In order to take the  $RL$  load impedance into account

$$\begin{bmatrix} v_{qs} \\ v_{ds} \end{bmatrix} = (R_l + pL_l) \begin{bmatrix} i_{lq} \\ i_{ld} \end{bmatrix} \quad (3.42)$$

or

$$p \begin{bmatrix} i_{lq} \\ i_{ld} \end{bmatrix} = L_l^{-1} \begin{bmatrix} v_{qs} \\ v_{ds} \end{bmatrix} - L_l^{-1} R_l \begin{bmatrix} i_{lq} \\ i_{ld} \end{bmatrix} \quad (3.43)$$

In this case (3.36), (3.38) and (3.41) will represent the SEIG connected to a resistive load while (3.36), (3.38) and (3.43) will correspond to the SEIG feeding an  $RL$  load.

### 3.3 Approach to Skin Effect Modelling

It is known that eddy currents are closed loops of induced current circulating in planes perpendicular to a magnetic flux. They concentrate near the surface adjacent to current source (i.e. an excitation coil) and their strength decreases with distance from the coil. The current density in this circumstance decreases exponentially with depth. The alternate explanation of skin effect is that it is a phenomenon where an alternating current has the tendency to concentrate near the outer part or “skin” of the conductor through which it is flowing. For a steady unidirectional current through a homogeneous conductor, the current distribution is uniform throughout the cross section, that is, the current density is the same at all points in the cross section. With an alternating current this is not the case. As the frequency increases, the current is displaced more and more towards the surface. Consequently in the squirrel cage rotor bars of an induction machine the leakage flux tends to crowd towards the top of the bar adjacent to the air gap as shown in Figs. 3.7(a) – (c). This non-uniform distribution of induced currents in the conductors of the rotor has a huge influence on the resistance and inductance of the rotor circuit. As the flux produced by the rotor current crossing the air gap to link the stator increases, the leakage flux in the rotor will decrease. A decrease in the rotor flux per unit current decreases the rotor leakage inductance [9]. On the other hand since the effective area used by the current decreases, the effective resistance increases. These changes in magnitudes of rotor parameters have an impact on the dynamic behaviour of the machine.

As mentioned earlier, when an SEIG is loaded, both the magnitude and frequency of the induced emf are affected by the rotor speed, the value of the excitation capacitor and the load impedance [11]. Unlike induction generators connected to the grid, both frequency and magnetizing reactance of the SEIG vary with loading conditions even when the speed of the rotor is held constant [13].

To explain the variation of frequency it is assumed that the generator losses are small and negligible, the rotor speed is held constant and that the connected load is purely resistive. In such a case, an increase in load i.e. decreases in load resistance, will require a higher torque. This will result in a decrease in stator frequency to provide higher torque to match the increment in output power [14].

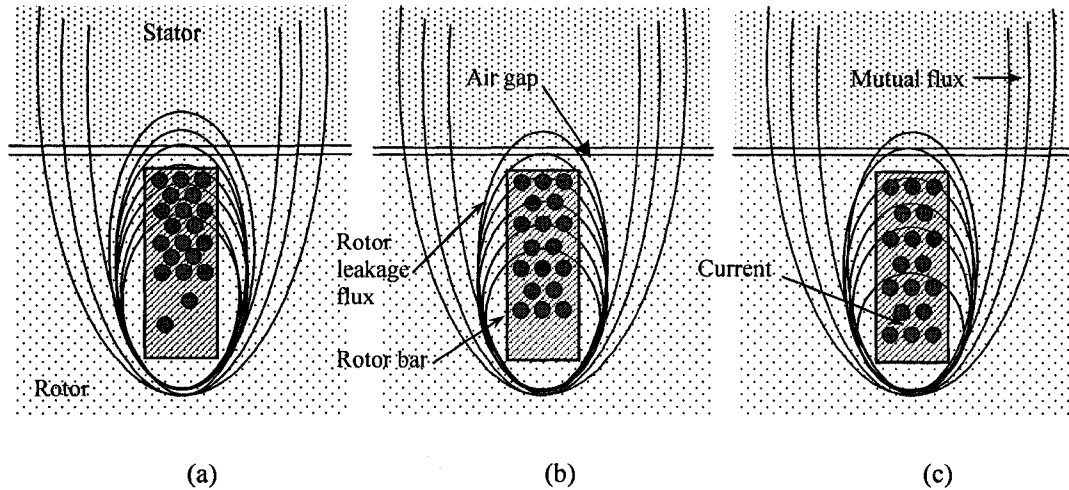


Fig. 3.7. Influence of skin effect on the flux and current distribution in the rotor bars. (a) High frequency, (b) Intermediate frequency, (c) Low frequency.

In wind turbine applications variations in turbine speed and load are common phenomena. These variations affect the stator frequency of SEIG, which in turn influence the magnitude of the machine impedances and consequently its performance.

When an SEIG is used in wind turbine applications, the actual machine behaviour during the steady state or transient condition should be precisely determined. In this research, an improved model of an SEIG incorporating skin effect has been developed to demonstrate its dynamic performance. In order to incorporate skin effect and the effect of main flux saturation, mathematical models are developed making it applicable for open circuit,  $R$  load and  $R-L$  load conditions. This inclusion of main flux saturation and skin effect is required in order to predict the results accurately. In the conventional model machine parameters have been used for simulation of dynamic behaviour while in the improved model skin effect have been taken into account for the parameters that are influenced by it. In development of the machine models the following assumptions have been made:

- Saturation effect is considered for both models, skin effect is considered for the proposed model.
- Harmonic content of the mmf wave is neglected.
- Iron losses are neglected.
- Rotor speed is held constant at base speed.

The d-q axis model based on the generalized machine theory [8] has been used. Figs. 3.6(a) and (b) show the arbitrary  $d$ - $q$  axis reference frame equivalent circuit for a three phase induction machine with excitation capacitance and  $R$ - $L$  load. As mentioned earlier, the  $d$ - $q$  axis model provides a very convenient way of representing the induction machine for numerical solution using the 4<sup>th</sup>-order Runge-Kutta method.

Due to migration of induced current owing to skin effect, the conductor's effective cross-section is reduced. As a result the resistance and energy dissipation are increased while the apparent inductance of the rotor conductors is reduced compared with the values for a uniformly distributed current. Subsequently skin effect will cause a decrease in the leakage inductance causing higher amplitudes of current, whereas the resistance will increase resulting in higher copper losses [15]. The effective resistance and inductance of the rotor bar are given by (3.44) and (3.45) respectively, where  $R_{r0}$  and  $L_{lr0}$  are the resistance and inductance in direct current condition.  $K_r$  and  $K_l$  are defined by (3.46) and (3.47) respectively. The magnitude of the rotor parameters, i.e. resistance and inductance of a squirrel cage machine is also dependent on the shape of the rotor bars. For bars with simple rectangular shapes, solving Maxwell's equation provides an accurate expression for rotor impedance as a function of frequency [16]. The analytical formula to relate the resistance and inductance, as a function of its dimensions and frequency are shown in [17]-[20].

$$R_r = K_r R_{r0} \quad (3.44)$$

$$L_{ls} = K_l L_{lr0} \quad (3.45)$$

where

$$K_r = \xi \left[ \frac{\sinh(2\xi) + \sin(2\xi)}{\cosh(2\xi) - \cos(2\xi)} \right] \quad (3.46)$$

$$K_l = \frac{3}{2\xi} \left[ \frac{\sinh(2\xi) - \sin(2\xi)}{\cosh(2\xi) - \cos(2\xi)} \right] \quad (3.47)$$

where

$$\xi = h_r \sqrt{\mu_0 \pi \sigma f \frac{b_r}{b_s}} \quad (3.48)$$

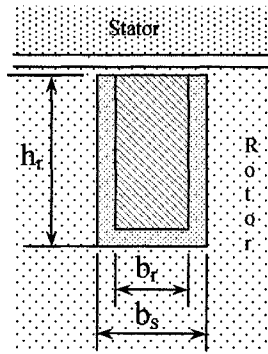


Fig 3.8. Dimensions of a rectangular rotor bar.

$h_r$  = height of rotor slot

$b_r$  = width of rotor bar

$b_s$  = width of rotor slot

$\mu_o$  = permeability of free space

$\sigma$  = conductivity of bar

$f$  = frequency of induced current

The variation of frequency with rotor speed and load has been studied on the two laboratory 7.5 hp induction machines. In Fig. 3.8 the dimensions of the rotor bar are also shown. The variation of the resistance coefficient  $K_r$  and inductance coefficient  $K_l$  with frequency of the test machine for variable speed, constant excitation capacitance and open circuit are shown in Fig. 3.9.

In order to take the skin effect into account in the machine model described in the previous section, the rotor resistance and inductance in (3.28) are modified using (3.44)-(3.48).

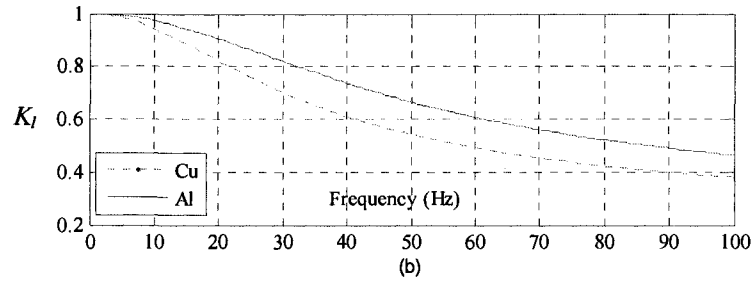
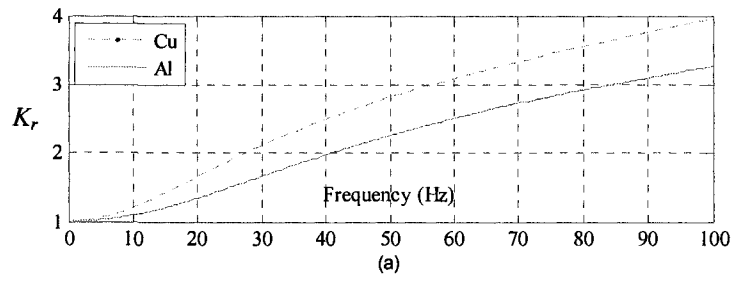


Fig. 3.9. Variation of rotor resistance coefficient (a) and inductance coefficient (b) with stator frequency.



### 3.4 Bibliography

- [1] N.H. Malik and S.E. Haque, "Steady State Analysis and Performance of an Isolated Self Excited Induction Generator," *IEEE Transaction on Energy Conversion*, pp. 134-139, 1986.
- [2] N.H. Malik and A.H. Al-Bahrani, "Influence of the Terminal Capacitor on the Performance characteristic of a Self Excited Induction Generator," *IEE Proceedings* Vol. 137, Pt. C, No. 2, pp. 168-173, Mar. 1990.
- [3] N.H. Malik and A.A. Mazi, "Capacitance Requirements of Self Excited Induction Generators," *IEEE Transaction on Energy Conversion*, Vol. EC-2, No. 1, pp. 62-69, Mar. 1986.
- [4] T.F. Chan, "Analysis of Self Excited Induction Generators using Iterative Method," *IEEE Transaction on Energy Conversion*, Vol. 10, No. 3, pp. 502-507, Sep.1995.
- [5] —, "Capacitance requirements of Self-Excited Induction Generators," *IEEE Transactions on Energy Conversion*, Vol. 8, No. 2, pp. 304-311, Jun. 1993.
- [6] A.M. Eltamaly, "New Formula to Determine Minimum Capacitance required for Self Excited Induction Generator," *IEEE 33rd Power Electronics Specialists Conference*, Vol. 1, pp. 106-110, Jun. 2002.
- [7] N.H. Malik and AA. Mazi, "Capacitance Requirements for Isolated Self Excited Induction Generators," *IEEE Transaction on Energy Conversion*, Vol. EC-2, No. 1, pp. 62-68, Mar. 1987.
- [8] P.C. Krause and C.H. Thomas, "Simulation of Symmetrical Induction Machinery," *IEEE Transaction on Power Apparatus and Systems*, Vol. PAS-84, No. 11, pp. 1038-1044. Nov. 1965.
- [9] D. Seyoum, "The Dynamic Analysis and Control of a Self-Excited Induction Generator driven by a Wind Turbine," Ph. D. Dissertation, The University of New South Wales, Australia, 1999.
- [10] P.C. Krause, *Analysis of Electric Machinery and Drive Systems*, 2<sup>nd</sup> Edition, IEEE Press, 2002.

- [11] G. Scutaru and C. Apostoiaia, "Matlab-Simulink Model of a Stand-Alone Induction Generator," *Proceedings of International Conference on Optimization of Electrical and Electronic Equipment*, pp. 155-162, May 2004.
- [12] L. Wang and C.H. Lee, "A Novel Analysis on the Performance of an Isolated Self-Excited Induction Generator," *IEEE Transaction on Energy Conversion*, Vol. 12, No. 2, pp.109-117, Jun. 1997.
- [13] T.F. Chan, "Steady State Analysis of Self Excited Induction Generators," *IEEE Transactions on Energy Conversion*, Vol.9, No. 2, pp.288-296, Jun. 1994.
- [14] Y.N. Anagreh and M. Refaee, "Teaching the Self Excited Generator using Matlab," *International Journal of Electrical Engineering Education*, Vol. 40, No. 1, pp. 55-65, Jan. 2003
- [15] J. Langheim, "Modeling of Rotor Bars with Skin Effect for Dynamic Simulation of Induction Machines," *Conference Record of the 1989 IEEE Industry Application Society Annual Meeting*, Vol. 1, pp. 38-44, 1989.
- [16] O.I. Okoro, "Analytical Method of computation of Rectangular Rotor Bar Impedance for Skin effect Using Matlab," *The Pacific Journal of Science and Technology*, Vol. 5, No. 2, pp. 16-25, Apr. 2003.
- [17] —, "Transient State Modeling of Asynchronous Generator with Skin Effect," *The Pacific Journal of Science and Technology*, Vol. 5, No. 2, pp. 63-71, Oct. 2004.
- [18] M. Kostenko and L. Piotrovsky, *Electrical Machines, Alternating Current Machines*, Vol. 2, Translated from Russian by A. Chernukhin, Mir Publishers, 1972.
- [19] P.L. Alger, *Induction Machines Their Behavior and Uses*, Gordon and Breach Science Publishers, New York, 1970.
- [20] H. Kabbaj, X Roboam, Y. Lefevre and J. Faucher, "Skin Effect Characterization in a Squirrel Cage Induction Machine," *Proceedings of the IEEE International Symposium on Industrial Electronics*, Vol. 2, pp. 532-536, 1997.

## 4 DETERMINATION OF ALUMINIUM-ROTOR AND COPPER-ROTOR INDUCTION MACHINE EQUIVALENT CIRCUIT PARAMETERS

### 4.1 Introduction

In order to determine the performance of the induction machine precisely, the machine equivalent circuit (Fig. 4.1) parameters need to be determined accurately. The tests required to determine the machine parameters are based on the conventional experimental methods described in texts [1], [2] and IEEE Standard [3]. These tests are carried out on the laboratory 7.5 hp induction machines. As mentioned earlier one of the machines has aluminium rotor while the other machine has copper as the rotor cage bars.

### 4.2 DC Resistance Test

The dc resistance test is carried out by passing a dc current through the phase winding of the stator and measuring the voltage drop across it. Several measurements are made and the dc resistance of the stator winding is taken to be the mean of all the calculated values of resistance.

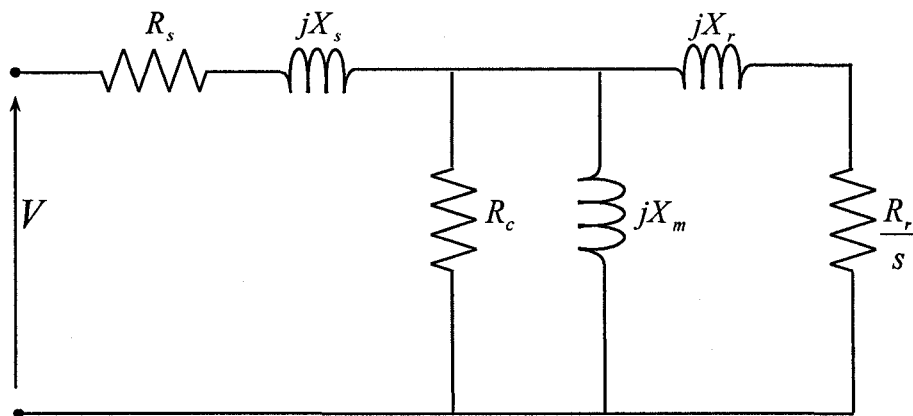


Fig. 4.1. Per-phase equivalent circuit of an induction machine.

### 4.3 Open-Circuit Test

Open-circuit test is conducted by driving the induction machine at its rated synchronous speed using an external prime mover which in this case is a dc motor. The stator terminals are supplied with rated voltage. When the machine is running at synchronous speed, the rotor slip is zero and hence the rotor circuit becomes open and the equivalent circuit reduces to the one shown in Fig. 4.2. In this figure, the parallel magnetizing reactance  $X_m$  and core loss resistance  $R_c$  can be converted into a series branch as shown in Fig 4.3. Here

$$R_M = \frac{R_c X_m^2}{R_c^2 + X_m^2} \quad (4.1)$$

and 
$$X_M = \frac{R_c^2 X_m}{R_c^2 + X_m^2} \quad (4.2)$$

In this case with

$V_o$  = open-circuit phase voltage

$I_o$  = open-circuit phase current

$P_o$  = open-circuit three phase input power

$s$  = slip, 0

$$Z_o = \frac{V_o}{I_o} \quad (\text{input impedance}) \quad (4.3)$$

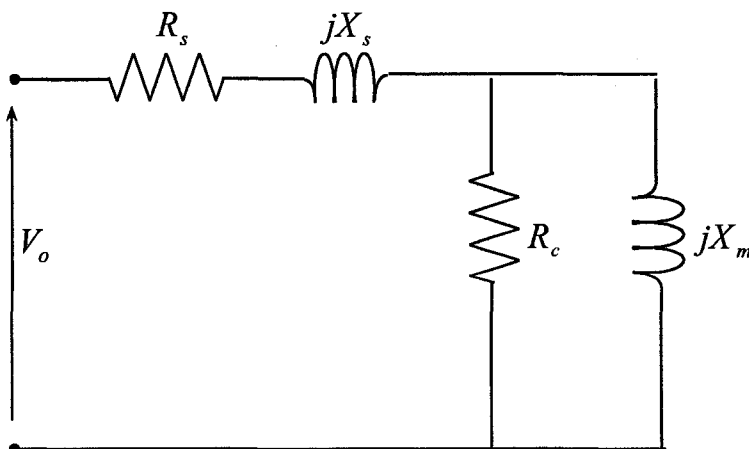


Fig. 4.2. Per-phase equivalent circuit of an induction machine at no load.

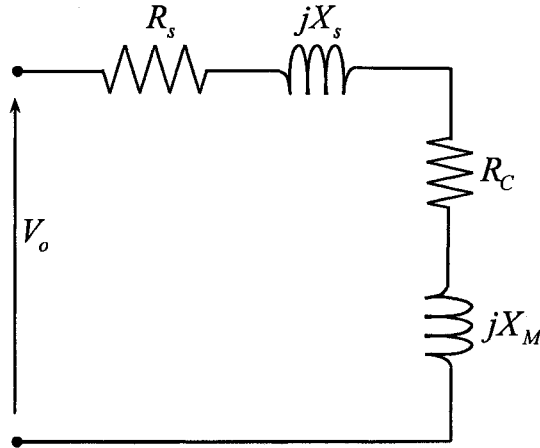


Fig. 4.3. Modified per-phase equivalent circuit of an induction machine at no load.

$$R_o = \frac{P_o}{3I_o^2} \quad (\text{input resistance}) \quad (4.4)$$

$$X_o = \sqrt{Z_o^2 - R_o^2} \quad (\text{input reactance}) \quad (4.5)$$

then

$$R_o = R_s + R_C \quad (4.6)$$

and

$$X_o = X_s + X_M \quad (4.7)$$

#### 4.4 Short-Circuit Test

The locked-rotor or short-circuit test is conducted by blocking the rotor by some means to prevent it from moving. Since under this condition the slip  $s$  is equal to one the equivalent circuit is modified and shown in Fig. 4.4. At standstill condition of the rotor, the rated current is supplied to the stator terminals.

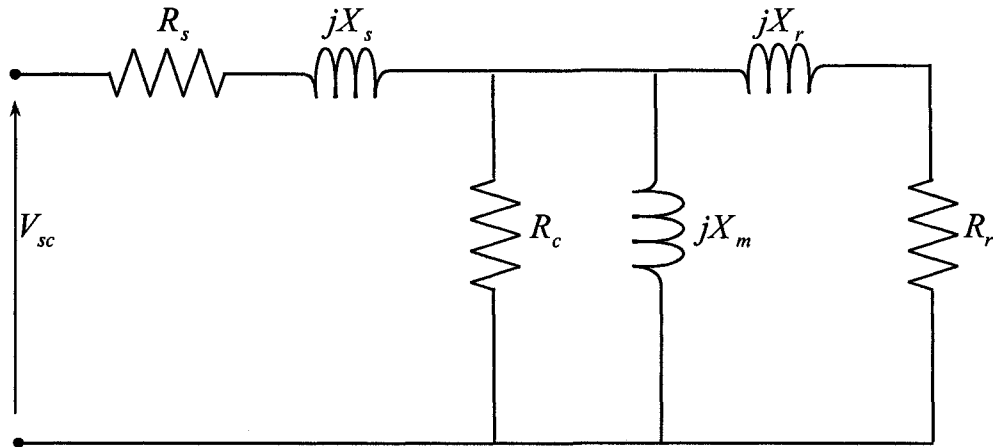


Fig. 4.4. Per-phase equivalent circuit of an induction machine at blocked-rotor condition.

In this case with

$V_{sc}$  = short circuit phase voltage

$I_{sc}$  = short circuit phase current

$P_{sc}$  = short circuit three phase input power

$s$  = slip, 1

$$Z_{sc} = \frac{V_{sc}}{I_{sc}} \quad (\text{input impedance}) \quad (4.8)$$

$$R_{sc} = \frac{P_{sc}}{3I_{sc}^2} \quad (\text{input resistance}) \quad (4.9)$$

$$X_{sc} = \sqrt{Z_{sc}^2 - R_{sc}^2} \quad (\text{input reactance}) \quad (4.10)$$

Details of the Matlab program [1] to determine the induction machine parameters are given in Appendix A.

The machines used in this investigation are 7.5 hp industrial type three-phase squirrel cage induction machines, one with aluminium rotor the other with copper rotor. Each machine has the option of two voltage-current configurations. The specifications of these machines are shown in Table I.

TABLE I  
NAME PLATE DATA AND OTHER FEATURES OF THE INDUCTION MACHINES.

	Unit	Aluminium-rotor	Copper-rotor
Manufacturer		General Electric	Siemens
NEMA Design		B	B
NEMA efficiency	%	89.5	92.4
Rated voltage	V	200/346	208-230/460
Rated current	A	20.9/12	20-19/9.5
Output power	hp	7.5	7.5
Connections		Delta/Wye	Wye/Wye
Number of poles		4	4
Rated speed	rpm	1755	1755
Rated frequency	Hz	60	60
Weight	kg	75.9	90
Diameter of rotor	mm	134.9	129.9
Length of rotor core	mm	135.7	165.8
Length of stator core	mm	135.5	166.0
Inside diameter of stator core	mm	135.16	130.16
Number of stator slots		48	48
Height of rotor bar	mm	25.79	26.6
Width of rotor bar	mm	5.62	5.6
Length of rotor bar	mm	136.8	167.8
Number of rotor conductors		40	40
Conductivity of rotor bar	$\mu\text{S}/\text{mm}$	37.71	59.61

The equivalent circuit parameters of the induction machines derived from the experimental investigations described earlier are calculated and presented in Table II.

TABLE II  
EQUIVALENT CIRCUIT PARAMETERS OF THE INDUCTION MACHINES

	Units	Parameters of Aluminium-rotor IM		Parameters of Copper-rotor IM	
Rated Voltage	V	208	346	208	460
Rated Current	A	20	12	20	9.5
Stator winding connection		Delta	Wye	Wye	Wye
$R_s$	pu	0.0157	0.0231	0.0273	0.0234
$R_r$	pu	0.0568	0.049128	0.0797	0.0578
$X_{ls}$	pu	0.0552	0.0556	0.0902	0.0744
$X_{lr}$	pu	0.0828	0.0835	0.1350	0.1115
$X_m$	pu	2.1795	2.4444	2.9662	2.4555
$R_c$	pu	33.0825	33.9227	43.09	34.961
$P_{rot}$	pu	0.0287	0.0297	0.0270	0.0232

#### 4.5 Saturation Characteristics

It is well known that the voltage build up of an isolated self-excited induction generator is attained through a transient process that reaches equilibrium due to saturation of the magnetic material of the machine. At the state of equilibrium, or steady-state operating condition, the magnetizing reactance of the machine must be equal to the slope of the reactance of the excitation capacitor. The evaluation of the saturation level and the mutual inductance term at a particular operating condition require the accurate representation of the magnetization curve of the induction machine under consideration. In order to model an SEIG accurately, the variation of the magnetizing inductance with current needs to be determined as the magnetizing inductance is the key element for voltage build-up and stability. In this research the saturation curve has been measured with the machine driven at synchronous speed by a shunt connected dc motor. A three phase balanced voltage is applied to the stator terminals. The voltage is gradually increased from 0 to about 120% of rated voltage and the corresponding current at each step is recorded. The saturation curves with the phase voltage as a function of current and



at rated frequency is shown in Fig. 4.5 for aluminium-rotor and Fig. 4.6 for copper-rotor induction machine. The measured points on the saturation characteristics are used to generate continuous curves using a 3<sup>rd</sup> order polynomial curve fitting method. The relationship between the magnetizing inductance and the magnetizing current is calculated from the saturation curve using  $X_m = \frac{|E_m|}{|I_m|}$  and shown in Fig. 4.7. It can be seen that the value of the magnetizing inductance decreases with the increase of magnetizing current owing to magnetic saturation. The magnetizing inductance can be represented by piecewise linearization [4] or by other mathematical functions [5].

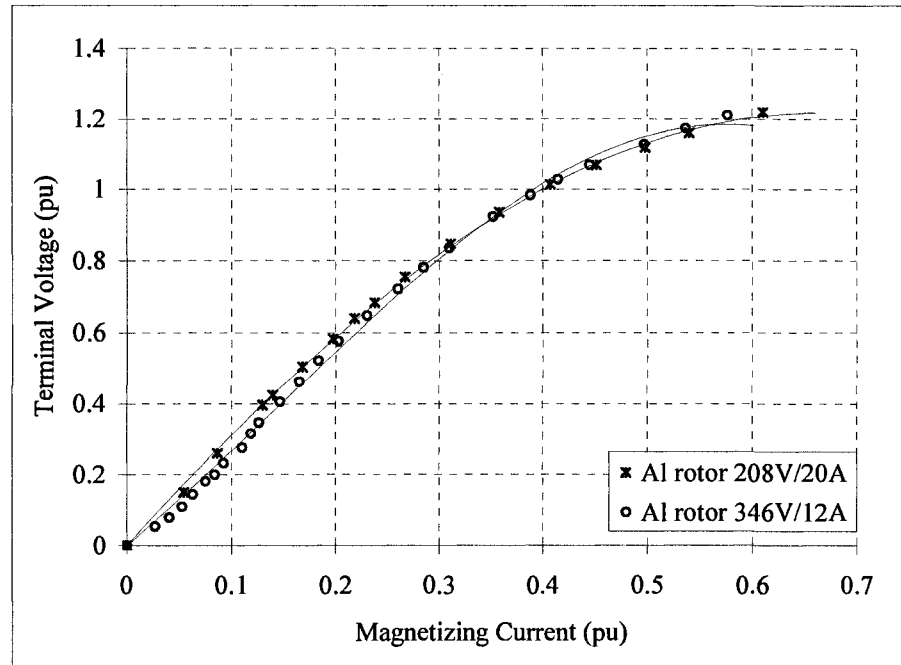


Fig. 4.5. Measured saturation characteristics of the aluminium-rotor induction machine for two voltage configurations.

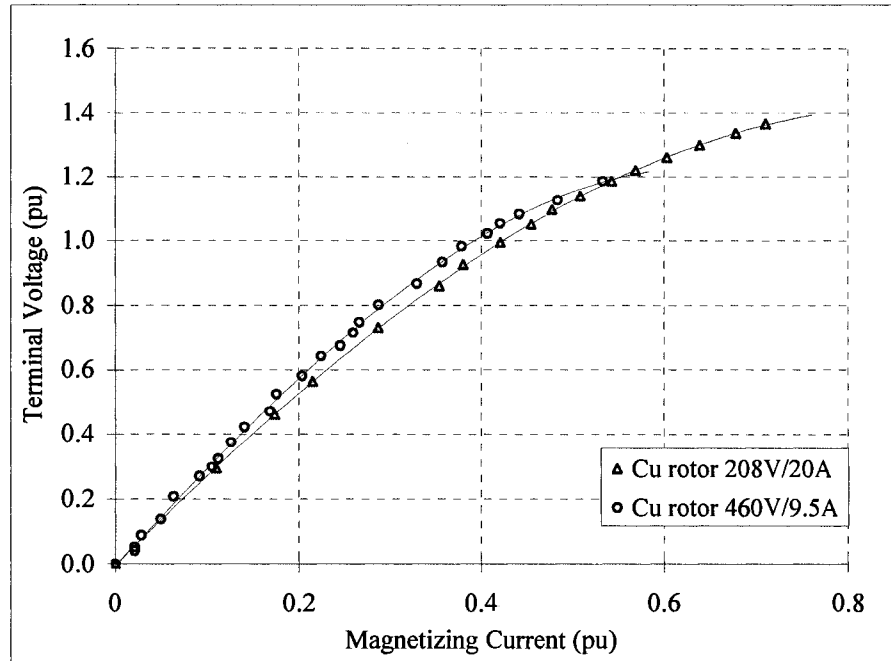


Fig. 4.6. Measured saturation characteristics of copper-rotor induction machine for two voltage configurations.

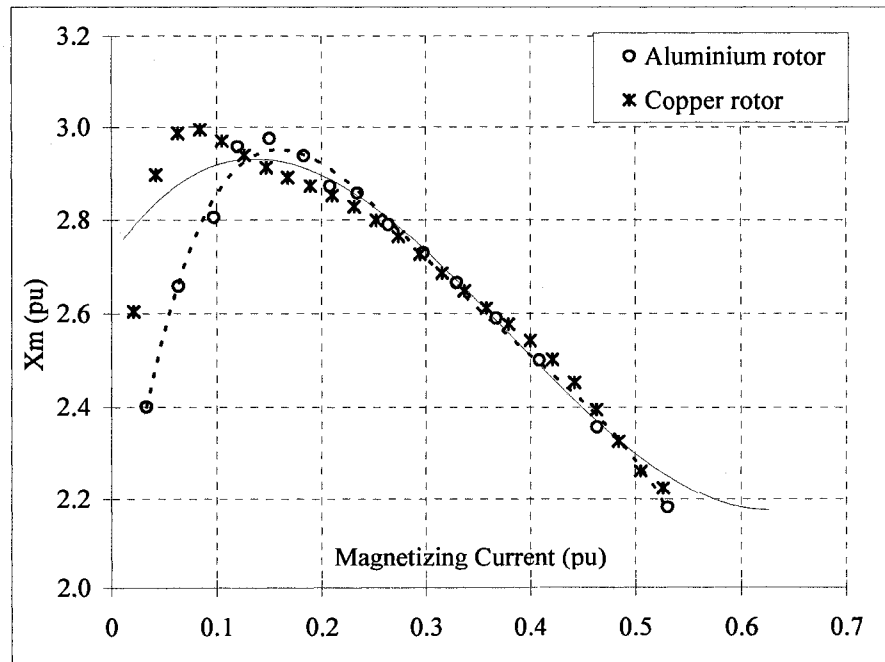


Fig. 4.7. Magnetizing reactance of the induction machines.

## 4.6 Bibliography

- [1] S. J. Chapman, *Electrical Machinery Fundamentals*, 4<sup>th</sup> edition. McGraw-Hill, New York, 2004.
- [2] M.S. Sharma, *Electric Machines Steady-State Theory and Dynamic Performance*, 2<sup>nd</sup> ed. PWS Publishing Company, Boston, 1994.
- [3] *IEEE Standard Test Procedure for Polyphase Induction Motors and Generators*, IEEE Std. 112-2004, IEEE Power Engineering Society, New York, USA, Nov. 2004.
- [4] T.F. Chan, "Capacitance Requirements of Self-Excited Induction Generators," *IEEE Transactions on Energy Conversion*, Vol. 8, No. 2, pp 304-311, Jun. 1993.
- [5] —, "Steady-State Analysis of Self-Excited Induction Generators," *IEEE Transactions on Energy Conversion*, Vol. 9, No. 2, pp 288-296, Jun. 1994.

## **5 NUMERICAL AND EXPERIMENTAL INVESTIGATION OF SEIGS WITH ALUMINIUM ROTOR AND COPPER ROTOR**

### **5.1 Physical Features of Aluminium-Rotor and Copper-Rotor SEIGs**

Aluminium die-cast rotors have been manufactured since 1930s. The die-cast technology has been the standard for motor manufacturers for a long time. Even though the benefits of copper have been appreciated by the motor manufacturers as well as researchers but the higher cost of copper and manufacturing difficulties in producing large number of integral horsepower motors has, until recently, prevented its adoption [1].

High melting point and resulting high cost for die-casting was for long a major barrier for copper-rotor induction machines. Several technological breakthroughs in copper die-casting have been recently achieved removing the barrier and clearing the way for industrial production [2].

Copper has higher electrical conductivity and higher thermal capacity per unit volume than aluminium leading to lower copper losses and lower temperature rise during operation. This improves overload capacity for a limited operation time and mitigates the effects of higher start up current. Direct substitution of rotor material by copper achieved a reduction of the total losses by 14% [3]. In test data for motors where copper has simply been substituted for aluminium with no change in design, the starting and locked rotor torque is reduced [1], [4].

Compared to aluminium, copper provides a lower coefficient of expansion, higher tensile strength and higher conductivity. Aluminium will creep and move approximately 33% more than copper. This large movement can eventually lead to fatigue in motor material due to thermal expansion and contraction. Since copper has a higher thermal capacity per unit volume compared to aluminium, it would lead to a lower temperature rise during operation. This in turn would lead to an increase in machine life.

Being three times stronger than aluminium, copper rotors will be able to withstand high centrifugal forces and repeated hammering of the current induced forces during each start. Copper can better withstand thermal cycling over the total life cycle of the machine.

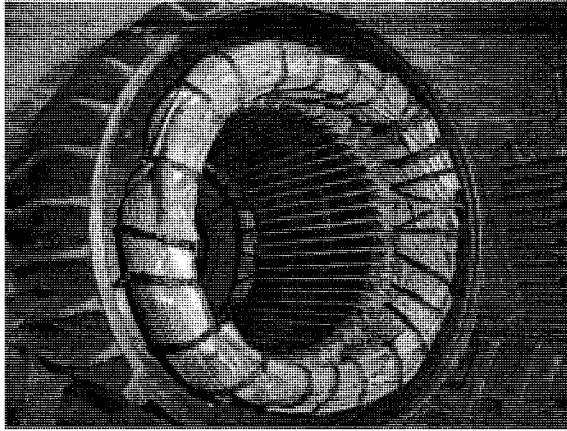
TABLE III  
PHYSICAL PROPERTIES OF ALUMINIUM AND COPPER

	Units	Aluminium	Copper
Electrical conductivity	$\mu\text{S}/\text{mm}$	37.71	59.61
Thermal capacity	$\text{kJ}/\text{l-K}$	2.43	3.44
Density	$\text{g}/\text{cm}^3$	2.70	8.91
Thermal conductivity at 20°C	$\text{W}/\text{m-K}$	230	397
Tensile strength	$\text{N}/\text{mm}^2$	50-60	200-250
Melting point	°C	660	1083
Coefficient of thermal expansion	$/^\circ\text{C}$	$22.2 \times 10^{-6}$	$16.5 \times 10^{-6}$
Specific heat	$\text{J}/\text{kg-K}$	900	385

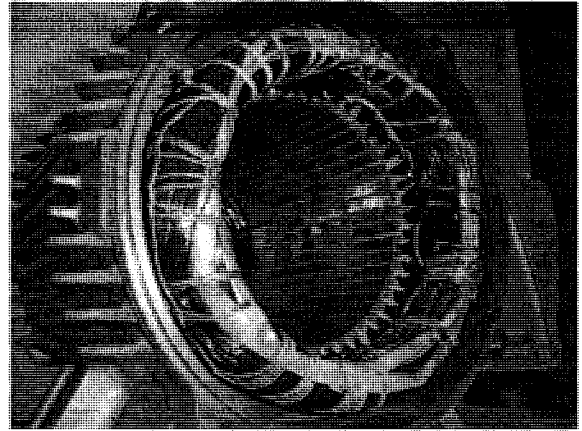
Aluminium has 35% higher temperature rise than copper for the same kW loss. A brief comparison of the physical properties of aluminium and copper are given in Table III.

As mentioned earlier, the two 7.5 hp industrial type induction machines one with conventional aluminium-rotor, 346V/12A and the other with copper-rotor 460V/9.5A, both wye connected as shown in Fig. 5.1 are studied in this research. Table I in the previous chapter shows the physical features of the two machines. It may be noted that these two machines are manufactured by two different companies. Even though the designs are consistent with NEMA guidelines, there are subtle dissimilarities in many areas. As can be seen, the aluminium cage rotor is skewed with the fan blades integrally cast on the end rings while the copper cage rotor is plain and without such blades attached to the end rings. The copper-rotor motor has comparatively longer core that lowers flux density while increasing cooling capacity and reducing magnetic and stray losses. Despite such subtle dissimilarities between these machines, a detailed qualitative performance analysis has been carried out.

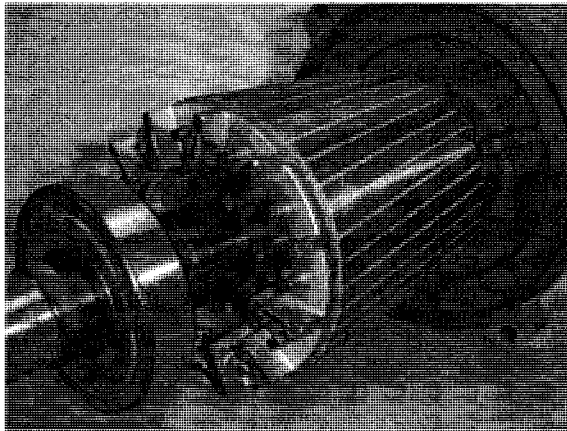
The machine equivalent circuit parameters are determined from the standard no load, dc and blocked rotor tests outlined in [5] and are shown in Table II in the previous chapter. The torque-speed characteristics of these two machines are calculated using these equivalent circuit parameters and are shown in Fig. 5.2(a) – (c). It can be seen from this figure that the starting and pull-out torques of the copper-rotor machine are relatively lower than the aluminium-rotor machine for the same rating.



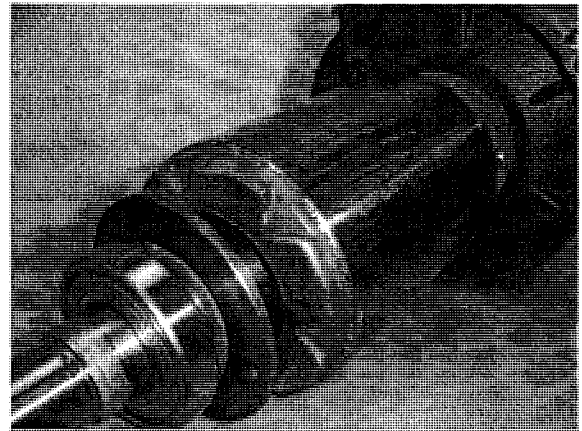
(a)



(b)

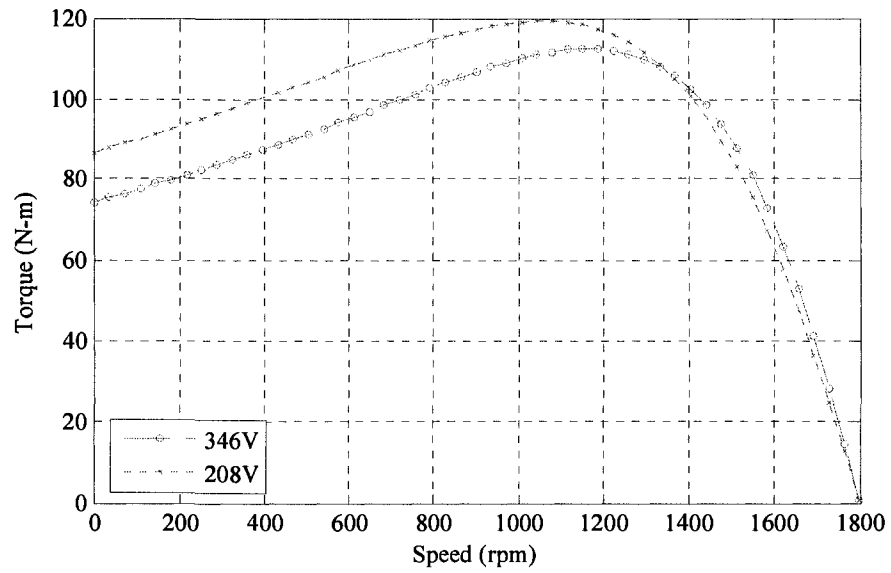


(c)

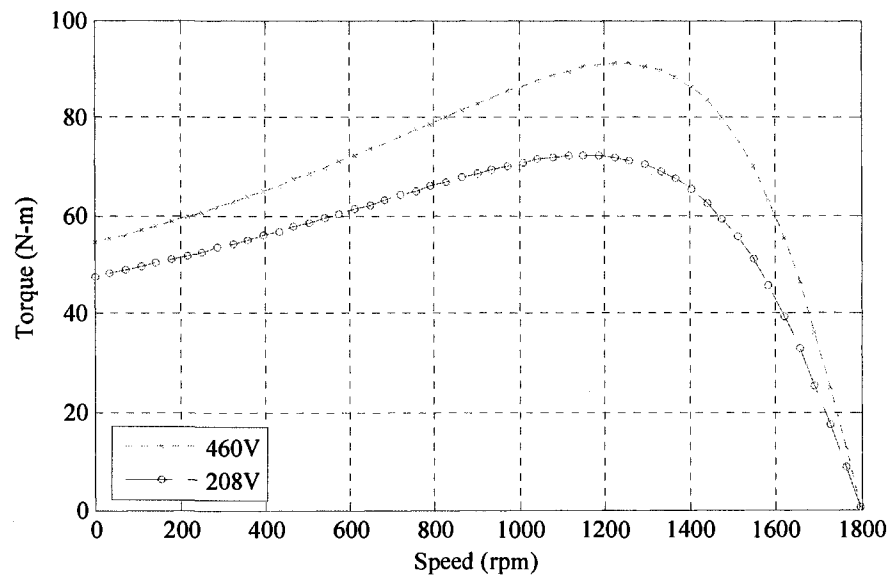


(d)

Fig. 5.1. Stators and rotors of the two 7.5 hp induction machines used in the investigations.  
(a) Stator of aluminum-rotor IM. (b) Stator of copper-rotor IM.  
(c) Aluminium rotor. (d) Copper rotor.



(a)



(b)

**Fig. 5.2 Torque-Speed characteristics of the induction machines.**  
**(a) Aluminium- rotor machine with 346V/12A and 208V/20A connections.**  
**(b) Copper-rotor machine with 460V/9.5A and 208V/20A connections.**

## 5.2 Voltage Build-up under Open Circuit Condition Ignoring Skin Effect

The dynamic model of the SEIG is helpful to analyze its transient and steady-state characteristics. The simulation of an SEIG gives an insight about its performance under various operating conditions. In order to represent the dynamic characteristic to study the performance, a mathematical model has been developed and presented in the previous chapter.

In the modelling of an SEIG, it is important that the variation of the magnetizing inductance is taken into consideration accurately, because it plays a significant role in the dynamics of voltage build up and stability. The saturation characteristics and the magnetizing inductance calculation are described in Section 4.4.

The generators used in this investigation are three phase 7.5 horse power squirrel cage induction machines whose parameters are measured and given in Table II. The saturation characteristics in actual quantities for both the machines are reproduced and given in Fig 5.3. It can be observed that the magnetizing curves of both the machines are similar in appearance, however the slope and saturation area of the mmf curve of the copper-rotor

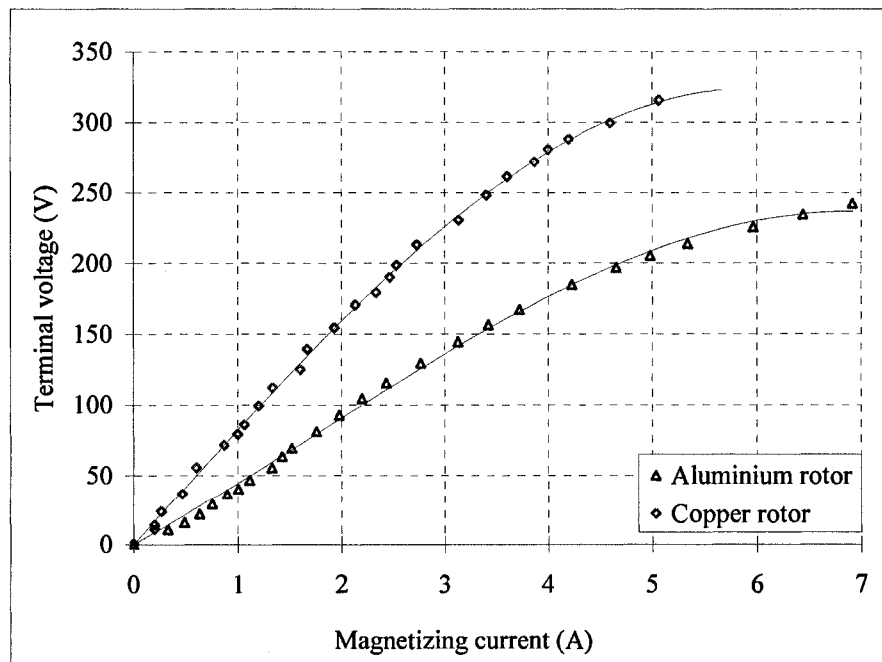


Fig. 5.3. Saturation characteristics of the two 7.5 hp SEIGs.



induction machine is more steep and accentuated than that of the aluminium-rotor one. This can be attributed to the air gap and susceptibilities of the rotor materials.

Simulations are carried out using d-q axis equivalent circuit and 4<sup>th</sup>-order Runge-Kutta method. The d-q reference frame is a well established method of analysing three phase machines and the Runge-Kutta method is a very popular means of numerical solution for higher order differential equations. For open-circuit condition, the model is developed using higher order differential equations and solved using a Matlab program.

In order to take the effect of magnetic saturation of the machines into account the saturation characteristics of the induction generator is determined from standard laboratory tests. The nonlinear relationship between the magnetizing inductance  $X_m$  and the magnetizing current  $i_m$  in actual quantities for the aluminium-rotor and the copper-rotor SEIGs are derived from its respective magnetizing characteristics and given in Fig 5.4 and Fig. 5.5 respectively. The nonlinear nature of the relationship can be expressed in several ways. Some authors have proposed piece-wise linearization [6][7], or by using higher order polynomials [8], [9] or a continuous function[10]-[12]. In this research a continuous function to express mathematically the relationship between magnetizing inductance and magnetizing current is proposed using curve fitting technique.

$$X_m = \alpha(\arctan(\beta * i_m - \gamma) + \delta) / i_m \quad (5.1)$$

where the coefficients  $\alpha$ ,  $\beta$ ,  $\gamma$  and  $\delta$  are determined from nonlinear least squares or nonlinear least-squares regression method using Matlab program.

At each integration step of the Matlab program, the magnetizing current is calculated from the relation

$$i_m = \sqrt{(i_{qs} + i_{qr})^2 + (i_{ds} + i_{dr})^2} \quad (5.2)$$

From the calculated value of  $i_m$  the value of  $X_m$  is derived from (5.1) and updated at each integration stage in the main Matlab routine.

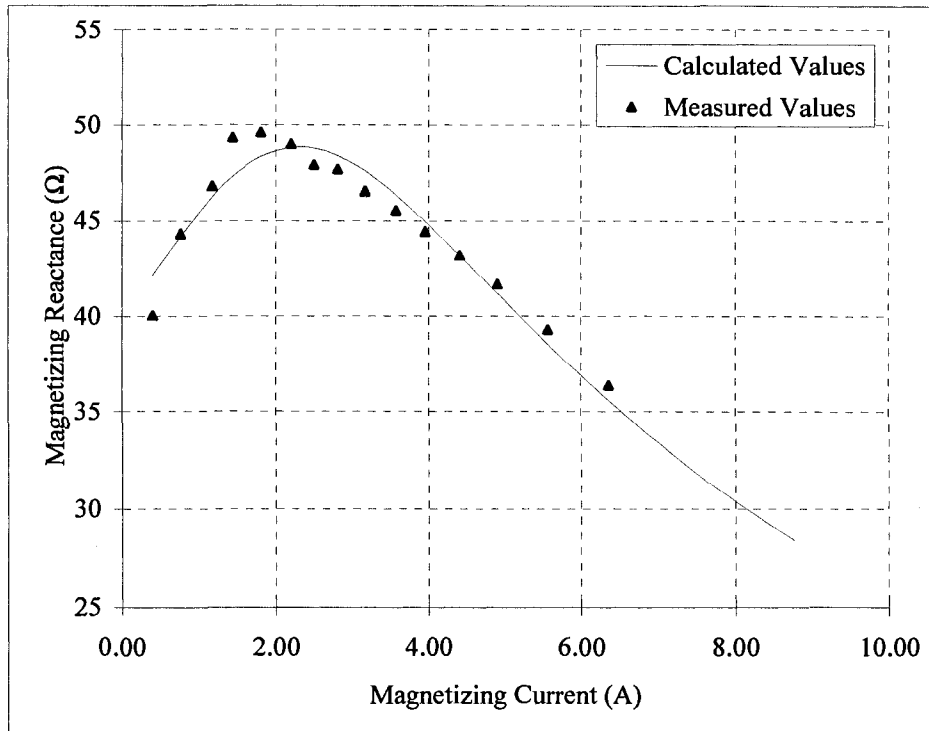


Fig. 5.4. Magnetizing reactance of 7.5 hp aluminium-rotor SEIG.

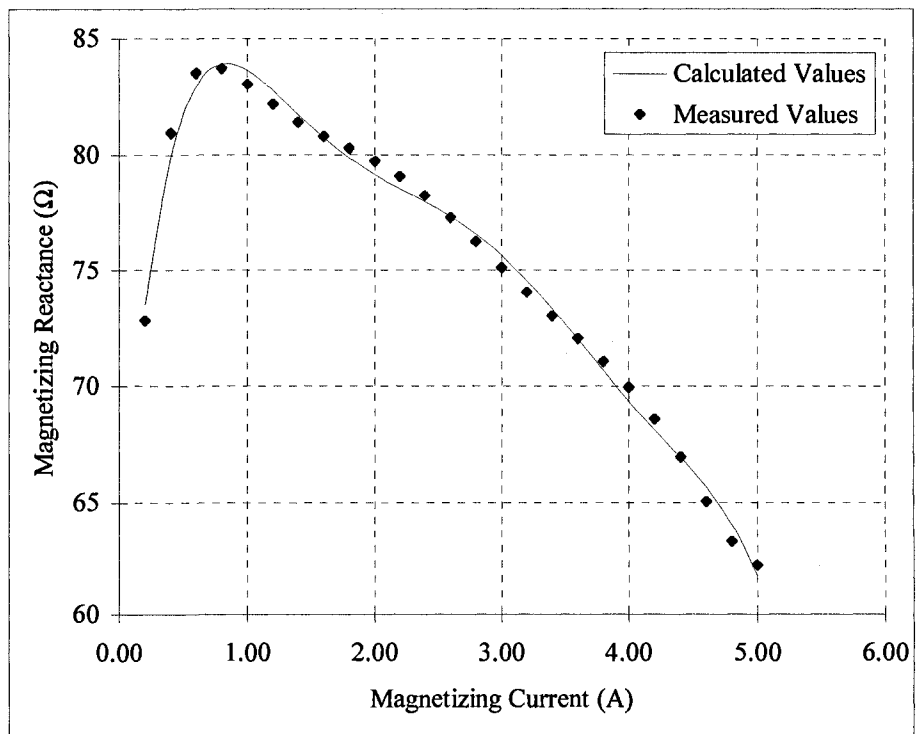


Fig. 5.5. Magnetizing inductance of 7.5 hp copper-rotor SEIG.

The voltage and current build-up in  $d$ - $q$  reference frame for aluminium-rotor induction generator is shown in Figs. 5.6 and 5.7 respectively.

The phase voltages and currents are calculated using the inverse of the classical transformation matrix  $T$ , where

$$T = \frac{2}{3} \begin{bmatrix} \cos(\omega t) & \cos(\omega t - \frac{2\pi}{3}) & \cos(\omega t + \frac{2\pi}{3}) \\ \sin(\omega t) & \sin(\omega t - \frac{2\pi}{3}) & \sin(\omega t + \frac{2\pi}{3}) \\ \frac{1}{2} & \frac{1}{2} & \frac{1}{2} \end{bmatrix} \quad (5.3)$$

and  $\omega$  is the speed of the rotating reference frame in the  $d$ - $q$  axes.

The voltage and current build-up in actual  $abc$  quantities for aluminium-rotor is given in Fig. 5.8.

For copper-rotor SEIG the same features are shown in Fig. 5.9 – Fig. 5.11.

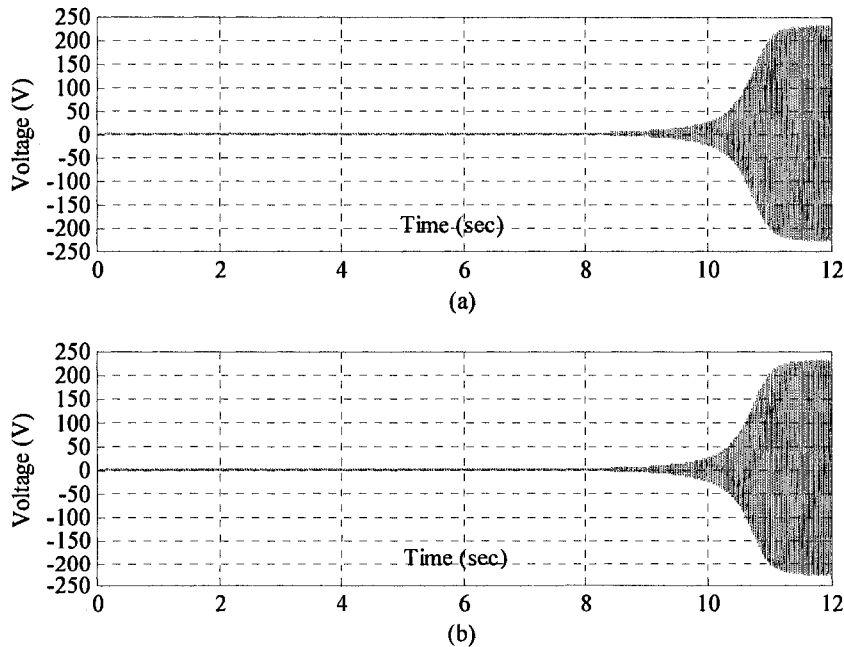


Fig 5.6. Stator voltage build up process of the aluminium-rotor SEIG under no load condition. (a)  $V_{qs}$ . (b)  $V_{ds}$ .

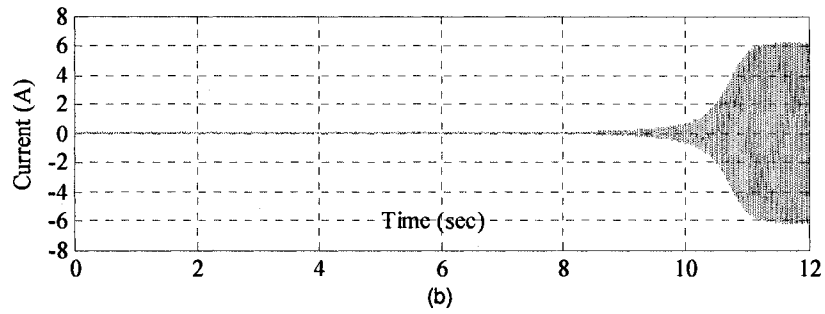
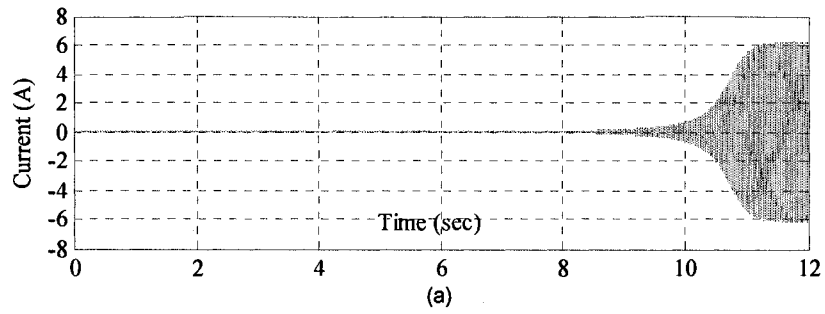


Fig. 5.7. Stator current build up process of the aluminium-rotor SEIG under no load condition. (a)  $I_{qs}$ . (b)  $I_{ds}$ .

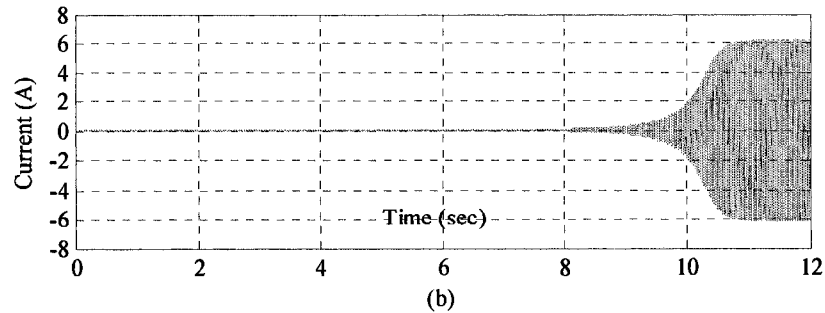
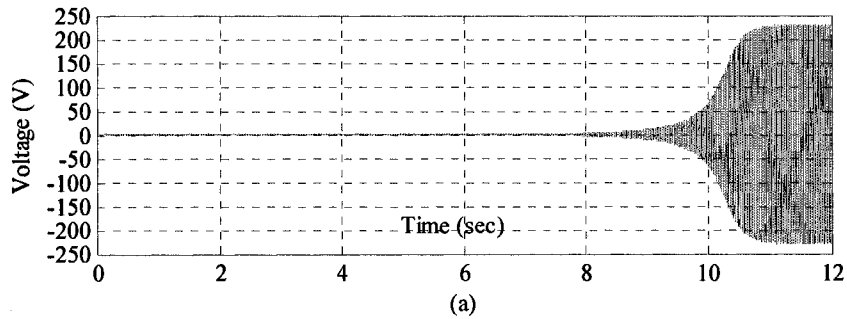


Fig. 5.8. Stator voltage and current build up process of the aluminium-rotor SEIG under no load condition. (a)  $V_a$ . (b)  $I_a$ .

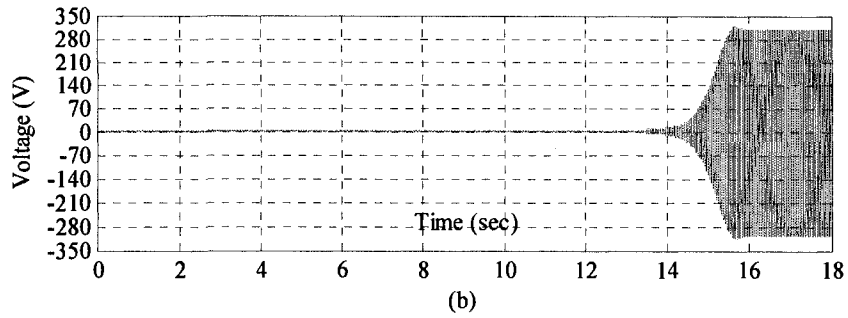
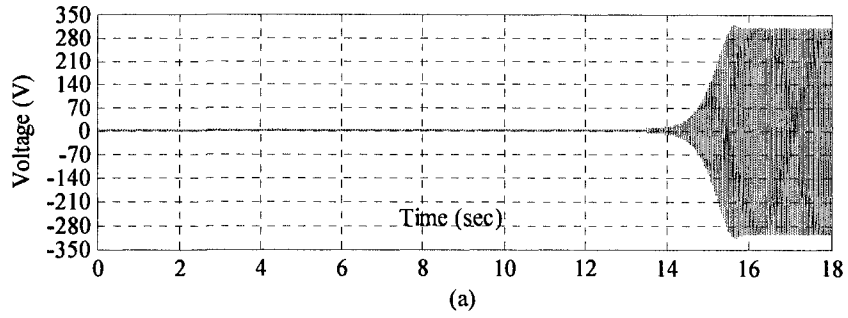


Fig 5.9. Stator voltage build up process of the copper-rotor SEIG under no load condition. (a)  $V_{qs}$ . (b)  $V_{ds}$ .

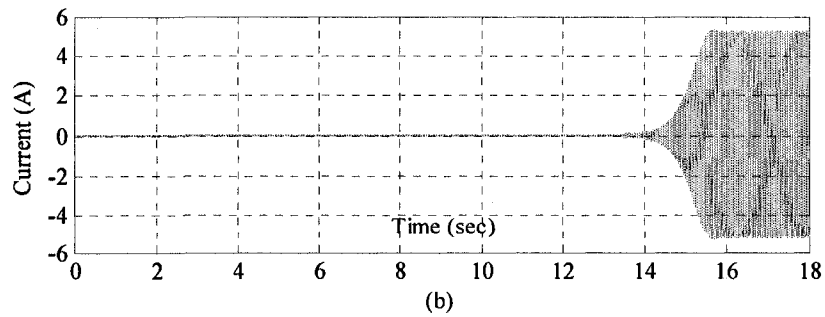
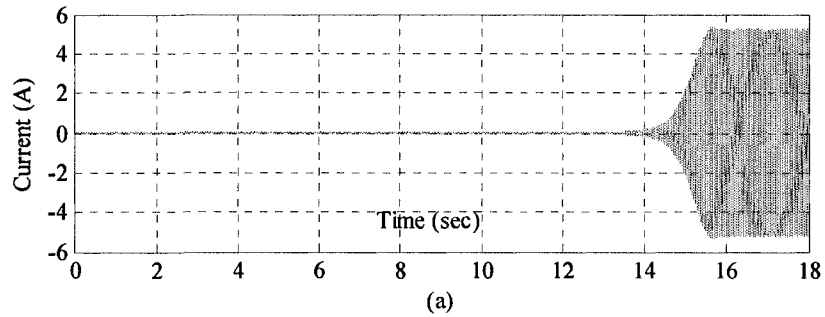


Fig. 5.10. Stator current build up process of the copper-rotor SEIG under no load condition. (a)  $I_{qs}$ . (b)  $I_{ds}$ .

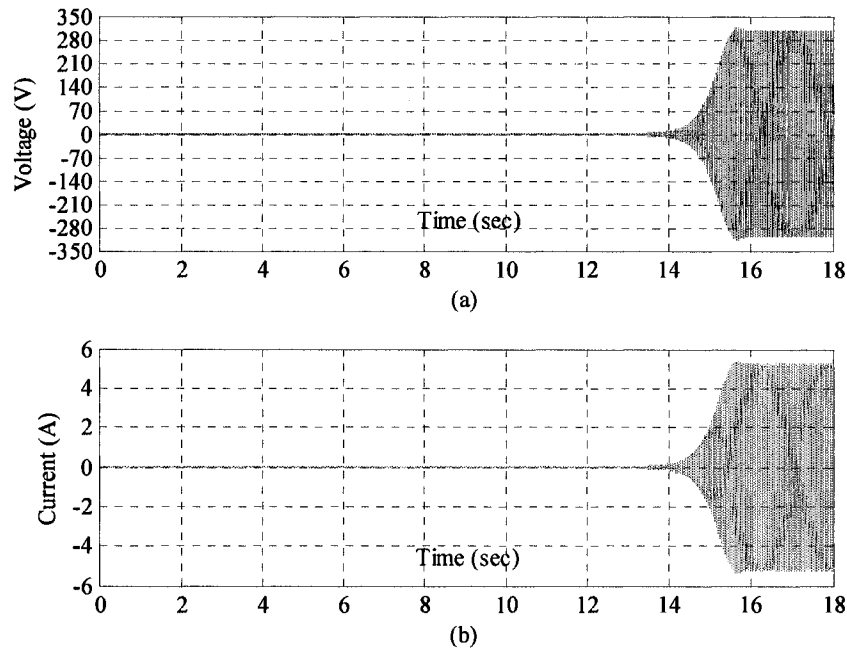


Fig 5.11. Stator voltage and current build up process of the copper-rotor SEIG under no load condition. (a)  $V_a$ . (b)  $I_a$

### 5.3 Simulation and Experimental Results Considering Skin Effect

As discussed earlier, in a conductor, if the current is dc, the current distribution is uniform over the entire cross section. But if the current is ac, then the current distribution will not be uniform because of skin effect.

When skin effect is taken into account in the mathematical analysis of the SEIGs, a sub-routine is incorporated in the main program. The value of the stator frequency is predetermined using this sub-routine, making use of the numerical expressions (3.44) and (3.45). Then by incorporating (3.46) and (3.47) in the machine model, the rotor resistance and inductance values are updated at each integration step. The flow chart to simulate the performance of the SEIGs is illustrated in Fig. 5.12.

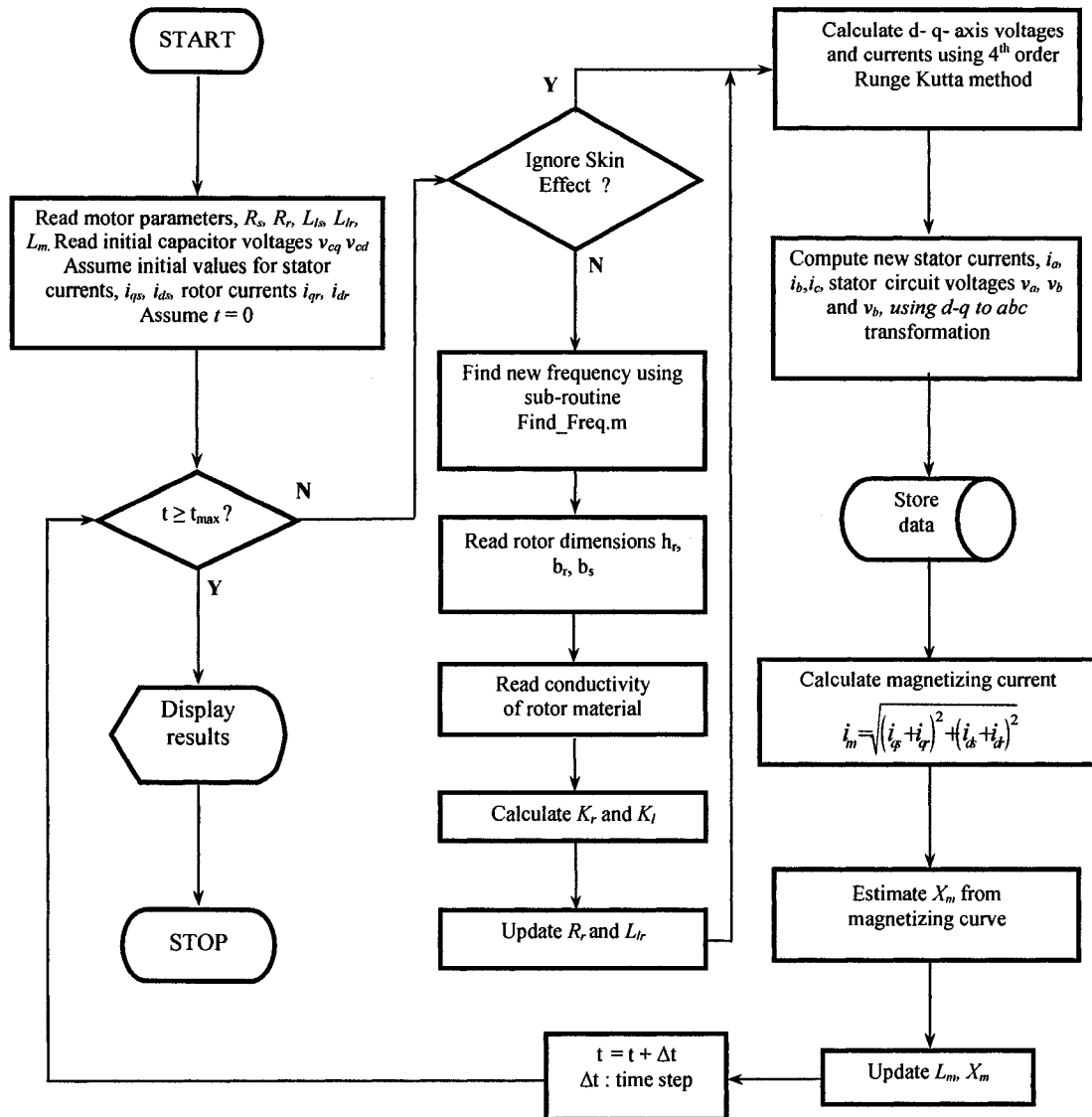


Fig. 5.12. Flowchart to calculate stator voltages and currents taking skin effect into account.

### 5.3.1 Experimental set-up

In order to verify the accuracy of the models of the SEIGs, experiments are carried out in the laboratory with the two 7.5 hp induction machines. Each SEIG set consists of a DC motor working as the prime mover directly coupled to the induction machine. A three-phase wye connected bank of industrial type capacitors is hooked to the terminals of the SEIG through an electrical switch. The load which consists of three-phase wye

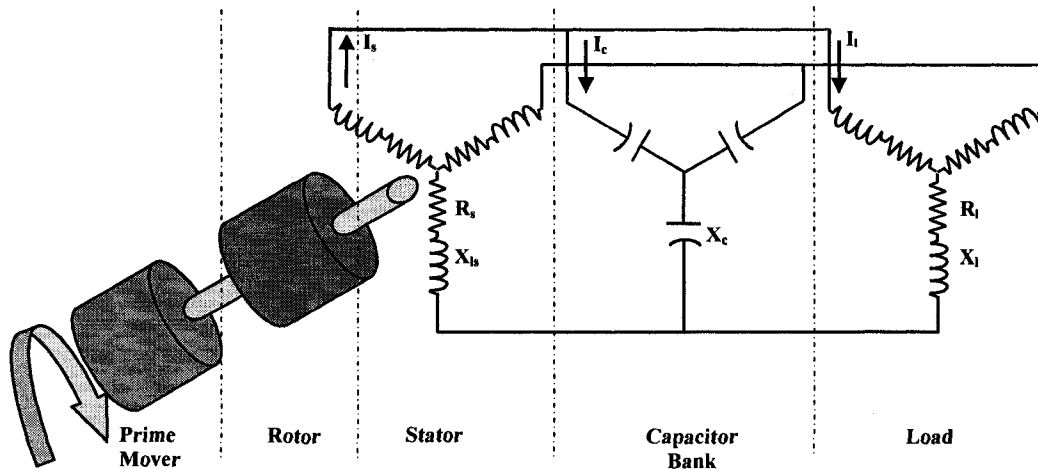


Fig. 5.13. Schematic diagram of the experimental set-up of the SEIG.

connected resistors is also connected through a switch. For  $RL$  load three-phase wye-connected resistors in series with inductances of appropriate values are used. The schematic diagram of experimental set-up is shown in Fig. 5.13. The actual laboratory set-up is presented in Figs. 5.14 – Fig. 5.16. The voltage and current waveforms and other electrical parameters are obtained from experimental set-up using a Tektronix 1002 Digital Storage Oscilloscope and Fluke 434 Power Quality Analyzer (PQA). Three current transformers with a ratio of 5:1 have been used with the PQA for current measurements.

### 5.3.2 Open-circuit condition

In order to verify the relationship between stator frequency and rotor speed experiments are performed by building up the terminal voltage with the help of the excitation capacitors. Then by varying the speed of the prime mover and measuring the frequency the relationship between the rotor speed and terminal frequency is obtained. The experimental values and simulation results are given in Fig. 5.17. The process of voltage build-up has been calculated both by ignoring and also including skin effect. It is



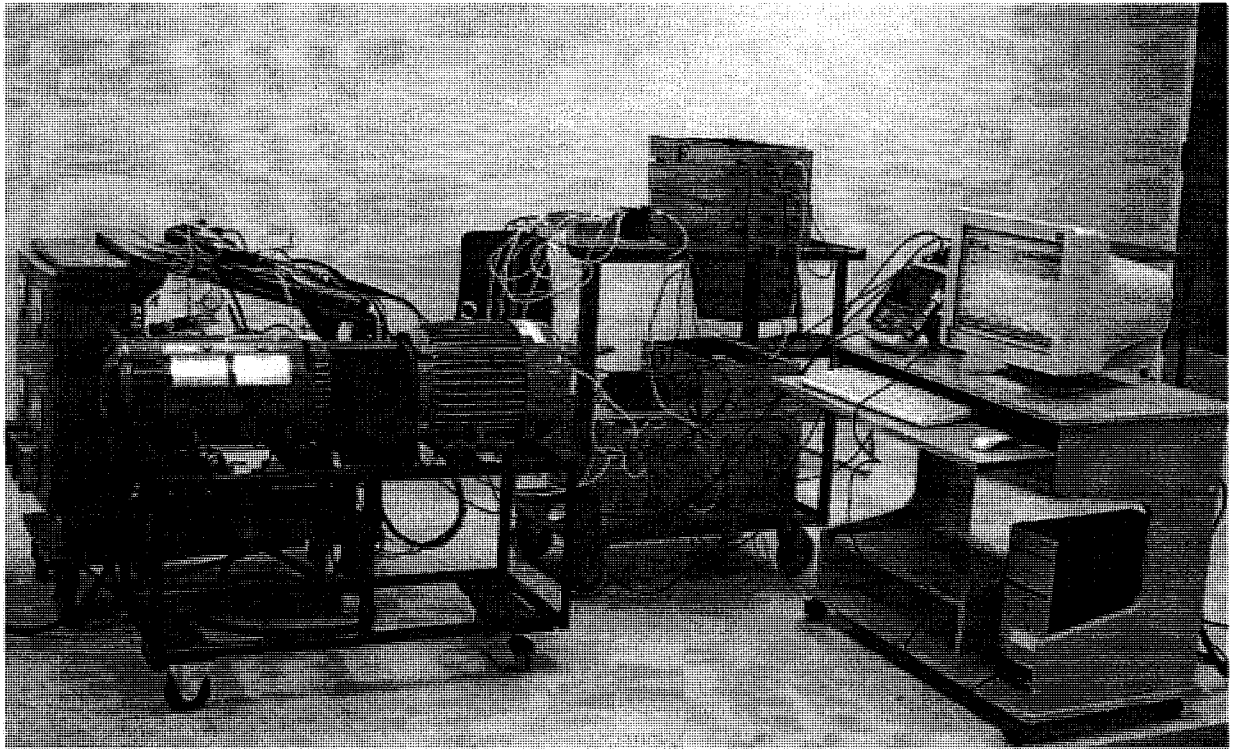


Fig. 5.14. Experimental set-up of the SEIG.  
A: Power supply. B: DC motor (Prime mover). C: Induction generator.  
D: Capacitor bank. E: Electrical load. F: Measuring instrument and monitoring system

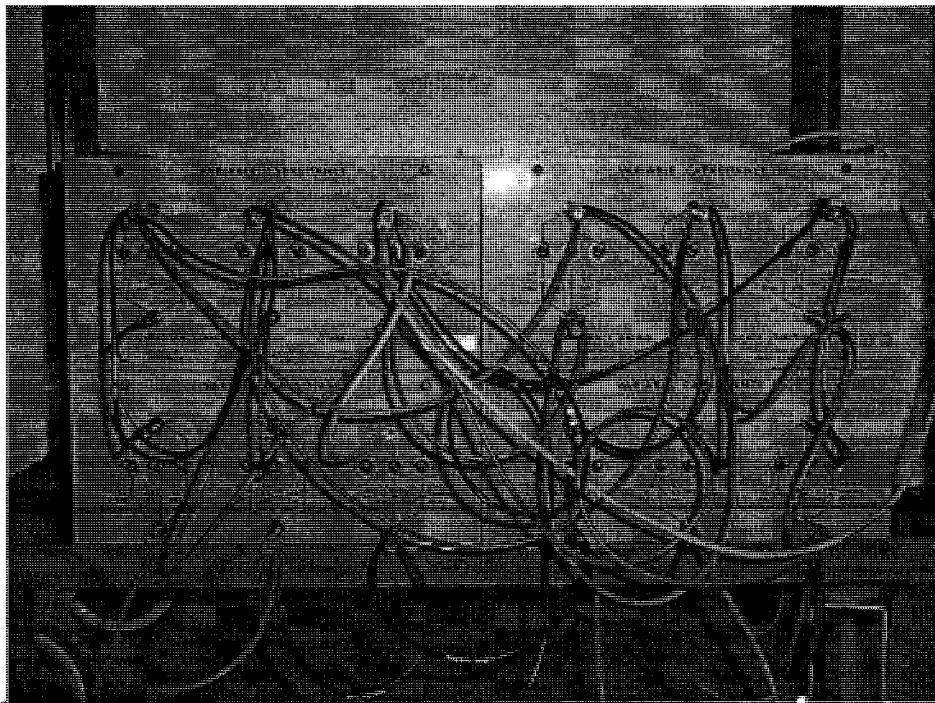


Fig. 5.15. Experimental set-up of the three-phase capacitor bank.

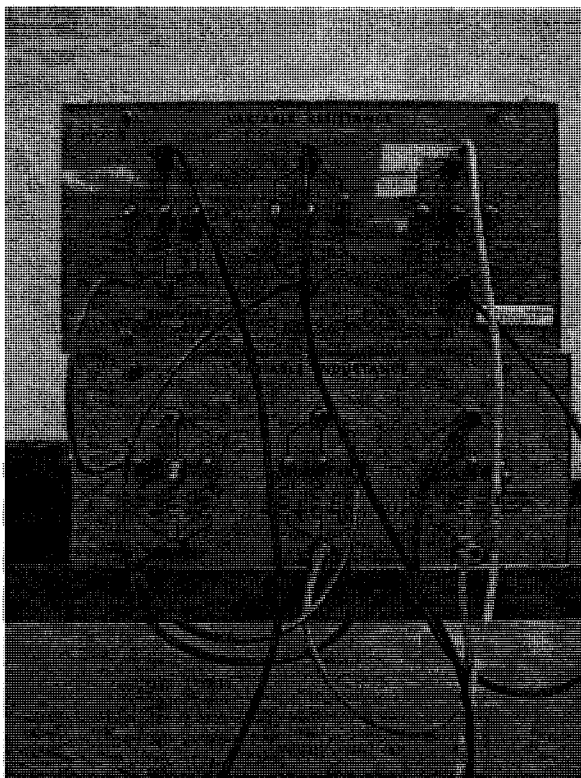


Fig. 5.16. Experimental set-up of the three phase  $RL$  load.

seen that there is a considerable difference in the build-up time in each case. The time taken for the voltage to reach the steady state level in case of the model that ignores skin effect is higher than by the model that considers it. This is true for both aluminium- and copper-rotor SEIGs. The results are presented in Figs 5.18 and Fig. 5.21 for aluminium- and copper-rotor machines respectively. The build-up time is measured using Tektronix Digital Oscilloscope (Fig. 5.19 and Fig 5.22) and also by Fluke Power Quality Analyser (Fig. 5.20 and Fig 5.23). In both cases the results calculated by the proposed model that considers skin effect are consistent with the measured values.

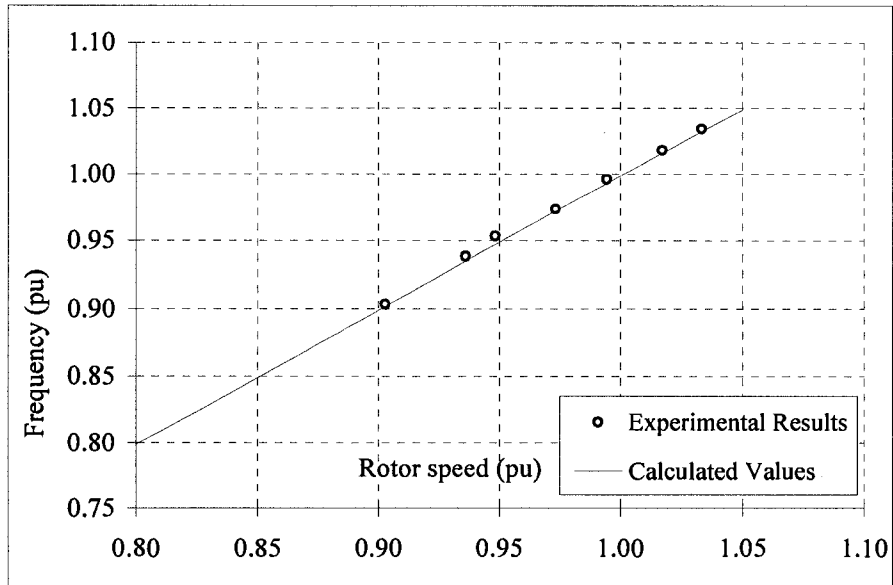


Fig. 5.17. Variation of frequency with rotor speed for the aluminium-rotor SEIG.

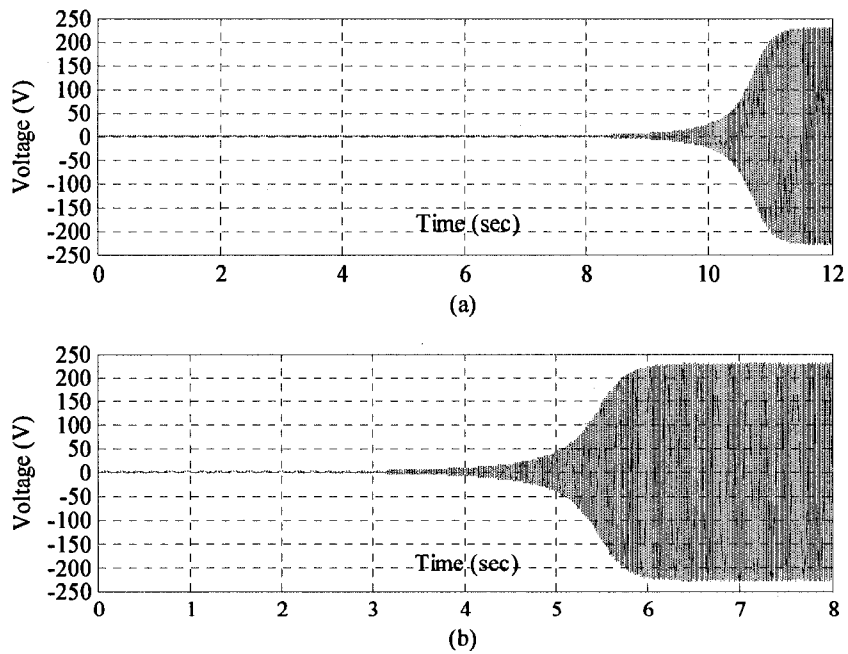


Fig. 5.18. Stator phase 'a' voltage build-up process under no load condition for aluminium-rotor SEIG (a) ignoring and (b) considering skin effect.

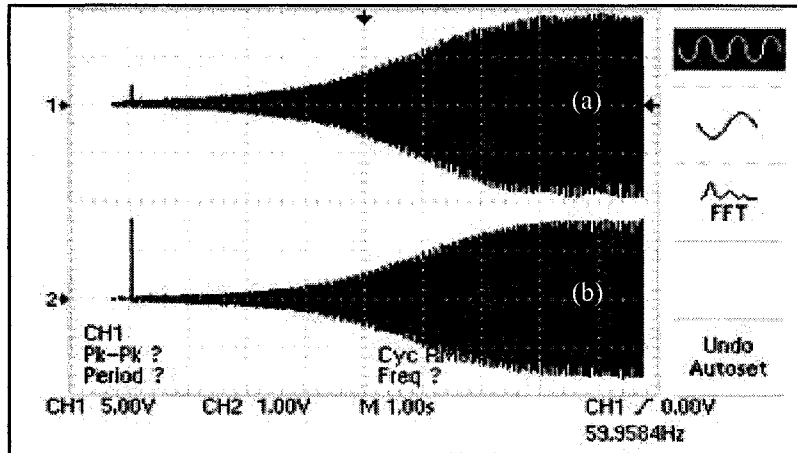


Fig. 5.19. Experimental results of stator voltage and current build-up for aluminum-rotor SEIG using Tektronix oscilloscope. (a) Voltage. (b) Current.

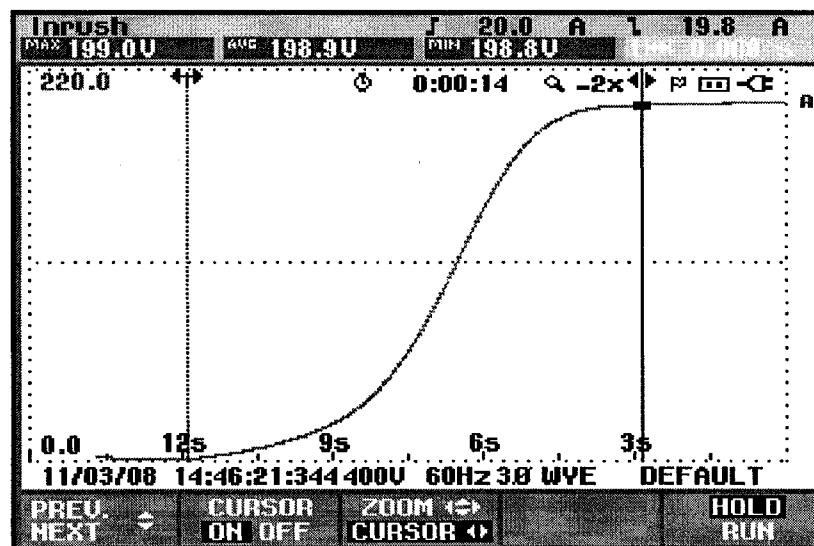


Fig. 5.20. Experimental results of stator phase 'a' voltage build-up for aluminum-rotor SEIG using Fluke Power Quality Analyzer.

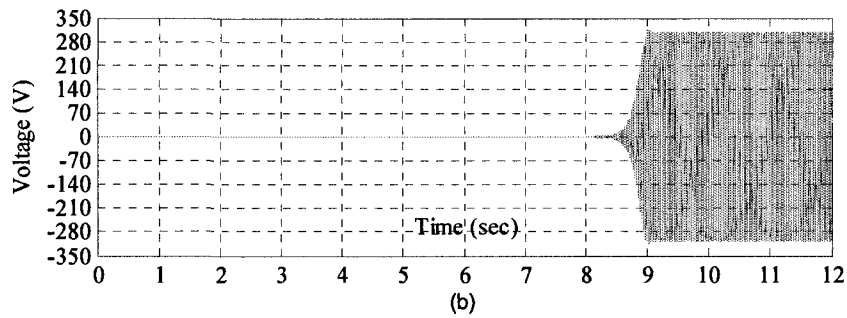
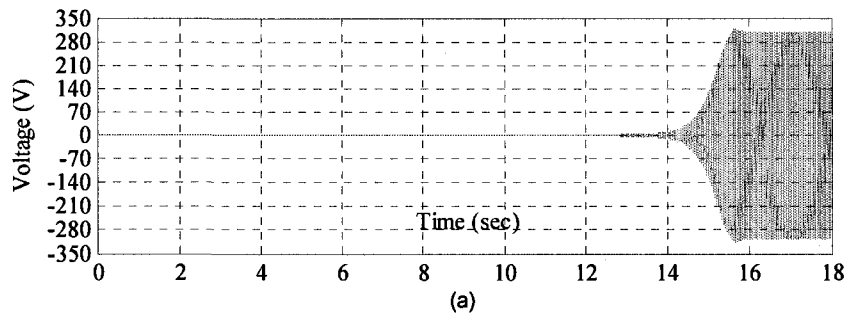


Fig. 5.21. Stator voltage build-up process under no load condition for copper-rotor SEIG (a) ignoring and (b) considering skin effect.

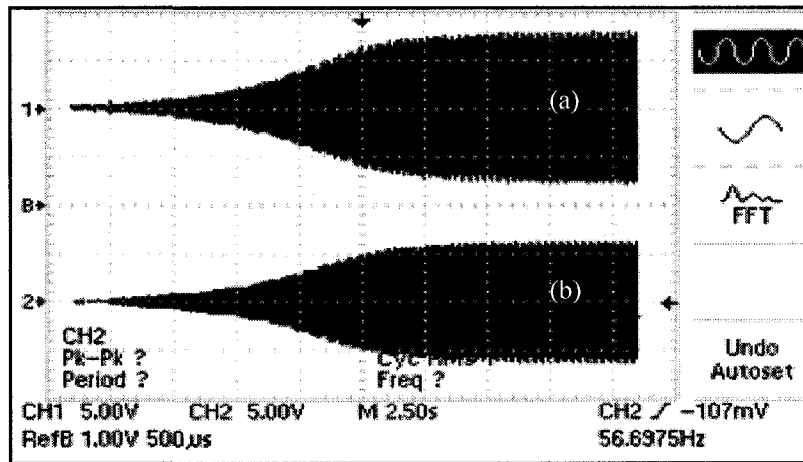


Fig. 5.22. Experimental results of stator voltage and current build-up for copper-rotor SEIG using Tektronix oscilloscope. (a) Voltage. (b) Current.

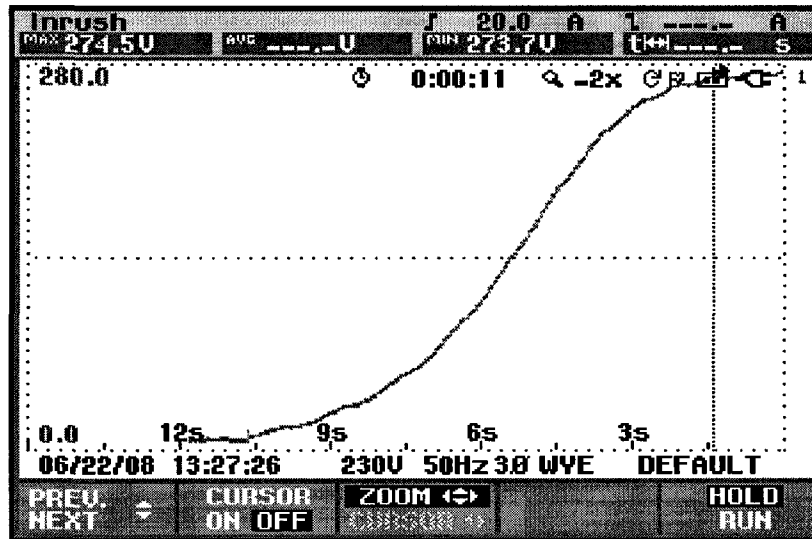
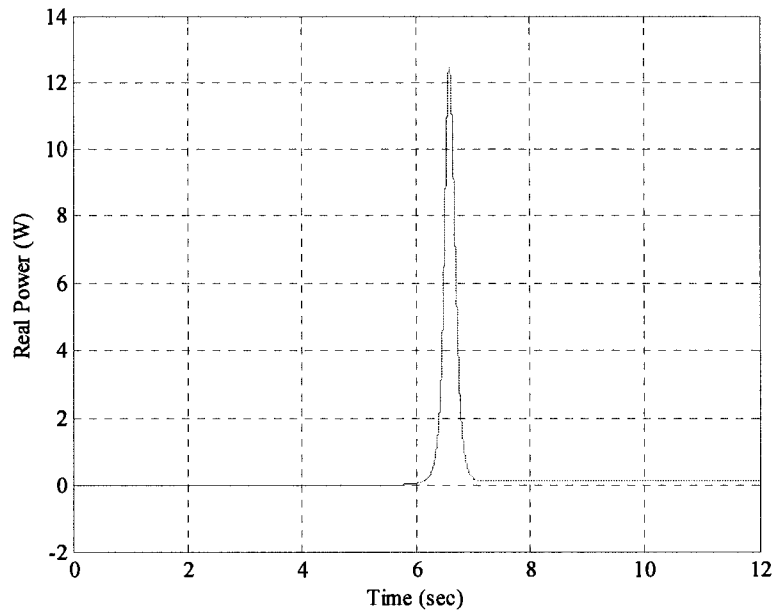
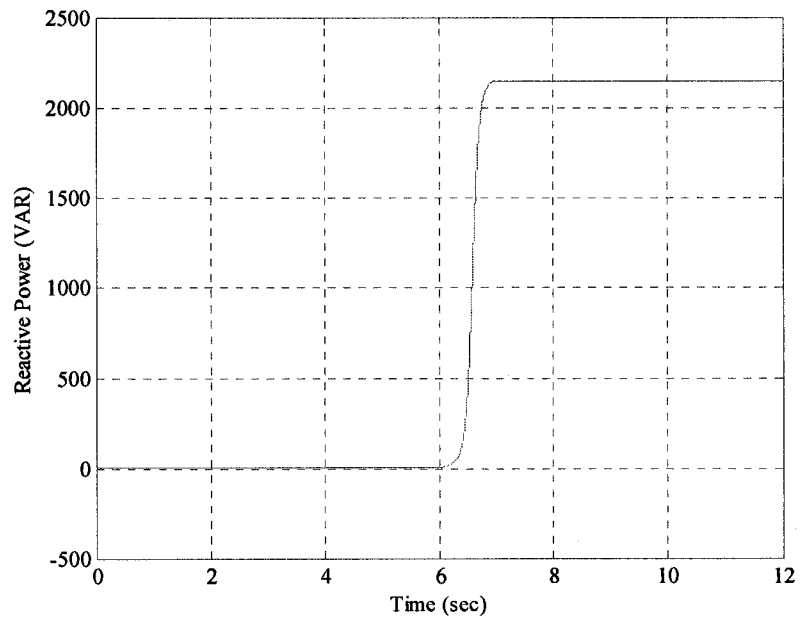


Fig. 5.23. Experimental results of stator voltage build-up for copper-rotor SEIG using Fluke Power Quality Analyzer.

The calculated real and reactive power output using the proposed model by taking skin effect into account are shown in Fig. 5.24 and Fig. 5.26 while the measured values are shown in Fig. 5.25 and Fig. 5.27 for aluminium- and copper-rotor SEIGs respectively.

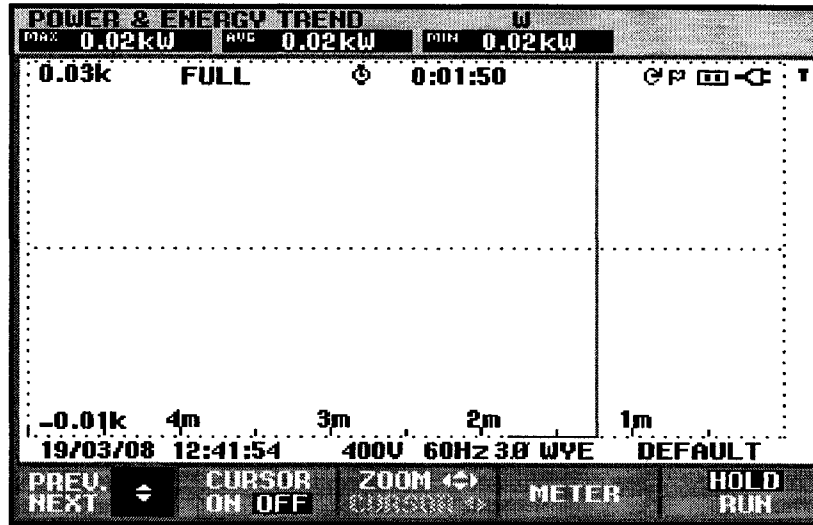


(a)

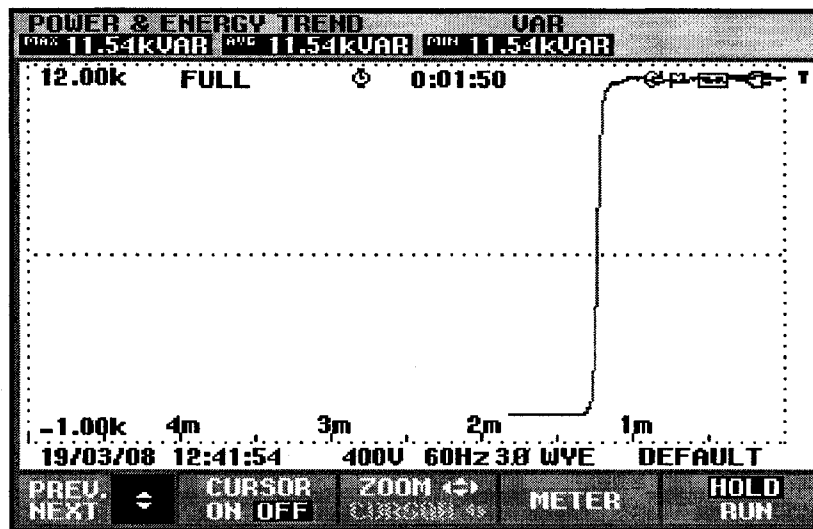


(b)

Fig. 5.24. Calculated real and reactive power under no load conditions for aluminium rotor SEIG. (a) Real power. (b) Reactive power.



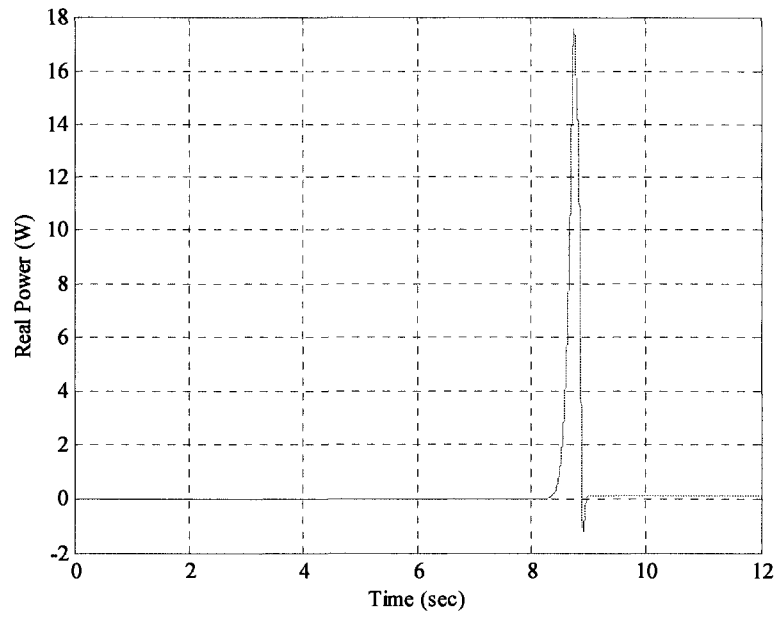
(a)



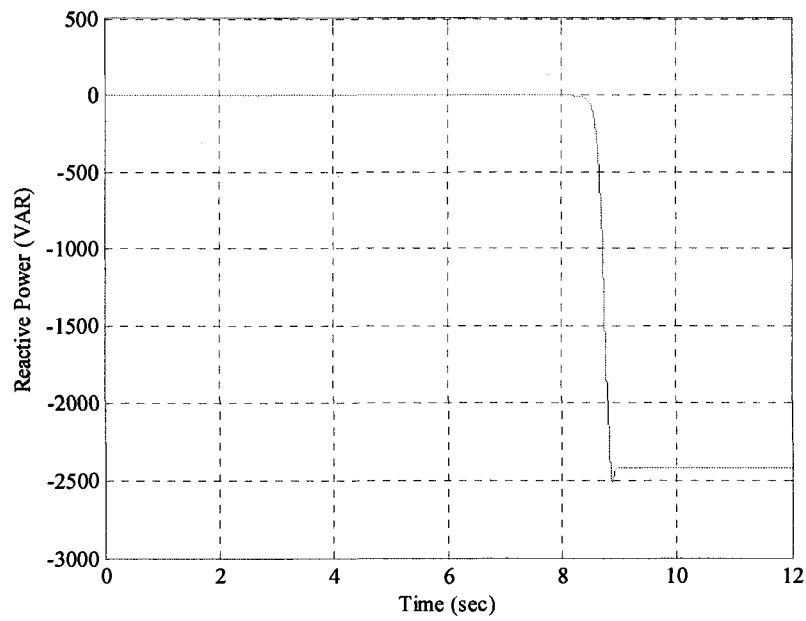
(b)

Fig. 5.25. Measured real and reactive power under no load condition for aluminium-rotor SEIG (CT ratio 5:1). (a) Real power. (b) Reactive power.



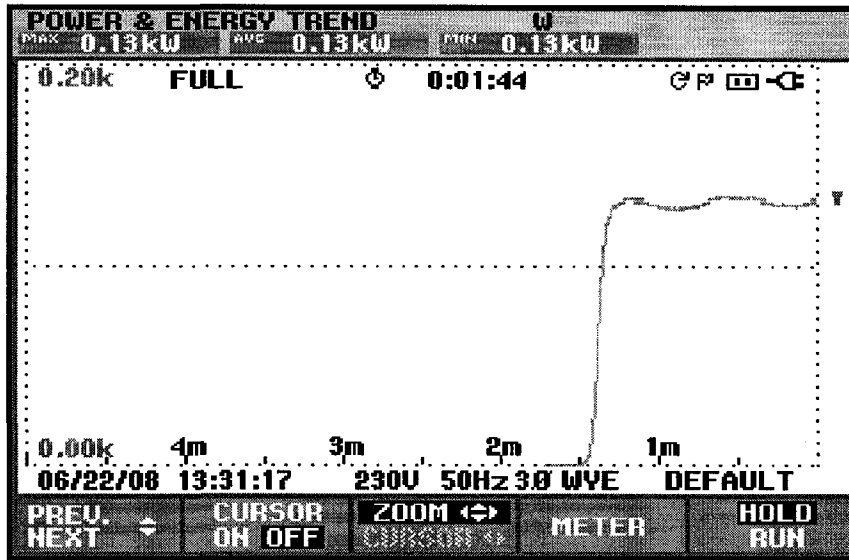


(a)

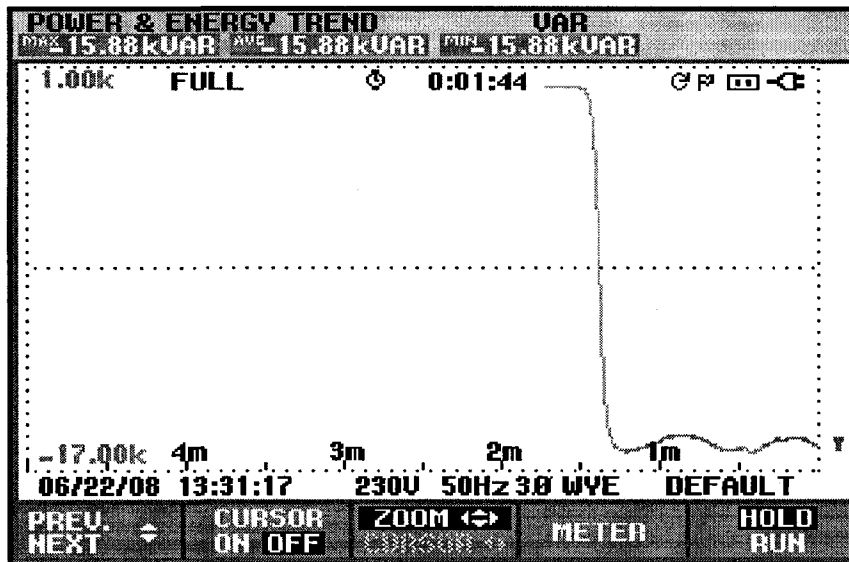


(b)

Fig. 5.26. Calculated real and reactive power under no load condition for copper-rotor SEIG. (a) Real power. (b) Reactive power.

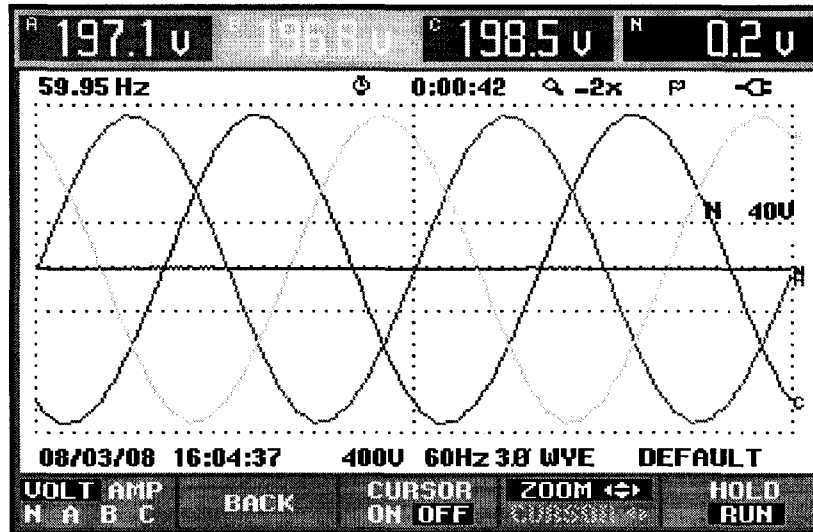


(a)

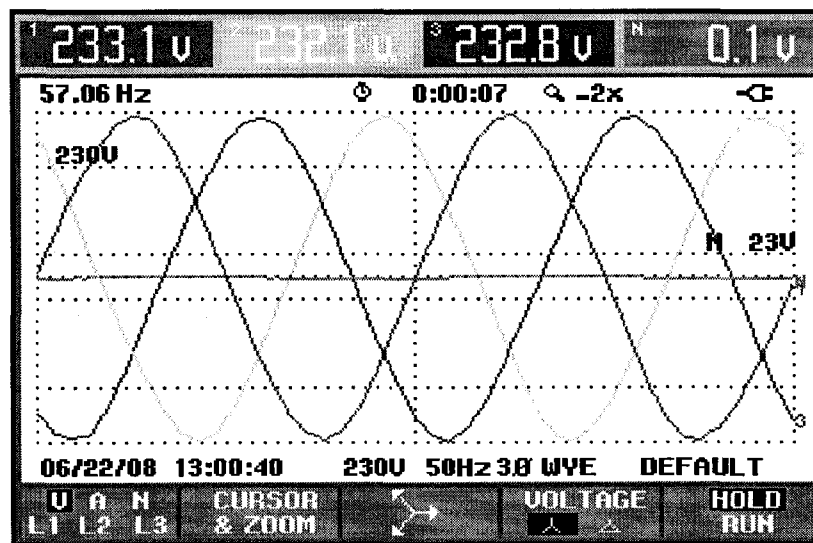


(b)

Fig. 5.27. Measured real and reactive power under no load condition for copper-rotor SEIG (CT ratio 5:1). (a) Real power. (b) Reactive power.



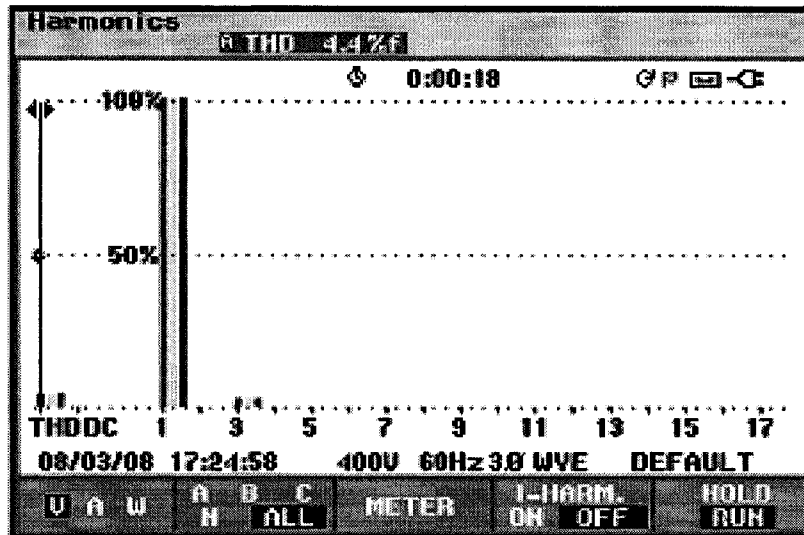
(a)



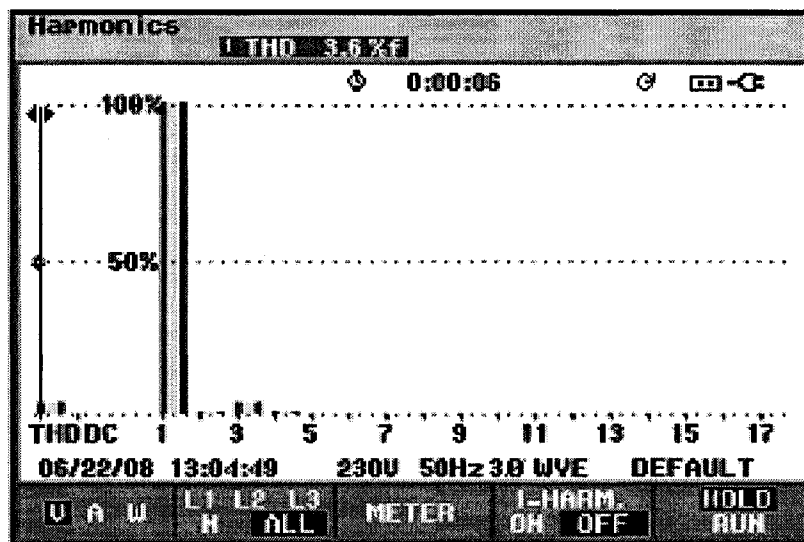
(b)

Fig. 5.28. Measured voltage wave forms of the three phases of SEIG.  
 (a) Aluminium-rotor (b) Copper-rotor.

The wave forms of the terminal voltages of the two SEIGs at no load conditions are measured (Fig. 5.28) using the Fluke instrument. It can be seen that the voltage waveforms are sinusoidal and displaced by 120 electrical degrees. In ideal condition the voltage at neutral should be zero. As the neutral is not grounded in this experiment, there is a small voltage recorded ( 0.2 V for aluminium and 0.1 V for copper-rotor IG). This



(a)



(b)

Fig. 5.29. Measured Total Harmonic Distortion.  
 (a) Aluminium-rotor SEIG. (b) Copper-rotor SEIG.

can be attributed to the small unbalance between the phases of the generator voltages. The departure from pure sinusoidal shape can be understood from Total Harmonic Distortion (THD) which is measured using the Analyser (Fig. 5.29). Table IV summarises the features of the voltage build-up of the two SEIGs.

TABLE IV  
VOLTAGE BUILD-UP CHARACTERISTICS OF THE TWO MACHINES

	Unit	Al-Rotor SEIG	Cu-Rotor SEIG
Capacitor	μf	61.6	39.6
Terminal Voltage	V	200	275
Build-up time (measured)	sec.	7.5	9
Build-up time (calculated)	sec.	5	9.5
Rotor speed	rpm	1800	1800
Terminal frequency	Hz	59.95	60.06
THD	%	4.4	3.6

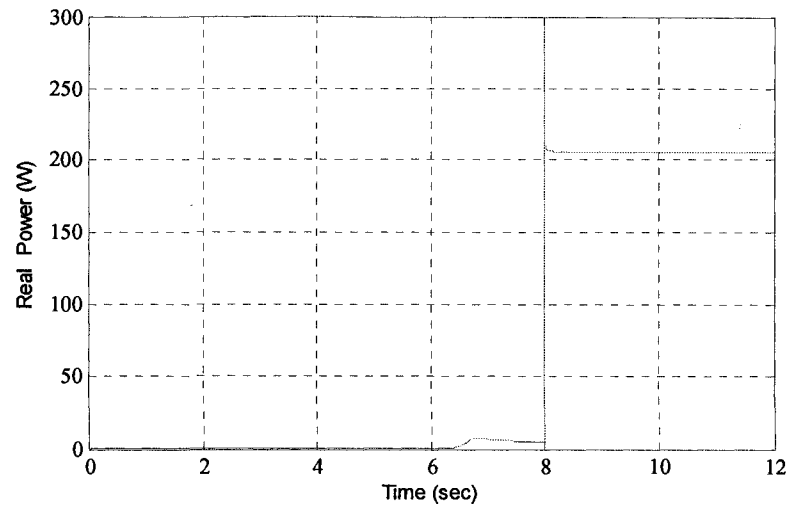
### 5.3.3 SEIG with resistive load

In order to take the load resistance  $R$  into account the equations developed earlier has to be modified. In this case (3.38) and (3.41) are combined to give

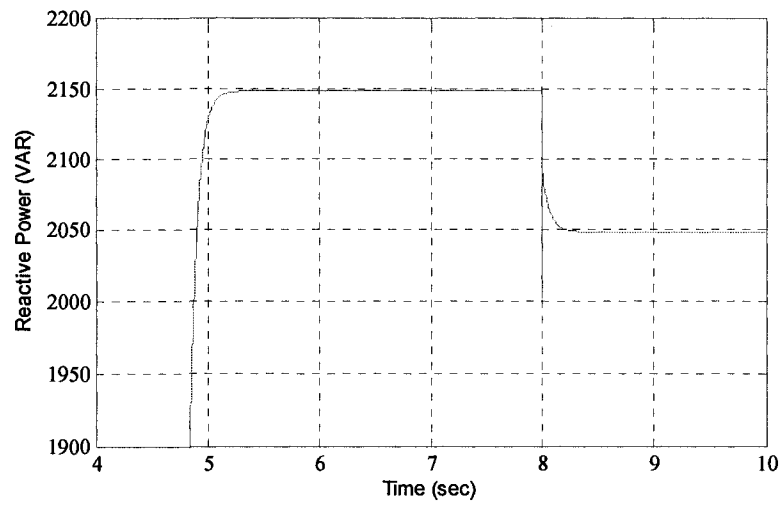
$$p \begin{bmatrix} v_{qs} \\ v_{ds} \end{bmatrix} = \begin{bmatrix} 1/C & 0 \\ 0 & 1/C \end{bmatrix} \begin{bmatrix} i_{qs} \\ i_{ds} \end{bmatrix} + \begin{bmatrix} -1/R_l C & -\omega \\ \omega & -1/R_l C \end{bmatrix} \begin{bmatrix} v_{qs} \\ v_{ds} \end{bmatrix} \quad (5.4)$$

In order to verify the SEIG model under resistive load and considering skin effect, a three-phase star connected resistance of 340 Ω was switched on at 8 sec. after the terminal voltage have reached steady state values. The simulated and measured values of the real and reactive power at the machine terminals are shown in Fig. 5.30 and Fig. 5.31.

For the copper-rotor SEIG three loading conditions have been considered. The values of the wye-connected resistance being 100 Ω, 63 Ω, and 46 Ω per phase. Only one set of results with 100 Ω are presented here in Fig. 5.32 and Fig. 5.33.

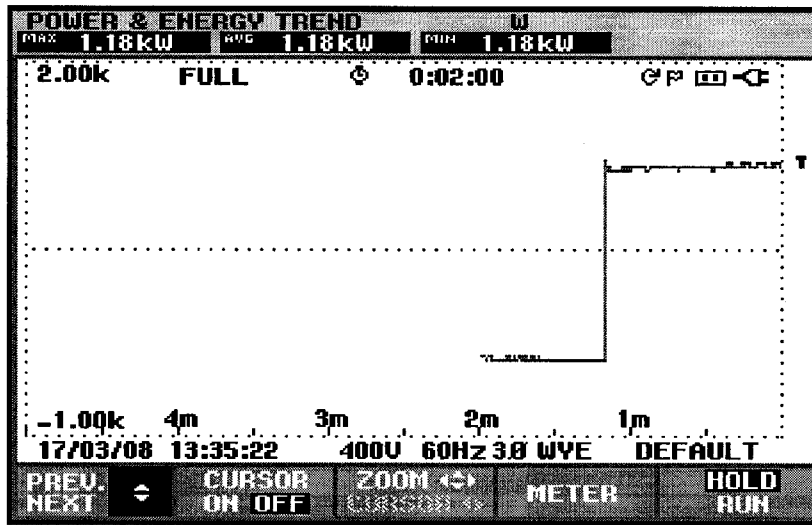


(a)

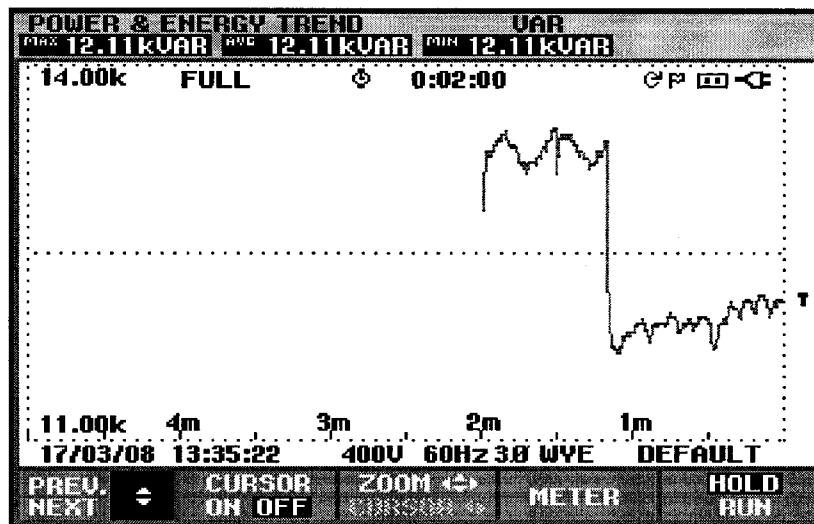


(b)

Fig. 5.30. Calculated power for aluminium-rotor SEIG under Resistive load condition. (a) Real power. (b) Reactive power.

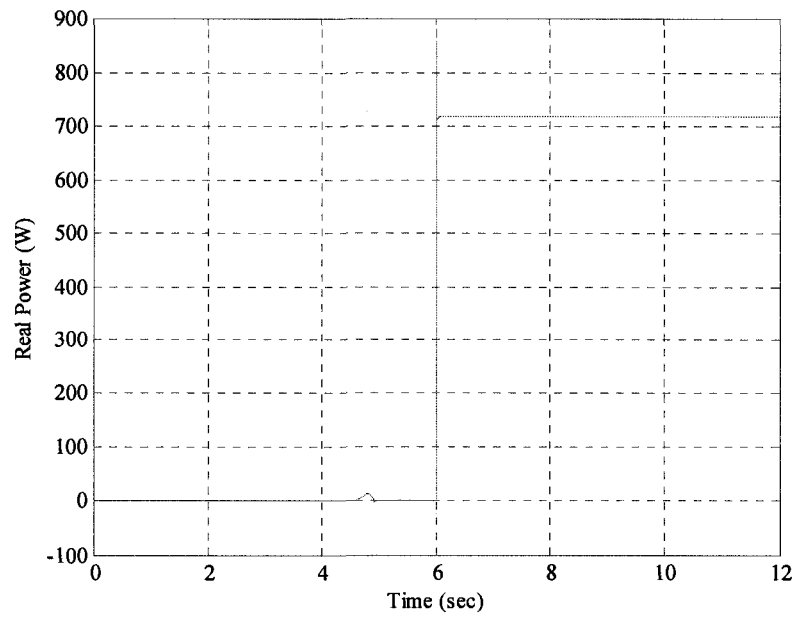


(a)

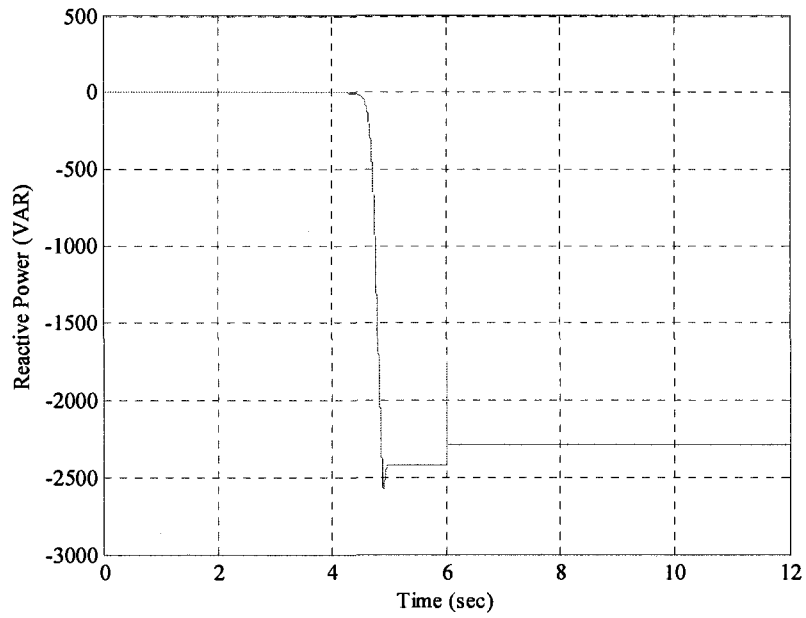


(b)

Fig. 5.31 Measured real and reactive power under resistive load condition for aluminium-rotor SEIG (CT ratio 5:1). (a) Real power. (b) Reactive power.



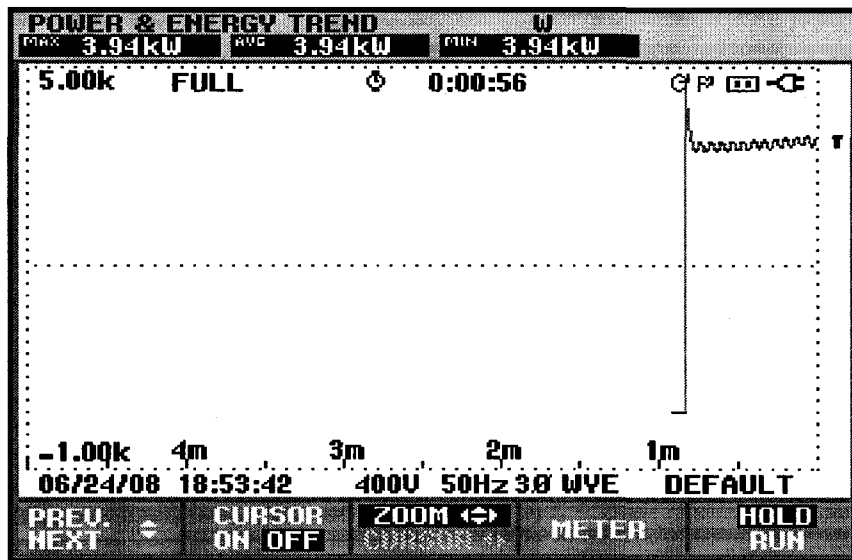
(a)



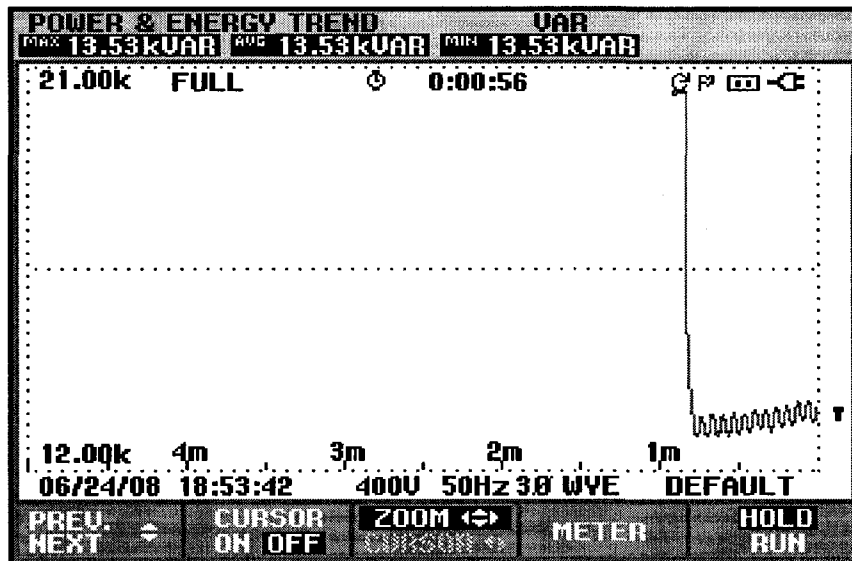
(b)

Fig. 5.32. Calculated real and reactive power for copper-rotor SEIG under Resistive load condition. (a) Real power. (b) Reactive power.





(a)



(b)

Fig. 5.33. Measured real and reactive power under resistive load condition for copper-rotor SEIG (CT ratio 5:1). (a) Real power. (b) Reactive power.

From these figures it can be observed that there is a close agreement between the calculated and measured values.

### 5.3.4 SEIG with $RL$ load

With the induction machine on load the load currents may be expressed as:

$$\begin{aligned} i_{qs} &= i_{cq} + i_{lq} \\ i_{ds} &= i_{cd} + i_{ld} \end{aligned} \quad (5.5)$$

$$\begin{aligned} v_{qs} &= (R_l + pL_l)i_{lq} \\ v_{ds} &= (R_l + pL_l)i_{ld} \end{aligned} \quad (5.6)$$

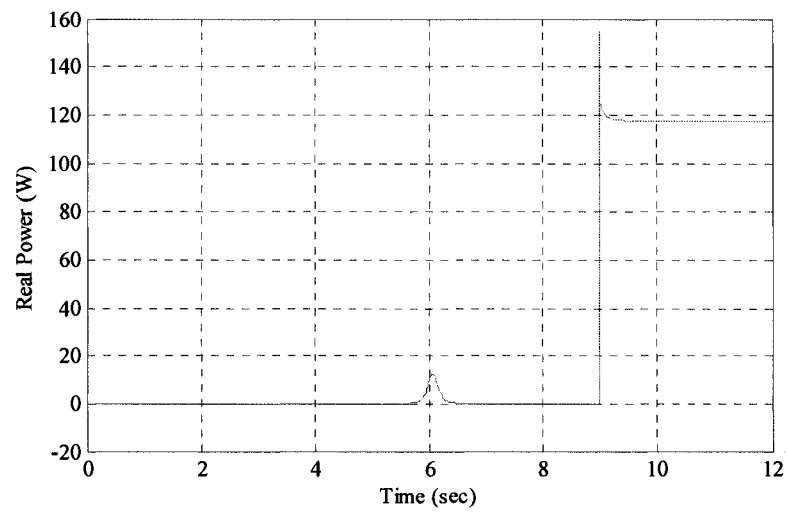
which can be rewritten as

$$\begin{bmatrix} i_{lq} \\ i_{ld} \end{bmatrix} = \begin{bmatrix} v_{qs} \\ v_{ds} \end{bmatrix} (R_l + pL_l)^{-1} \quad (5.7)$$

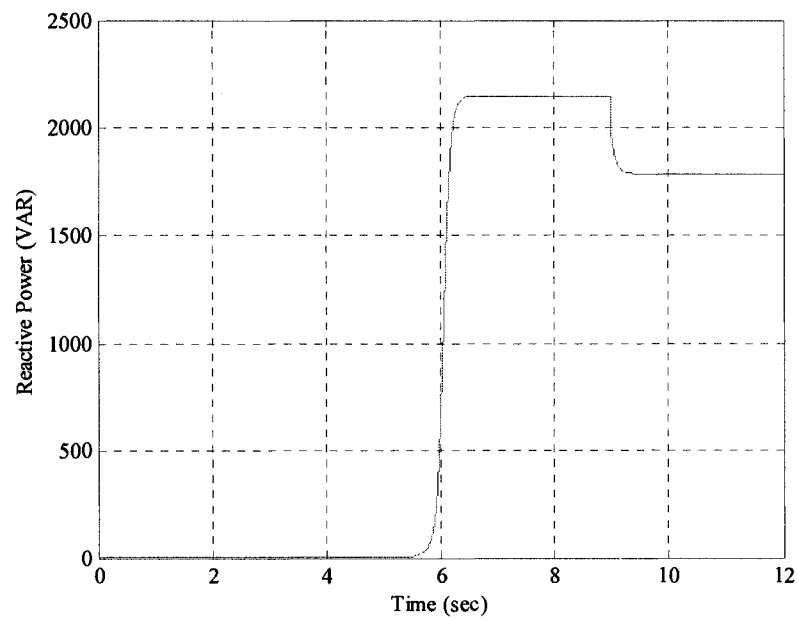
$$p \begin{bmatrix} v_{qs} \\ v_{ds} \end{bmatrix} = \begin{bmatrix} 1/C & 0 \\ 0 & 1/C \end{bmatrix} \begin{bmatrix} i_{qs} \\ i_{ds} \end{bmatrix} + \begin{bmatrix} -1/R_l C & -\omega \\ \omega & -1/R_l C \end{bmatrix} \begin{bmatrix} v_{qs} \\ v_{ds} \end{bmatrix} \quad (5.8)$$

$$p \begin{bmatrix} i_{lq} \\ i_{ld} \end{bmatrix} = \begin{bmatrix} L_l^{-1} & 0 \\ 0 & L_l^{-1} \end{bmatrix} \begin{bmatrix} v_{qs} \\ v_{ds} \end{bmatrix} - \begin{bmatrix} L_l^{-1} R_l & 0 \\ 0 & L_l^{-1} R_l \end{bmatrix} \begin{bmatrix} i_{lq} \\ i_{ld} \end{bmatrix} \quad (5.9)$$

Calculated and measured values for  $R = 171 \Omega$  and  $L = 0.4536 \text{ H}$ , are shown in Fig. 5.34 – Fig. 5.37 for both the machines. This load is applied at  $t = 9$  seconds after the stator voltage has reached steady state values.

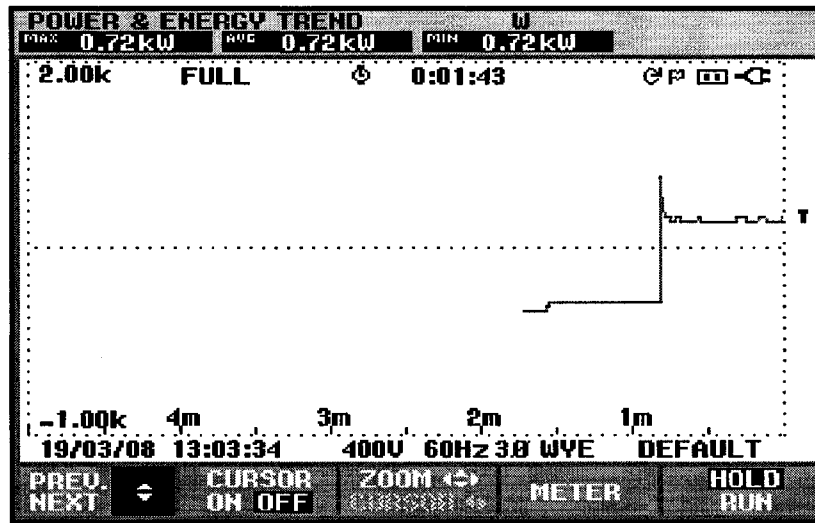


(a)

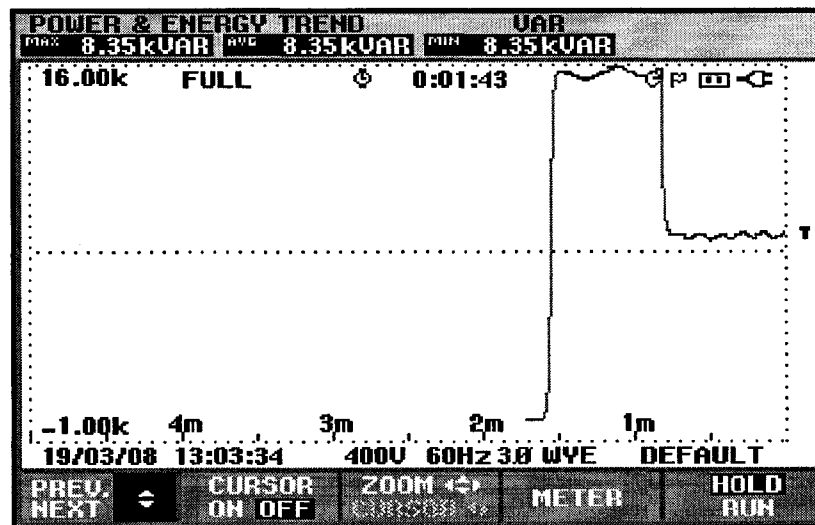


(b)

Fig. 5.34. Calculated real and reactive power for aluminum-rotor SEIG under  $R-L$  load. (a) Real power. (b) Reactive power.

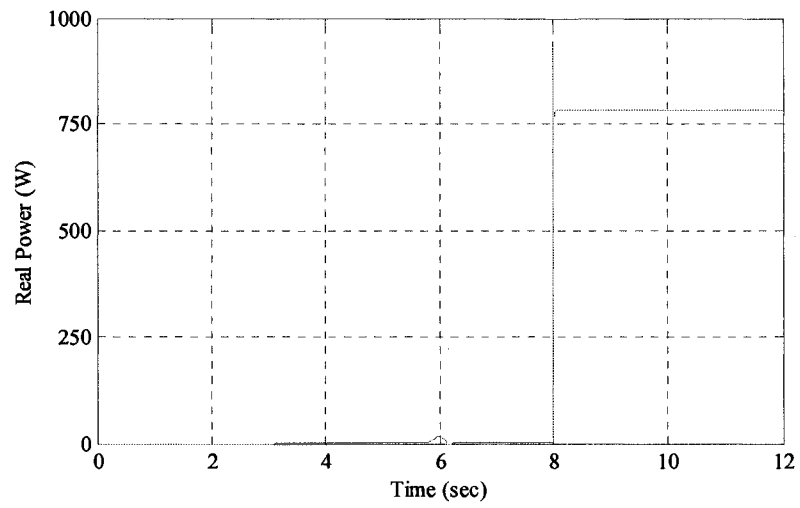


(a)

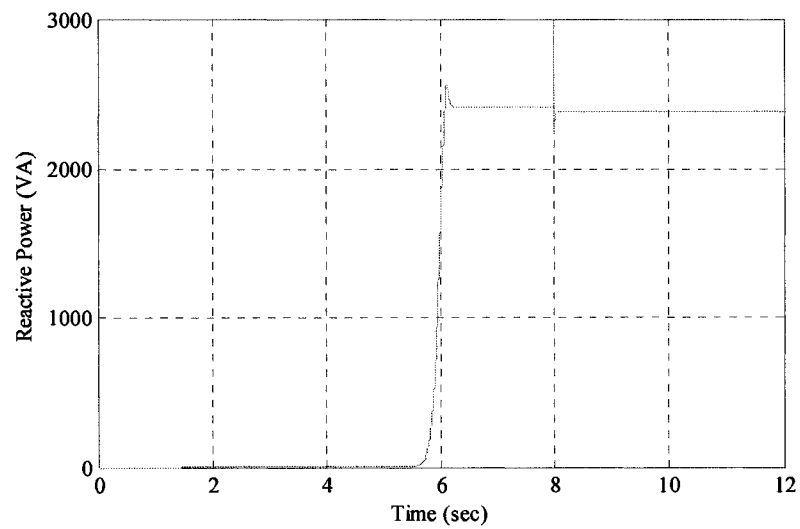


(b)

Fig. 5.35. Measured real and reactive power for aluminum-rotor SEIG under *RL* load (CT ratio 5:1). (a) Real power. (b) Reactive power.

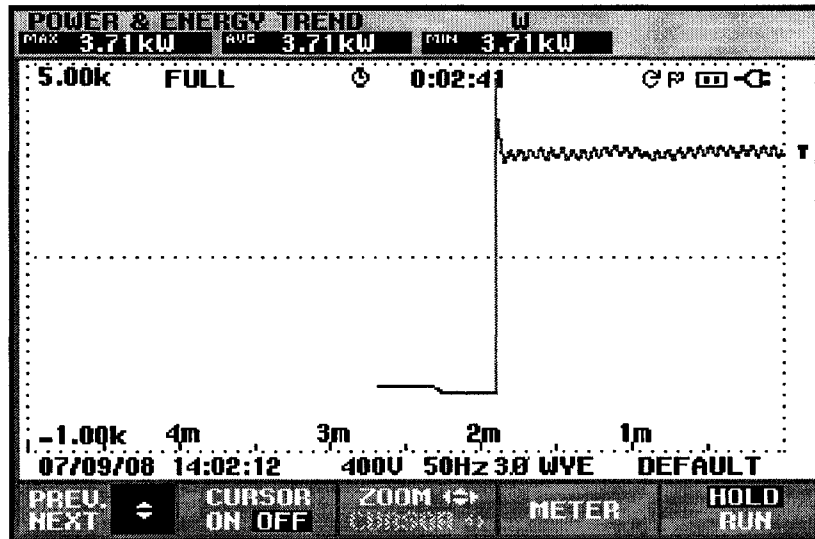


(a)

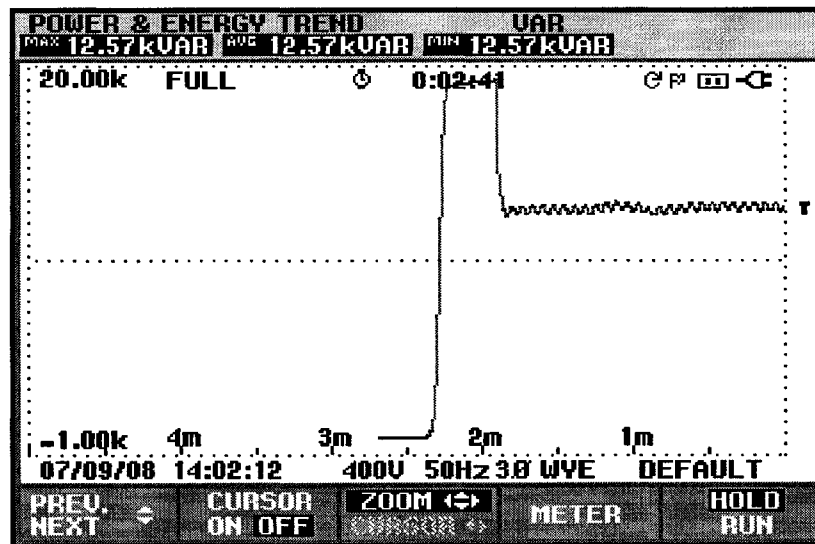


(b)

Fig. 5.36. Calculated real and reactive power for copper-rotor SEIG under *RL* load. (a) Real power. (b) Reactive power.



(a)



(b)

Fig. 5.37. Measured real and reactive power for copper-rotor SEIG under *RL* load. (CT ratio 5:1). (a) Real power. (b) Reactive power.

#### 5.4 Voltage Regulation of SEIGs

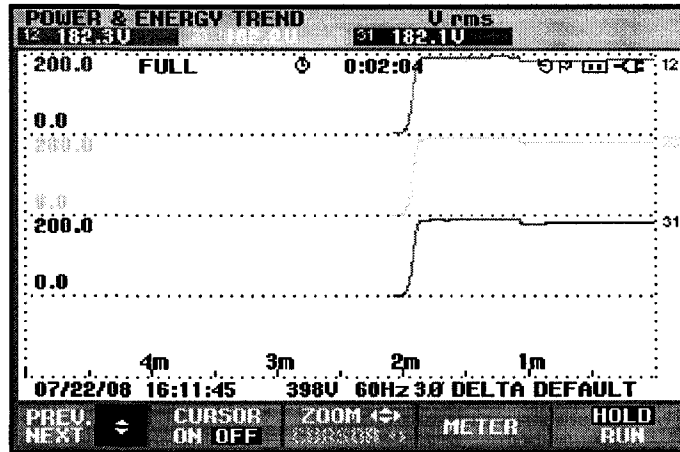
The main shortcoming of a self-excited induction generator such as the generator used in this research is its inherently poor voltage regulation [13]. As mentioned previously, when the induction generator operates in self-excitation mode, it determines

its own terminal voltage and frequency. These two quantities depend on the size of the excitation capacitor, the induction machine parameters, the electrical load, power factor of the load and the speed of the rotor. The most serious issue concerning the terminal voltage of an SEIG is that it varies widely with changes in load especially when the load is reactive.

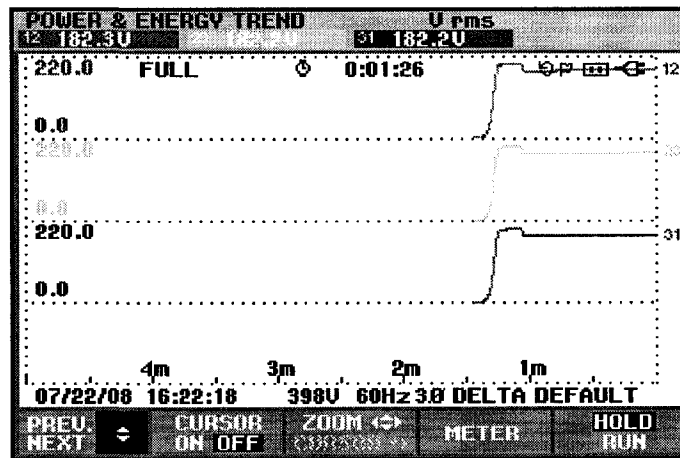
If the connected load is purely resistive then the impedance  $X_c$  of the excitation capacitance  $C$ , will dominate the parallel combination of the load resistance  $R_l$  and  $X_c$ . as long as  $R_l$  is high. However as  $R_l$  approaches zero the machine is loaded heavily and will be driven to cut off.

If the value of the excitation capacitance  $C$  is small or  $X_c$  is very large, then the load impedance  $R_l + jX_l$  will dominate the parallel combination of the load and  $X_c$ . The effect of  $X_c$  will be diminished driving the machine to cut off. On the other hand if  $R_l + jX_l$  is very large, then  $X_c$  dominates the parallel, combination of the load and  $R_l + jX_l$ . If  $C$  is large or  $X_c$  is small, further increase in  $C$  will result in reducing the capacitive component in the circuit, driving the machine to cut off [14].

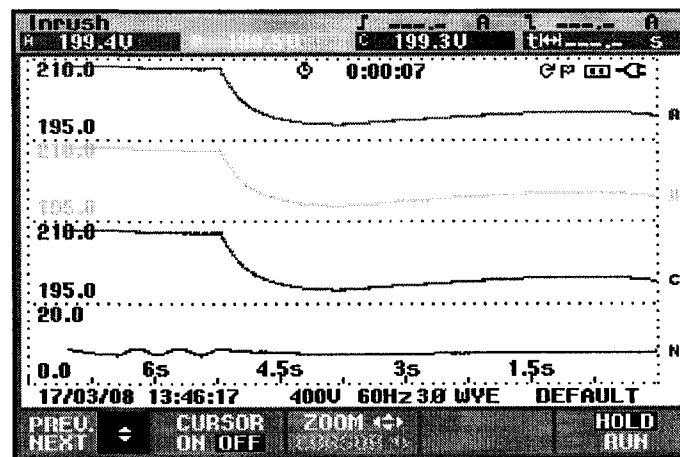
The voltage regulation of the two induction generators are determined by connecting resistances of 100  $\Omega$ , 63  $\Omega$  and 46  $\Omega$  and measuring the terminal voltages and current at each stage. For  $RL$  load an inductance of 0.4536 H in series with a resistance of 46  $\Omega$  is connected across the generator terminals. The resulting voltage traces are displayed in Fig. 5.38(a)-(c) for aluminium-rotor and 5.39(a)-(c) for copper-rotor SEIG. For  $RL$  load the voltage traces are shown in Fig. 5.40(a) and Fig. 5.40(b) for aluminium- and copper-rotor SEIG respectively.



(a)



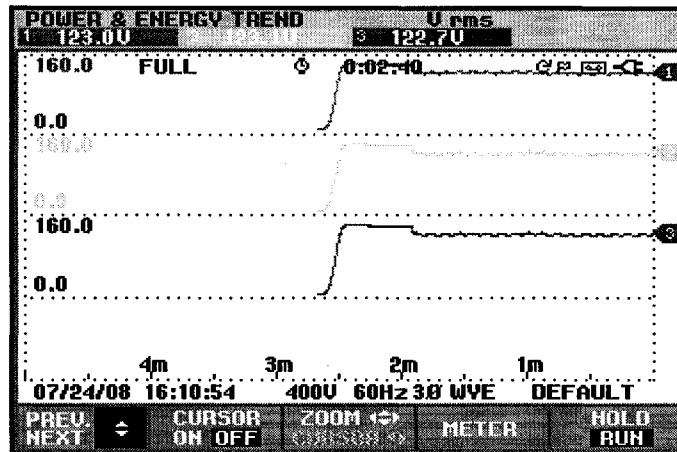
(b)



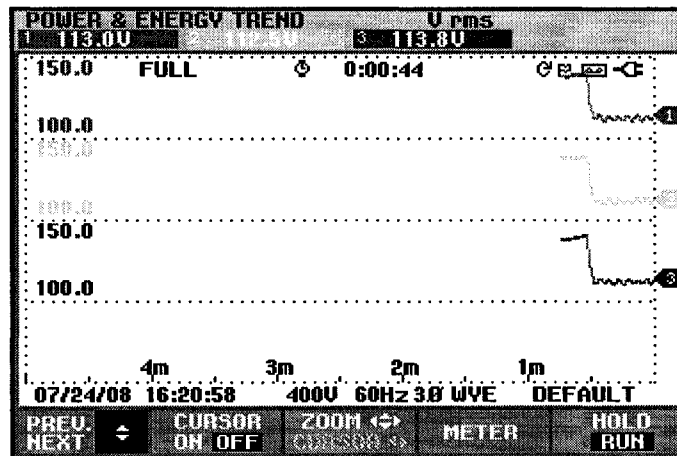
(c)

Fig. 5.38. Voltage regulation of aluminium-rotor SEIG with  $R$  load.  
 (a)  $R = 100 \Omega$ . (b)  $R = 63 \Omega$ . (c)  $R = 46 \Omega$ .

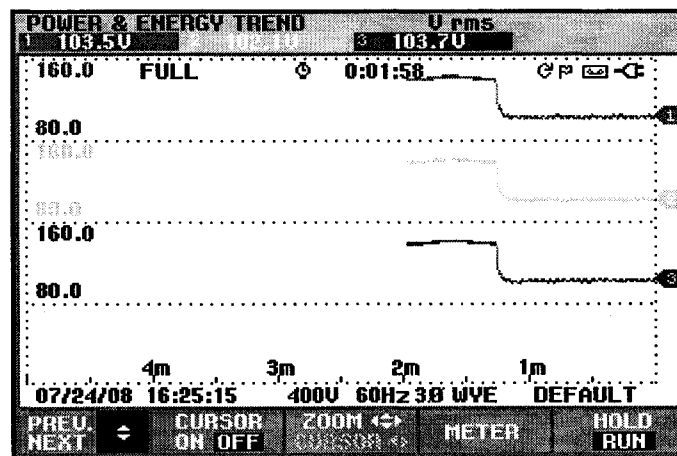




(a)

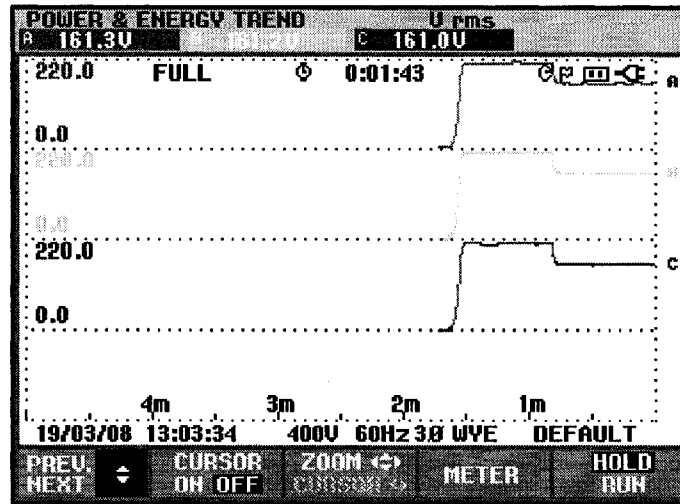


(b)

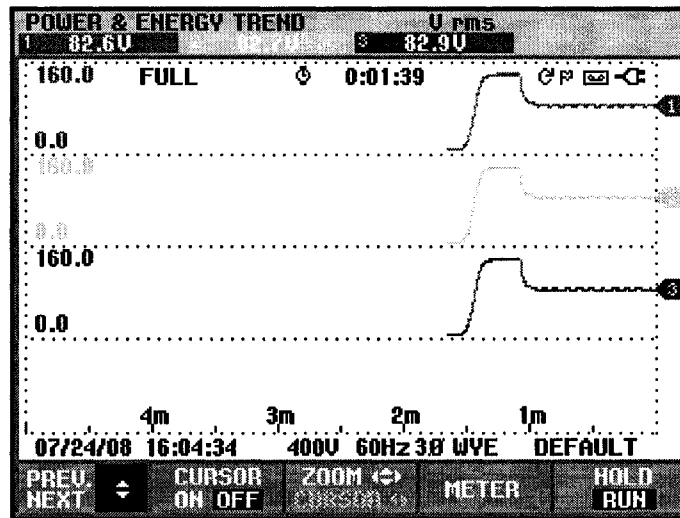


(c)

Fig. 5.39. Voltage regulation of copper-rotor SEIG with  $R$  load.  
 (a)  $R = 100 \Omega$ . (b)  $R = 63 \Omega$ . (c)  $R = 46 \Omega$ .



(a)



(b)

Fig. 5.40. Voltage regulation of the SEIGs with  $RL$  load.  
 (a) Aluminium-rotor.(b) Copper-rotor.

As can be seen from the above figures if the magnitude of the excitation capacitance is kept fixed and load is applied, the voltage regulation is poor and becomes more severe with the increase in load. The results are summarized and shown in Table V.

TABLE V  
VOLTAGE REGULATION OF THE MACHINES

	Al-rotor SEIG		Cu-rotor SEIG	
Load	Voltage Regulation (%)	Power measured at SEIG terminals (W)	Voltage Regulation (%)	Power measured at SEIG terminals (W)
100 $\Omega$	2.48	348	15.2	404
63 $\Omega$	9.3	540	20.1	572
46 $\Omega$	14.2	566	28.1	674
46 + j 171 $\Omega$	24.12	260	40.4	252

### 5.5 Copper Losses in a Self Excited Induction Generator

The copper losses in an SEIG for both the stator and rotor are calculated using the developed model of the machine. At the same time the power delivered by each of the induction generator at the terminals are calculated. As can be seen from Fig. 5.41 that the power delivered increases with the loading, i.e. decrease in the magnitude of the load

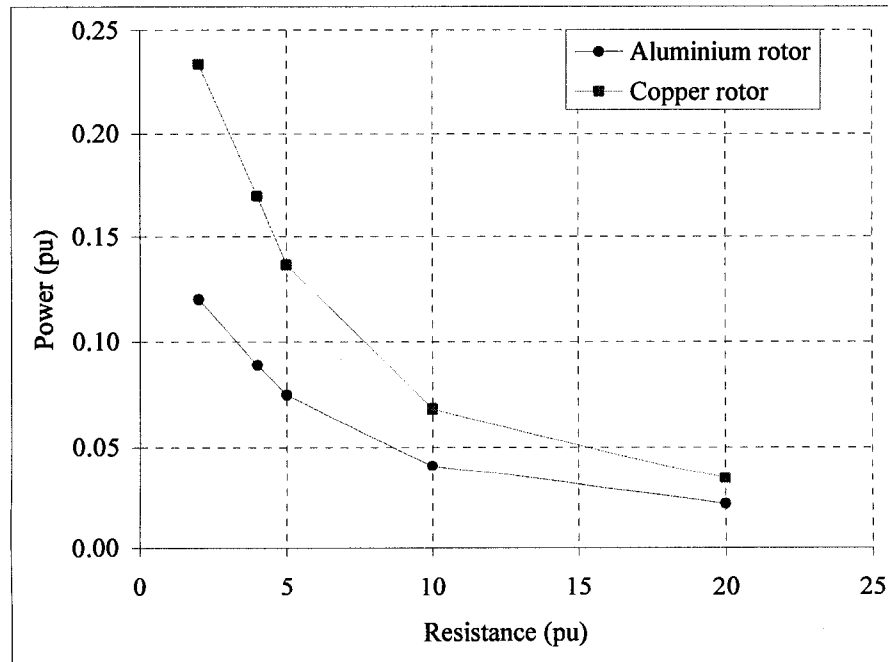


Fig. 5.41. Calculated power at delivered stator terminals for  $R$  load.

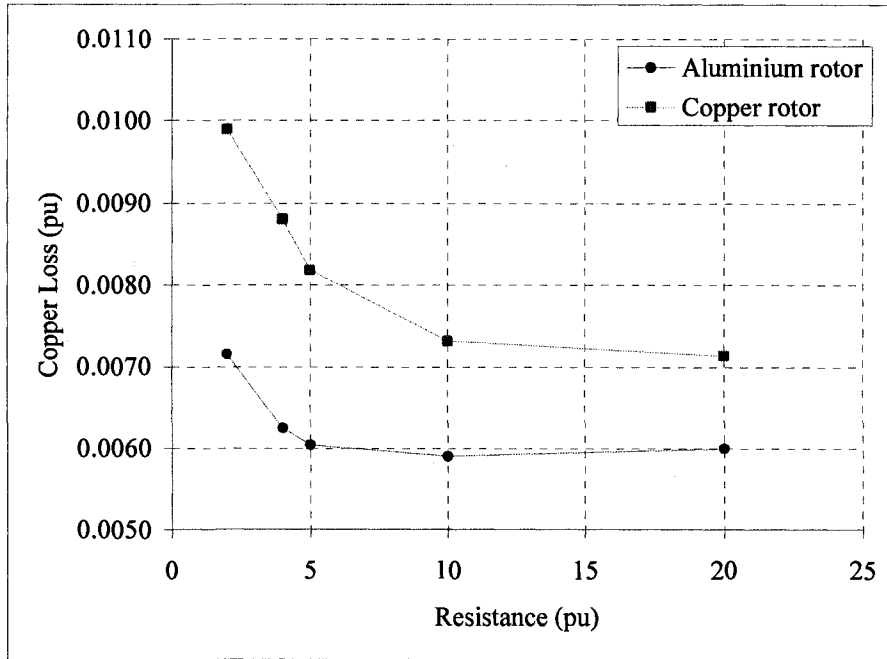


Fig. 5.42. Calculated stator copper loss for  $R$  load.

resistance. However due to poor voltage regulation of the machines the terminals voltage decreases along with a decrease in the stator currents. The copper losses have also been

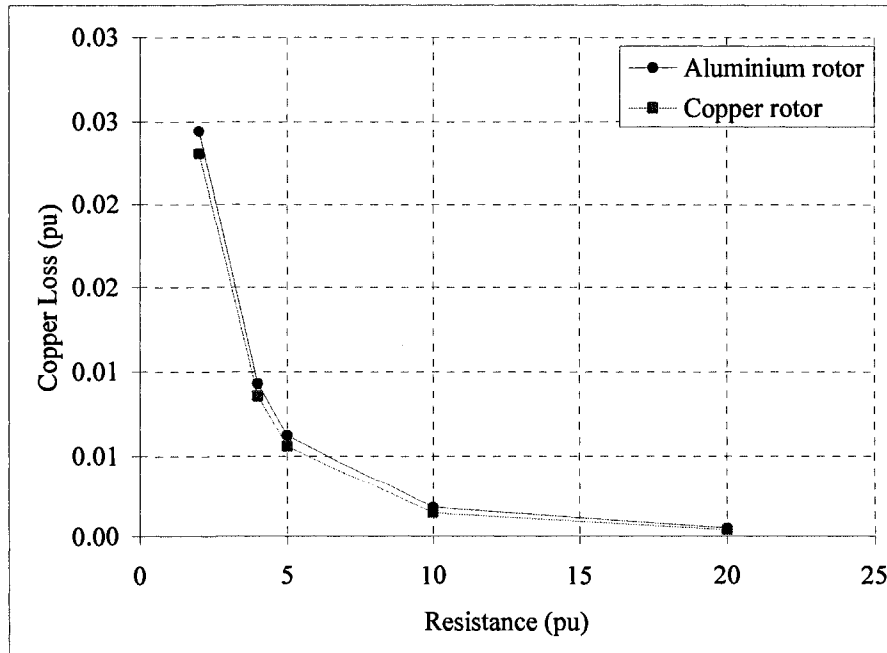


Fig. 5.43. Calculated rotor copper loss for  $R$  load.

calculated for the same loading conditions and shown in Fig. 5.42 and Fig 5.43 for stator and rotor respectively.

In spite of its many advantages, a self-excited induction generator has some severe limitations. Since it does not have a separate dc field excitation, the emf induced in the machine windings is solely due to the excitation capacitors connected to the terminals. The VARs demand by the machine is balanced by the VARs supplied by the capacitors. In case of *RL* load the parallel combination of the *RL* circuit and the excitation capacitance must be capacitive in order to maintain excitation at the generator terminals. This is due to the fact that under this condition the capacitor must feed the VARs required by both the machine and the load. As a result with the increase in the load, the operating point on the saturation curve of the SEIG goes further down towards cut off. This is seen in Fig. 5.44 where the power delivered by the generator sharply goes down due to lower terminal voltage and stator currents resulting in lower values of delivered power, close to cut off conditions.

The behaviour of the stator copper losses (Fig. 5.45) can be explained from this phenomenon. Due to decrease in the stator terminal voltage and subsequent decrease in

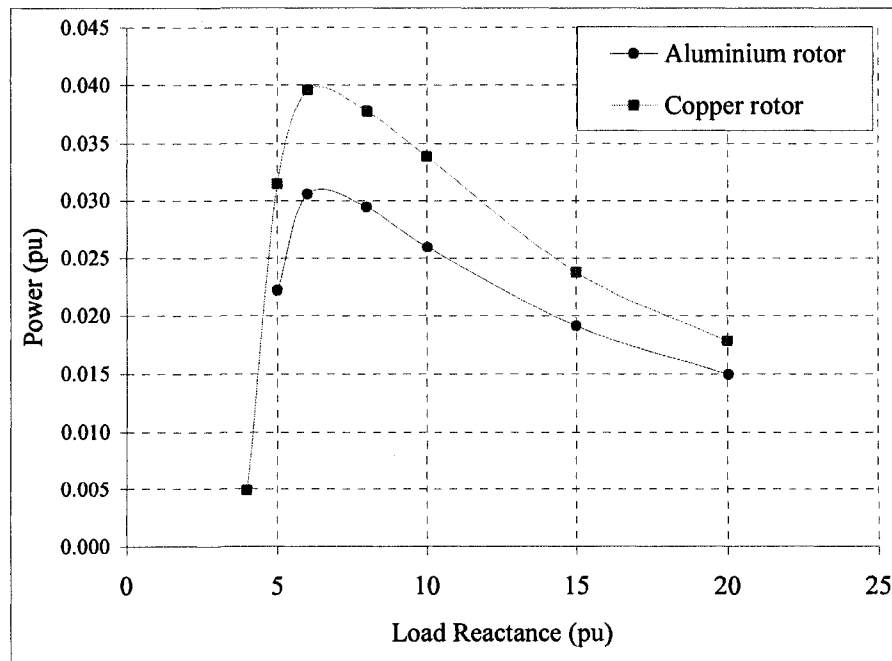


Fig. 5.44. Calculated power at delivered stator terminals for *RL* load.

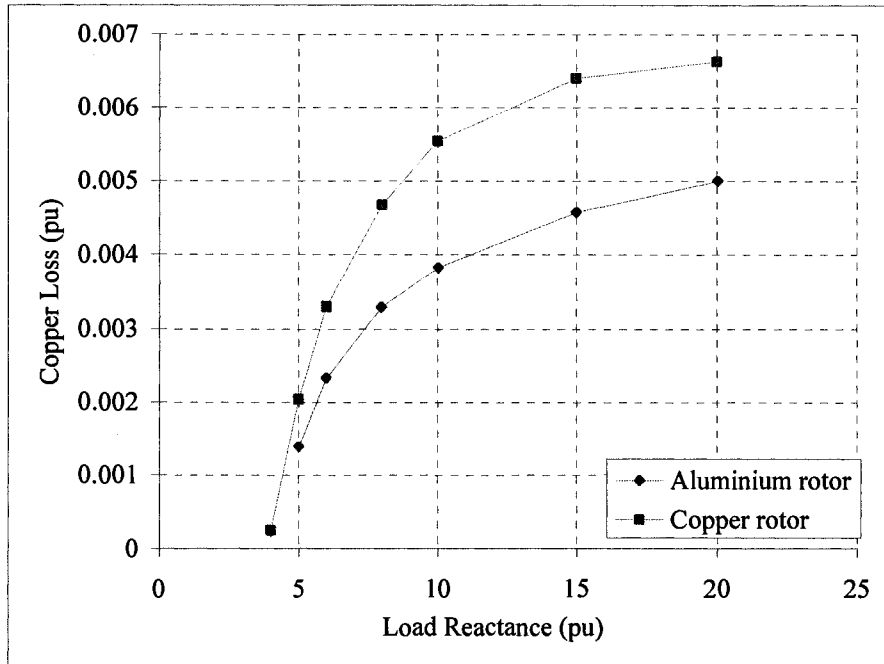


Fig. 5.45. Calculated stator copper loss for *RL* load.

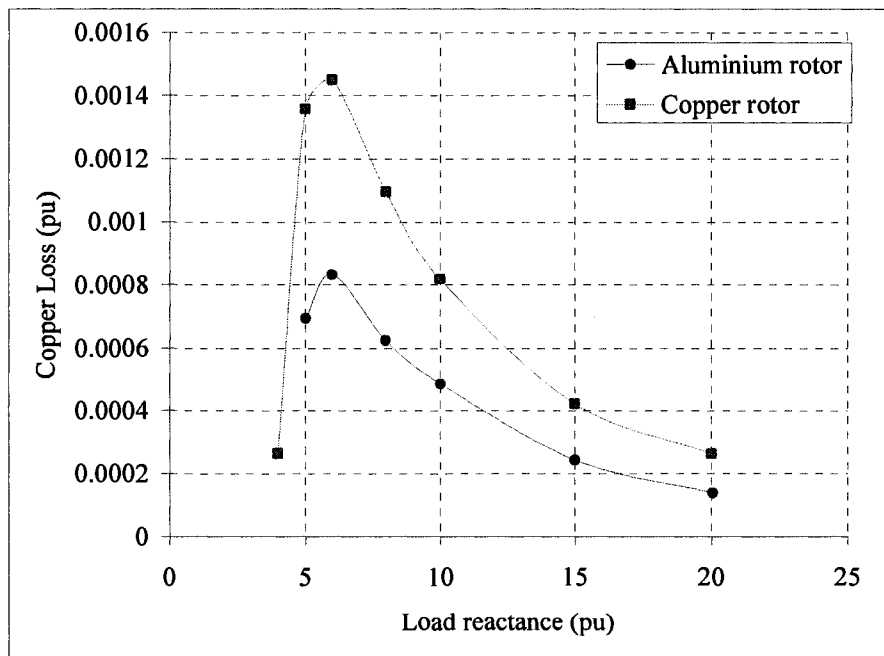


Fig. 5.46. Calculated rotor copper loss for *RL* load.

stator current owing to poor voltage regulation, the stator copper losses show decreasing trend with load.

Rotor copper losses (Fig. 5.46) show an increasing trend with load. However near cut-off conditions, at around a load of  $6 + j6$  pu, the losses sharply decline due to decrease in rotor current.

Copper losses are also calculated in an induction generator using the mathematical model where only the aluminium bars are replaced with copper and, in this case, the terminal voltage of the SEIG is kept constant by increasing the value of the excitation capacitance accordingly to  $160 \mu\text{f}$ . The stator and rotor copper losses are then calculated for both aluminium and copper rotor SEIGs for a 40% loading condition. It is observed that there is a 20% reduction in the rotor copper loss in the case of the copper rotor SEIG. As can be seen from Fig. 5.47, even though there is a slight decrease in the stator copper losses, the losses in the rotor is quite significant for the copper rotor SEIG.

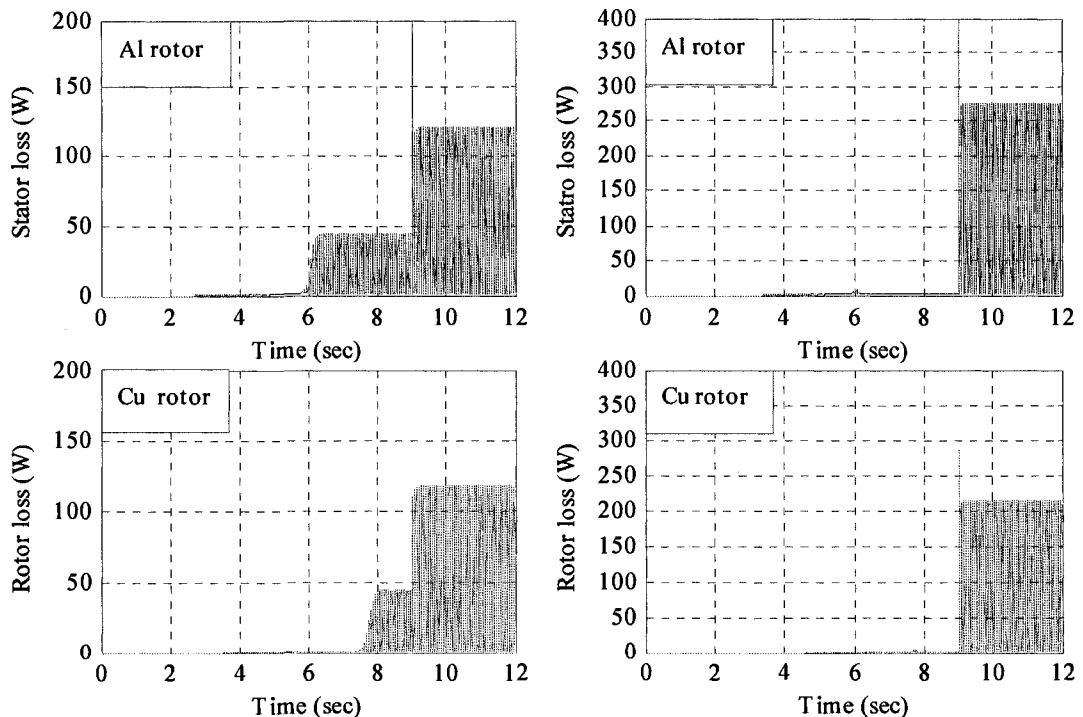


Fig. 5.47. Calculated rotor copper loss for aluminium-rotor and copper-rotor SEIGs under  $RL$  load for  $C= 160\mu\text{F}$ .

## 5.6 Bibliography

- [1] D.T. Peters, J.G. Cowie, E.F. Brush, Jr., M. Doppelbauer and R. Kimmich, "Performance of Motors with Die-cast Copper Rotors in Industrial and Agricultural Pumping Applications," *IEEE International Conference on Electric Machines and Drives*, pp. 987-992, May 2005.
- [2] Induction Motors with Die-Cast Copper Rotors, [http:// www.leonardo-energy.org](http://www.leonardo-energy.org), Feb. 2006.
- [3] E.F. Brush, Jr., J.G. Cowie, D.T. Peters, and D. J. Van Son, "Die-cast Copper Motor Rotors: Motor Test Results, Copper Compared to Aluminum," <http://www.arti-21cr.org/~/20030-final2.pdf>.
- [4] D.T. Peters, J.G. Cowie, E.F. Brush Jr., and D.J. Van Son, "Copper in the Squirrel Cage for Improved Motor Performance," *Proceedings of the IEEE International Electric Machines and Drives Conference*, Vol. 2, pp. 1265-1271, 2003.
- [5] S. J. Chapman, *Electrical Machinery Fundamentals*, 2<sup>nd</sup> edition. McGraw-Hill, New York, 1998.
- [6] A.K. Tandon, S.S. Murthy and G.J. Berg, "Steady State Analysis of Capacitor Self-Excited Induction Generators," *IEEE Transactions on Power Apparatus and Systems*, Vol. PAS-103, No. 3, pp. 612-617, Mar. 1984.
- [7] L. Wang and C.H. Lee, "A Novel Analysis on the Performance of an Isolated Self-Excited Induction Generator," *IEEE Transactions on Energy Conversion*, Vol. 12, No. 2, pp. 109-117, Jun. 1997.
- [8] L. Wang and C.M. Cheng, "Selection of Magnetizing Curves for Accurately Simulating a Three-Phase Self-Excited Induction Generator Feeding a Single-Phase Load," *IEEE Power Engineering Society Winter Meeting*, Vol. 1, No. 1, pp. 286-290, 2000.
- [9] D. Seyoum, C. Grantham and F. Rahman, "A Novel Analysis of an Isolated Self-Excited Induction Generator Taking Iron Loss into Account," *IEEE Transaction on Industrial Applications*, Vol. 35, No. 3, Apr. 2003.
- [10] S.S. Kou and L. Wang, "Dynamic Eigenvalue Analysis of a Self-Excited Induction Generator Feeding an Induction Motor," *IEEE Power Engineering Society Winter Meeting*, Vol. 3, No. 1, pp. 1393-1397, 2001.



- [11] —, Steady-State Performance of a Self-Excited Induction Generator Feeding an Induction Motor,” *Electric Power Components and Systems*, Taylor and Francis, pp. 581-593, 2002.
- [12] O. Ojo, “Minimum Air Gap Flux Linkage Requirement for Self-Excitation in Stand Alone Induction Generators,” *IEEE Transaction on Energy Conversion*, Vol. 10, No. 3, pp. 484–492, Sept. 1995.
- [13] H.C. Rai, A.K. Tandan, S.S. Murthy, B. Singh and B.P. Singh, “Voltage Regulation of Self Excited Induction Generator using Passive Elements,” *Sixth International Conference on Electrical Machines and Drives*, pp. 240-245, Sep. 1993.
- [14] T.C. Sekhar, and B.P. Muni, “Voltage Regulators for Self Excited Induction Generator, *IEEE Region 10 Conference TENCON*, Vol. C, pp. 460-463, Nov. 2004.

## 6.0 CONCLUSION

It has been an endeavour in this research work, to analyse the performance of self excited induction generators. A novel mathematical model has been developed to represent the system using higher order differential equations. The stationary reference frame of the two axes theory, with the d-q axes  $90^\circ$  apart in space, has been used. The mathematical model has further been enhanced to include skin effect and the material of the rotor cage bars. In this investigation, this model of the SEIG has been applied to both aluminium- and copper-rotor machines of similar power ratings to analyze their performance. The electrical parameters of each induction generator and the saturation characteristics of their respective main fluxes have been taken into account so that the dynamic model is more appropriate to represent the actual machines. The dynamic models have been experimentally verified with results that are obtained from the two 7.5 hp, G.E. and Siemens industrial type induction machines in the laboratory. Results obtained using the model by ignoring and also by considering skin effect in the case of no load,  $R$  and  $RL$  load conditions have been compared with the experimental ones. For both the machines the models that considered skin effect produced acceptable results.

As can be seen from the magnetizing characteristics of each SEIG, the curve for the copper-rotor machine is steeper compared to the aluminium-rotor machine. This may be attributed to the smaller rotor diameter, longer length and susceptibility of the rotor-bar material of the copper-rotor machine as compared to the aluminium counterpart. As a result for the same value of excitation capacitance, the no load output voltage will be higher in case of copper-rotor SEIG. For the same voltage output, a higher value of capacitance will be required for the aluminium-rotor machine. The values of the excitation capacitors used in this experiment are  $61.6 \mu\text{f}$  and  $33 \mu\text{f}$  for the aluminium and copper-rotor machine respectively.

From the equivalent circuit parameters determined from the standard tests, the torque-speed characteristics of the two machines have been calculated. It is seen that the starting and pull-out torques of the copper-rotor machine are relatively lower than the aluminium-rotor machine for rated condition.

The voltage and current build-up time under open circuit condition is found to be considerably higher in case of the model that ignores skin effect. When skin effect is

considered in the mathematical models, there is a close concurrence between the calculated and measured values for both the aluminium- and copper-rotor machines. It is also observed that the transients settle down faster in case of the model that takes skin effect into account.

The output voltage wave shapes have been observed to be sinusoidal, with a small third harmonic component for both the SEIGs. The ratio of the sum of the square of all the harmonic voltages amplitudes to the square of the fundamental voltage is a measure of the quality of the generated voltage and known as Total Harmonic Distortion (THD). The THD is measured and found to be higher in case of the aluminium-rotor machine.

One of the main drawbacks of a self excited induction generator is its poor voltage regulation, since there is no separate dc excitation system. As load is applied, the VARs supplied by the capacitance of the parallel combination of the excitation capacitance and the connected load must match the VARs demanded by the machine that is dictated by the magnetizing curve. In other words the VARs required by the machine to maintain self excitation and the VARs demanded by the connected load must be provided solely by the excitation capacitor. Consequently as the load is increased there is a decrease in the magnitude of the terminal voltage and frequency due to change in the reactive power requirement.

As the load becomes more inductive the VARs that can be supplied by the capacitors is distributed between the machine and the load. Consequently the VARs available to the machine are less than under the open circuit conditions. As can be seen from the results, the voltage decreases further with the application of load. Since the magnetizing curve of the copper rotor SEIG is steeper than the aluminium rotor machine studied in these investigations, for each unit decrease in the magnetizing current the decrease in voltage is more in the case of copper-rotor SEIG as compared to the aluminium one.

In order to evaluate the efficiency of an induction generator, all the losses must be taken into account. Copper losses in the stator and rotor are attributed to the respective currents in the stator and rotor of the machine. In simulations where in an SEIG the aluminium bars are substituted by copper and the terminal voltages are kept steady by augmenting the excitation capacitors, a significant decrease in rotor copper losses is observed.

In the numerical investigations using the measured equivalent circuit parameters, copper losses have been calculated for both machines without changing the magnitude of the respective excitation capacitor. It has been noted that the losses have similar behaviour in both the machines under similar loading conditions, the losses being higher in the copper-rotor SEIG. It is also observed that the losses are greatly influenced by the terminal voltage of the SEIGs which in turn is affected by the load and power factor.

The following topics are suggested for further research in the area of SEIGs:

- Voltage control
- Frequency control of the terminal voltage
- Dynamic analysis taking variation of rotor speed into account
- Measurement of efficiency

## **LIST OF CONTRIBUTIONS**

### **Journal Papers**

- [1] K. Hafiz, F. Farran, H. Allawaha, M. Ayoub, M. Chafei, and N. C. Kar, "Auxiliary Power Unit for Truck Idling Reduction," *International Journal of Environmental Studies*, Vol. 64 No. 4, August 2007.

### **Conference Papers**

- [1] K. Hafiz, N. Gaurav, and N.C. Kar, "Skin Effect Modeling of Self Excited Induction Generator in Wind Power Application," *Proceedings of IEEE Canadian Conference on Electrical and Computer Engineering*, May 2008.
- [2] K. Hafiz, N. Gaurav, and N.C. Kar, "Comparative Performance Analysis of Aluminum Rotor and Copper Rotor SEIG considering Skin Effect", *Proceedings of IEEE International Conference on Electrical Machines*, Portugal, September 2008.

### **Electrical Machines and Drives Research Laboratory Management**

- [1] Designed and fabricated single phase and three phase variable ac power supply.
- [2] Designed and fabricated single phase and three phase full wave bridge rectifier for low voltage high current dc supply.
- [3] Designed and build experimental set-up for Aluminium-rotor SEIG and Copper-rotor SEIG.

## APPENDIX A

Matlab Program to Calculate the Equivalent Circuit Parameters of an Induction Machine

```
clear all;
% Test data from 7.5 hp motor

p = 4; %% number of poles
f =60; %% frequency of supply voltage
design ='B'; %% NEMA Class
Rdc = 0.3884; %% DC resistance of the stator winding

%% Blocked rotor test

Vbr = 31.53667/sqrt(3); %% voltage per phase
lbr = 20.26667; %% Line current
Pbr = 558.5/3; %% input power
fbr =60; %% line frequency

%% No load test

Vnl = 200.5667/sqrt(3); %% voltage per phase
Inl = 8.26667; %% input current
Pnl = 280/3; %% input power
nsl = 1799.6; %% rotor speed

%% Calculations

Req = Pbr/lbr^2; Zbr = Vbr/lbr; Xeq = f/fbr*sqrt(Zbr^2-Req^2);

R1 = 1.05*Vdc/Idc/2; R2pr=Req-R1;
if design =='B'; X1 = .4*Xeq; X2pr = .6*Xeq;
elseif design =='C'; X1= .3*Xeq; X2pr = .7*Xeq;
else X1 = .5*Xeq; X2pr=.5*Xeq;
end

thetanl = acos(Pnl/Vnl/Inl); ns =120*60/p; s = (ns-nsl)/ns;
E1=Vnl-Inl*exp(-j*thetanl)*(R1+j*X1); I2pr = E1/(R2pr/s+j*X2pr);
E1=abs(E1); I2pr=abs(I2pr);
Pc = Pnl-Inl^2*R1-I2pr^2*R2pr/s; Rc=E1^2/Pc;
if Pc<0; disp('Check data for error');
end
Qm = Vnl*Inl*sin(thetanl)-Inl^2*X1-I2pr^2*X2pr; Xm= E1^2/Qm;
Parameter=[' R1 ' 'R2pr ' 'x1 ' 'x2PR ' 'Rc ' 'Xm ' ]
format short e
[R1 R2pr X1 X2pr Rc Xm]
```

## **APPENDIX B**

### **Auxiliary Power Unit for Truck Idling Reduction**

Reproduced from International Journal of Environmental Studies,  
Vol. 64, No. 4, pp. 433-443, August 2007

This article was downloaded by:[Canadian Research Knowledge Network]  
[Canadian Research Knowledge Network]

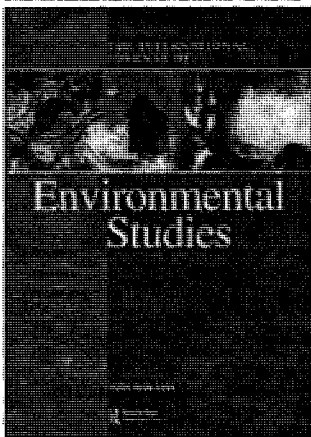
On: 11 July 2007

Access Details: [subscription number 770885180]

Publisher: Taylor & Francis

Informa Ltd Registered in England and Wales Registered Number: 1072954

Registered office: Mortimer House, 37-41 Mortimer Street, London W1T 3JH, UK



## International Journal of Environmental Studies

Publication details, including instructions for authors and subscription information:  
<http://www.informaworld.com/smpp/title-content=t713642046>

### Auxiliary power unit for truck idling reduction

Online Publication Date: 01 August 2007

To cite this Article: Hafiz, Khurshid, Farran, Fatima, Allawnha, Hani, Ayoub, Mohamad, El-Chafei, Mohammad and Kar, Narayan C. , (2007) 'Auxiliary power unit for truck idling reduction', International Journal of Environmental Studies, 64:4, 433 - 443

To link to this article: DOI: 10.1080/00207230701382057

URL: <http://dx.doi.org/10.1080/00207230701382057>

PLEASE SCROLL DOWN FOR ARTICLE

Full terms and conditions of use: <http://www.informaworld.com/terms-and-conditions-of-access.pdf>

This article maybe used for research, teaching and private study purposes. Any substantial or systematic reproduction, re-distribution, re-selling, loan or sub-licensing, systematic supply or distribution in any form to anyone is expressly forbidden.

The publisher does not give any warranty express or implied or make any representation that the contents will be complete or accurate or up to date. The accuracy of any instructions, formulae and drug doses should be independently verified with primary sources. The publisher shall not be liable for any loss, actions, claims, proceedings, demand or costs or damages whatsoever or howsoever caused arising directly or indirectly in connection with or arising out of the use of this material.

© Taylor and Francis 2007



## **Auxiliary power unit for truck idling reduction**

**KHURSHID HAFIZ, FATIMA FARRAN, HANI ALLAWNHA, MOHAMAD AYOUB,  
MOHAMMAD EL-CHAFEI AND NARAYAN C. KAR\***

Department of Electrical and Computer Engineering, University of Windsor, 401 Sunset Avenue,  
Windsor, Ontario, Canada N9B 3P4

*(Received 4 April 2007)*

Idling the engine of heavy-duty truck is the only way a driver can control the temperature in the cab/sleeper and have power for auxiliary devices when the truck is parked. It is an inefficient and noisy process that wastes thousands of litres of fuel per year while standing stationary in a parking lot. Almost all heavy-duty trucks idle about 20–40% of the time when the engine is running, depending on season, geographic location and trucking operation. This extensive engine idling has many disadvantages, including pollutant emissions, noise pollution, unnecessary fuel and maintenance costs, and driver discomfort. This paper discusses the problems related to truck idling and proposes an auxiliary power generation unit that can significantly reduce the fuel consumption, cut the costs, enhance engine life and reduce pollution. A control methodology is presented to regulate the output voltage of the auxiliary power unit under variable load conditions.

*Keywords:* Heavy-duty diesel truck; Idling; Pollution; Auxiliary power unit

### **1. Introduction**

Heavy-duty trucks consume billions of litres of fuel each year. A significant amount of this fuel is burned by the engines that are left idling to run heaters, air conditioners, refrigerators, microwave ovens, televisions, etc. inside the cab and to run block heaters in cold weather to avoid start-up problems [1]. The combustion of fuel in internal combustion engines of heavy-duty vehicles during idling contributes significantly to the air pollution in Canada particularly in the urban areas. Air pollution is a serious health problem and many premature deaths can be attributed to this factor. In this paper, the amount of idling by heavy-duty truck traction engines has been quantified and an efficient auxiliary power unit has been proposed to replace the main traction engine during idling.

The US Federal Motor Carrier Safety Administration enforces rules on the hours of service by a truck driver [2]. One of the rules limits truck drivers to driving only 11 hours after 10 consecutive off-duty hours. This off-duty period of 10 hours is associated with truck drivers taking a long idling stop to rest and operate some of their components such as heating or air conditioning. During the days of heating or cooling, truck drivers have few options other than to idle the large horsepower engine that can generate 400–500 horsepower in order to supply

---

\*Corresponding author. Email: nkar@uwindsor.ca; website: www.uwindsor.ca/electrical

power to considerably small loads which only require a small amount of electrical power to function. This results in the engine of the truck running at low efficiency for a long period of time, as well as the extra emissions of pollution to the atmosphere. Long-duration truck idling results from the need to provide heating, air conditioning, and ventilation and also to operate on board appliances for several hours at a time. A truck driver might also experience short-term idling for example when refuelling, conducting vehicle checks, waiting for loading and unloading, or while simply stuck in traffic. Other factors also contribute to idling such as engine and fuel temperatures.

Emissions from the combustion of fossil fuels include nitrogen oxides ( $\text{NO}_x$ ), volatile organic compounds (VOCs), sulphur oxides ( $\text{SO}_x$ ), carbon monoxide (CO), fine particulate matter, benzene, 1,3-butadiene, formaldehyde, acetaldehyde and other toxic or potentially toxic substances [3,4]. In this regard, transportation may be considered as one of the largest contributors to environmental pollution in Canada. Emissions attributed to diesel fuel include particulate matter (PM), oxides of nitrogen ( $\text{NO}_x$ ), carbon dioxide ( $\text{CO}_2$ ), and carbon monoxide (CO). Emissions from idling trucks are highly localized and concentrated. Figure 1 shows the concentration of  $\text{SO}_2$  and NO in 2002 in various cities in Ontario, Canada [3]. Of particular interest is the city of Windsor where thousands of vehicles like cars, pick-up trucks, minivans and sport utility vehicles and heavy-duty vehicles like trucks and buses crisscross the Windsor–Detroit border. Figures 2 and 3 show the average and maximum concentration of nitric oxide and sulphur dioxide at Windsor West station of Ministry of Environment, Ontario during the year 2004 [3]. As a result of such high levels of  $\text{SO}_2$  and NO in the air in Windsor, truck idling is now attracting increased attention from local and federal authorities.

There are also economic reasons to reduce truck idling. Argonne National Laboratory study stated that a typical heavy-duty freight-hauling truck on an average idles six hours/day or about 1818 hours/year [5,6]. Using alternative idling reduction technologies, less fuel is burned, resulting in cost savings. Cost savings include not only those for fuel, but also less frequent oil changes and more miles between repairs and overhauls. Studies by the Edison Electric Institute and the Argonne National Laboratory show that idling a truck engine for 2500 hours annually is the equivalent of 200,000 extra miles of engine wear, burning 3750 gallons of diesel fuel, and adding operation costs between US\$4000 and US\$7000 per truck per year [5,6].

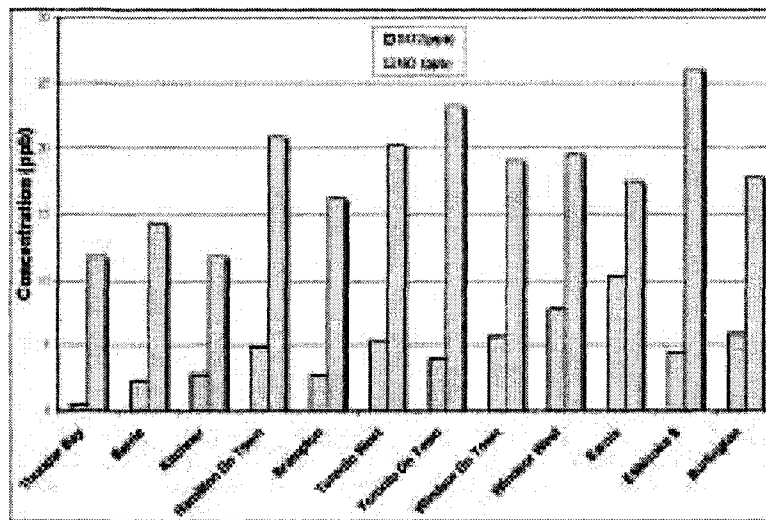


Figure 1. Concentration of  $\text{SO}_2$  and NO in Ontario cities.

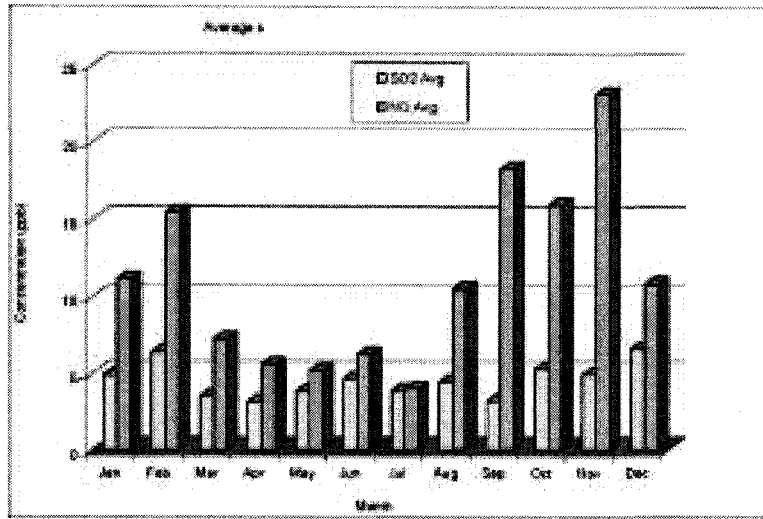


Figure 2. Average concentration of SO<sub>2</sub> and NO in Windsor West.

One of the alternative technologies to reduce idling, auxiliary power units (APUs), is being investigated by automotive and truck industries and the research community [1,7–17]. The APU system should be capable of providing electrical power to meet all the requirements of the truck sleeper cabin and its auxiliaries. The electrical generator provides electrical power for the heating, ventilation and air conditioning (HVAC) for the cab/sleeper compartment, battery top up, to keep the engine warm and ready to start and go, for TV, microwave, fridge, computer and radios inside the sleeper compartment. This paper presents an efficient power generation system that can meet the variable electric power demand from the loads during truck idling. A survey was conducted on heavy-duty trucks to determine the maximum power that the APU has to deliver when the truck main engine is idling. A digital control system has been developed which integrates all the equipment in the APU system to optimize electrical power output and keep fuel consumption to a low level. The proposed control system is

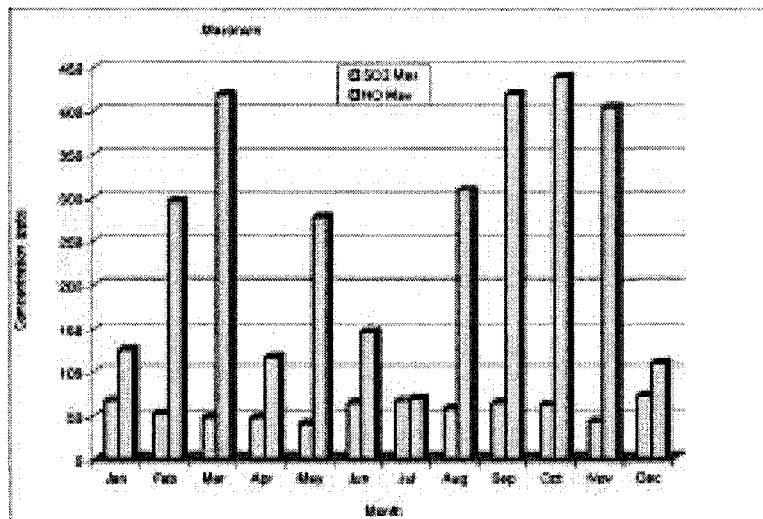


Figure 3. Maximum concentration of SO<sub>2</sub> and NO in Windsor West.

capable of regulating the output voltage of the APU under variable load conditions. A laboratory auxiliary power unit has been developed using a DC motor, a DC generator and the control system. Experimental investigations have been performed on this laboratory APU system to determine its steady-state performance.

## 2. Duration of idling and power consumption during idling

For the purpose of this paper, a survey was conducted on heavy-duty trucks travelling through the city of Windsor to determine the duration of idling and the amount of power consumed by the electrical equipment while the driver is resting. The types of in-cab appliances used by drivers were also investigated. A communication device such as CB radio, entertainment devices such as TV, computer and stereo, kitchen appliances such as refrigerator, and microwave oven, cab comfort devices such as heater, and air conditioner are the most common appliances. Also, block heaters are used in cold weather to keep the engine warm. Figures 4 and 5 illustrate the results of this survey. In these figures, the minimum and maximum power consumptions of a typical truck in one day when the truck is idling are shown. It can be seen from figure 5 that an approximate maximum power of 4000 W will be required for an APU to deliver, when the truck main engine is idling. The graphs show a typical 24-hour period. Hour one on the graph starts at 5:00 am. The results of the survey show that a significant amount of the emissions is produced by the long period of idling. Fuel consumed during the idling of trucks can be reduced by installing an auxiliary power unit that can run all the electrical equipment mentioned previously when the truck driver is resting. Some of the respondents of this survey were aware of the benefits such as fuel savings, less pollution, and less engine wear resulting from the use of idling reduction technologies. Most indicated they are likely to purchase idling reduction technologies.

## 3. Existing truck idling reduction technologies

To reduce truck idling, several alternative technologies are currently available. Idling reduction technologies include idle limiting devices like idle shut down timers, auxiliary

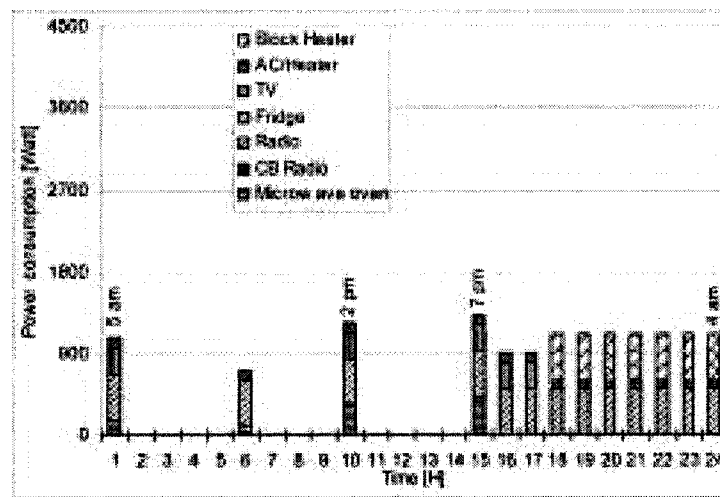


Figure 4. Minimum power APU has to deliver.

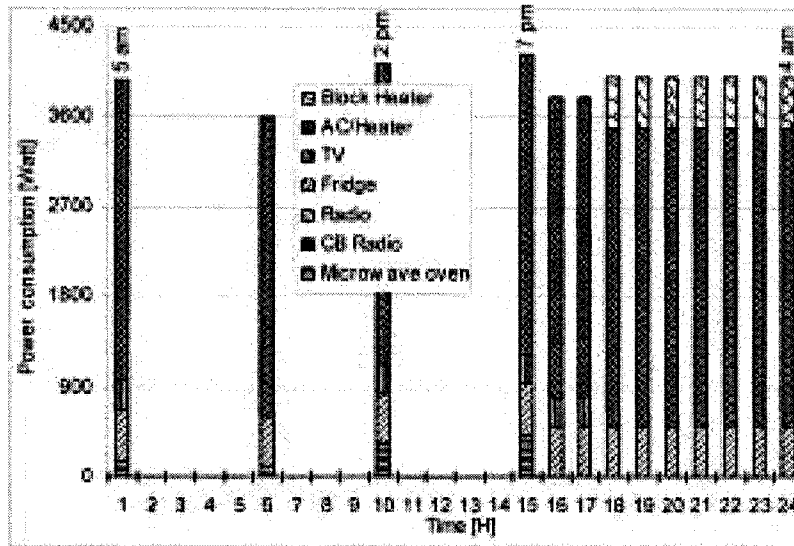


Figure 5. Maximum power APU has to deliver.

devices like direct-fired heaters, thermal storage, auxiliary power unit and truck stop electrification.

Idle limiting devices [17] range from systems that automatically stop and restart the engine as necessary to maintain the engine and cab/sleeper temperatures, to those which automatically shut down the engine after a specific idle time and maintain battery voltage within preset limits. Most engines now have a built-in idle shut down timer that enables the engine to shut off if left in idle for more than a pre-set period of time. This system is only offered as a factory option by several truck manufactures. For this system to work, the driver must set the parking brake while the truck is in neutral, and must have the ignition on 'ON' with the hood closed. The system is disabled by turning off the ignition or while the driver is driving. There are two options when choosing the type of system desired, either an 'engine only' mode or a 'cab comfort' mode. The 'engine only' mode monitors engine oil temperature and battery voltage, while the 'cab comfort' mode includes monitoring of engine mode parameters as well as cab/sleeper temperature.

The use of auxiliary devices such as direct-fired heaters and auxiliary power units could also be used as alternatives to truck idling. Direct-fired heaters [17,18] are small and inexpensive heaters that provide heat to both the cab/sleeper and/or engine. They consume far less diesel fuel and are more efficient than the heater of an idling diesel engine. Unfortunately the disadvantages of this sort of technology are its inability to provide cooling and its amount of use of the truck's battery. An Auxiliary Power Unit (APU) [17,19], on the other hand, provides electricity to charge the truck's batteries, heat the vehicle's engine, and heat/cool the sleeper compartment. One of the suppliers of APU [19], in their cost-saving analysis, indicated that a truck engine consumes fuel 1 gal/hr under light load condition, and 2 gal/hr under full load condition. On the other hand, their commercial APU, named Pony Pack, consumes fuel 0.075 gal/hr under light load condition and 0.3 gal/hr under full-load condition. Comparing the two rates together it is apparent that the APU is fuel efficient. The fuel cell APU [1] is an auxiliary source that has a promising future in eliminating truck idling emissions. Fuel cells offer a clean and efficient conversion of the chemical energy of fuel directly into electrical power in a controlled chemical reaction. Fuel cell APUs provides enough power to

heat/cool a cab/sleeper compartment and also run onboard electrical equipment. The disadvantages of this sort of system are the unavailability of a suitable fuel, higher production costs of the units and integration of the units with other on-board truck systems.

Truck stop electrification (TSE) is another alternative to reduce emissions resulting from idling trucks where a specially designed electrical power system supplies power to the truck components [17,20]. This system will provide 120 Volt AC electrical power and provide the truck driver with the option of running the components when idling. TSEs need to be equipped with electrical outlets and, also, the trucks need to be equipped with electrical power connections. Two of the electrical components that will be needed in the truck are charger and inverter; the charger is used to charge the truck batteries and the inverter is used to convert the battery 12V DC supply to 120V AC electrical power supply. The TSE system has several disadvantages, including the cost of the equipment that is added to the truck, and the availability of using the system since it is limited only to the truck stops.

#### 4. System configuration of the proposed auxiliary power unit

An internal combustion (IC) engine such as Honda 6.5 HP, air cooled four-stroke engine is usually the prime mover for the direct-coupled electric generator of an actual APU. But in the investigations of this paper, a separately-excited DC motor energized from a laboratory DC source, is used as the prime mover as shown in the schematic diagram of the proposed laboratory APU in figure 6. This DC motor is connected to DC power supply through a power electronics system that controls the voltage applied to the armature terminals of the motor. The voltage applied to the armature of the motor is controlled to yield the desired torque and speed. The voltage applied to the field circuit remains constant. The DC motor is

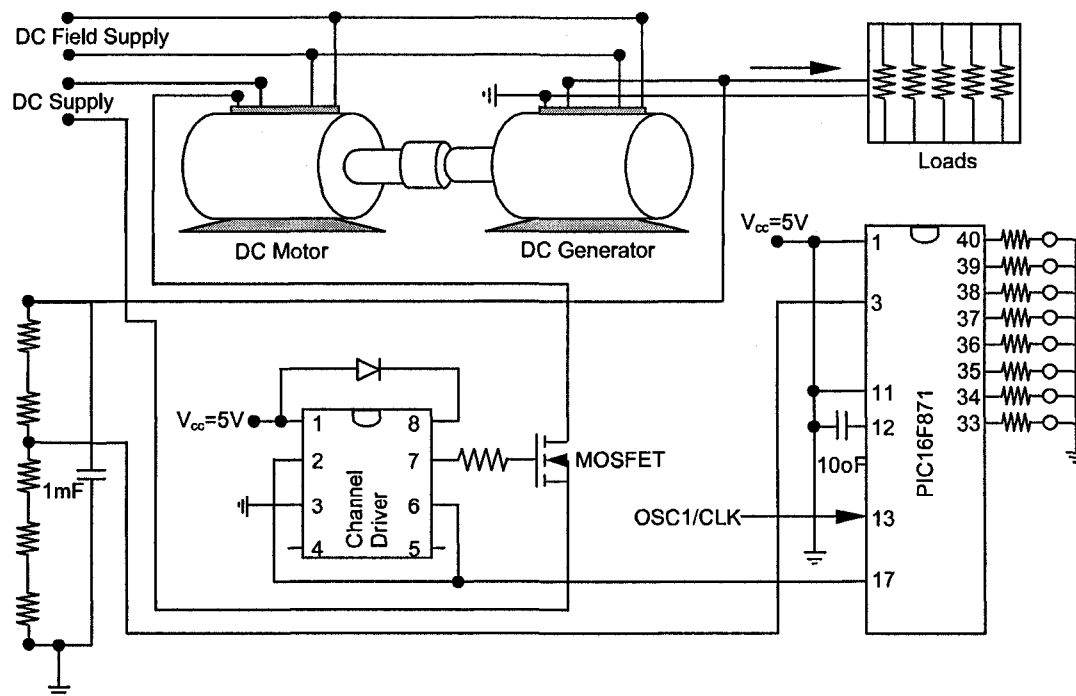


Figure 6. System configuration of the auxiliary power unit (APU).

then mechanically coupled to a DC generator that delivers electrical power to the loads during truck idling.

An energy management controller controls all APU activities. The microprocessor in the system controls the speed of the motor by varying the terminal voltage of the motor. This is achieved by adjusting the duty cycle of the waveform into the channel driver. PIC16F871 microprocessor provides the system with the ability to perform all required applications. The two desired features in this IC are A/D converter and the pulse width modulator. The A/D converter receives an analogue signal from the generator terminal voltage via a voltage divider. This analogue signal represents the power demand by the loads during idling. This signal is then converted into a digital signal which is processed within the microprocessor. The microprocessor has been programmed to compare and adjust the speed of the DC motor by using the pulse-width modulation technique.

Five resistive loads of equal resistance value are connected at the generator terminals in parallel. The terminal voltage of the DC generator is compared with a reference voltage (desired APU terminal voltage) in the microcontroller. Depending on the discrepancy between the actual generator terminal voltage and the reference voltage, the duty cycle of the channel driver is modified. The buck DC-DC converter in figure 6 with a given input voltage produces a controlled average output voltage depending on the value of the duty cycle. A change in the voltage applied to the armature of the DC motor will change the torque developed by the motor. Because of the discrepancy between the developed electromagnetic torque and the load torque at the motor shaft, the operating speed of the motor will change. Thus, the operating speed of the motor becomes approximately proportional to the duty cycle of the converter.

It may be mentioned here that the authors are in contact with International Truck & Engine Corporation (ITEC) in Chatham, Ontario and looking for possible collaboration to implement the proposed system. In this case, an IC engine will replace the DC motor. IC engines are characterized by highly nonlinear and time varying dynamics (ambient temperature, speed and power output) making them difficult to control by means of conventional control techniques. Thus, the main challenge will be to develop a control system that can be applied to regulate fuel injection to the IC engine to control the engine torque output. The authors anticipate that the performance of the APU system with the IC engine as the prime-mover will be the same qualitatively but may be different quantitatively.

## **5. Experimental investigations**

To determine the steady-state performance, experimental investigations have been performed on the proposed APU system illustrated in figure 6. The experimental setup is shown in figure 7. Two 120 W, 120 V, 1A, 1800 rpm laboratory DC machines have been used in the investigations. The experimental setup in figure 7 illustrates the basic concept behind an APU system. The actual rating (power, voltage, current, etc.) of an APU system and its control requirements will depend on the design objectives, load requirements, etc. The motor and generator terminal voltages and currents, power input and output, speed, and torque at various loading conditions are measured with and without the controller. The desired generator terminal voltage has been set to 90 V. Figures 8–11 show some of the results of these investigations.

Figures 8 and 9 show the relationships between the developed torque, speed, load power demand and the control system. The speed of the motor increases and the motor develops

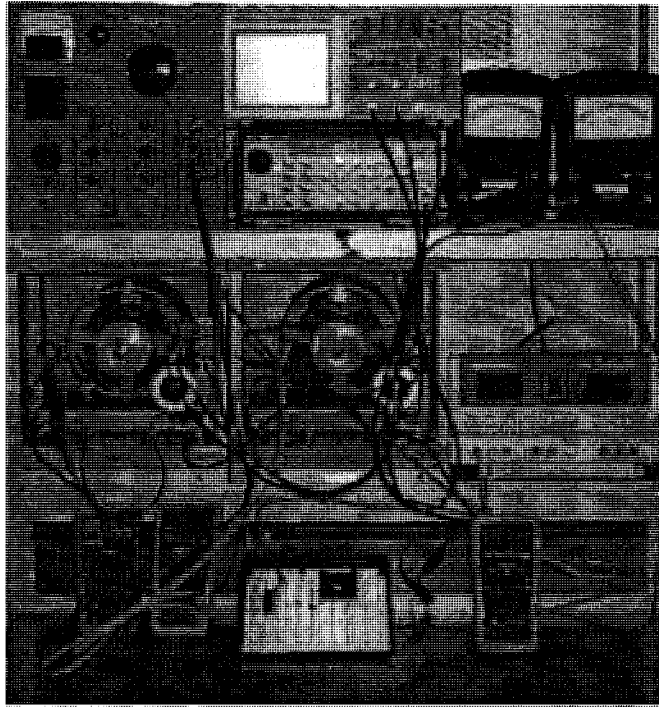


Figure 7. Experimental setup.

more electromagnetic torque with the increase of the load demand if the control system is engaged. It can be seen from figure 9 that the speed of the motor falls significantly with the increase of the load demand if the control system is not employed. The speed regulation in such a case has been found to be 20.93%. But, with the application of the control system, both the motor torque output (figure 8) and the speed of the motor (figure 9) increase to meet the increasing load demand.

Figure 10 illustrates the measured external volt-ampere characteristics of the DC generator in the APU system. The terminal voltage of a DC generator is related to the load current and the internal electromotive force (emf). The internal emf is a function of the machine field current and the rotor speed. The field current of the generator was held constant. If the control system is not employed, as can be seen from figure 9, the speed decreases with an increase in the load current, which in turn reduces the internal generated emf. This, in addition to the machine armature resistance drop, causes the terminal voltage of the generator to fall significantly as the load current increases as shown in figure 10. The voltage regulation without the control system has been found to be 34%. But, if the control system is engaged, the terminal voltage applied across the DC motor is increased with the increase of load and, thus, the motor delivers required speed and torque to the generator. The generator terminal voltage becomes independent of the load current with the application of the control system. This is due to the fact that the microcontroller senses a decrease in the terminal voltage due to an increase in the load current and modifies the PWM signal to increase the duty cycle so that the voltage applied to the DC motor terminal increases. An increase in the applied voltage increases the motor speed and the torque output. As the speed of the generator increases it brings the terminal voltage up to the desired level of 90 V.



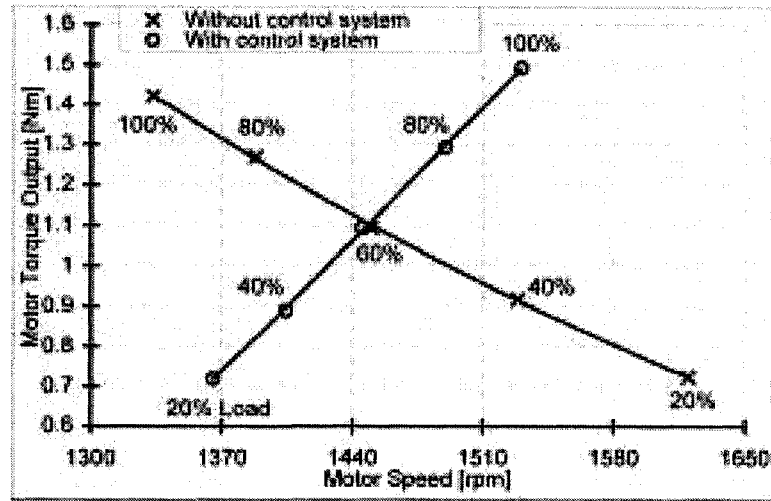


Figure 8. Variation in the measured motor torque output as a function of motor speed for different loading conditions with and without the control system.

The measured generator output power and generator output power per unit motor input torque as a function of load with and without the proposed control scheme are shown in figure 11. It can be seen from this figure that the effect of the control system is to increase the generator output power per unit applied input torque especially in the high load region.

## 6. Conclusions

This paper discusses the problems related to truck engine idling and proposes an auxiliary power generation system with improved power and efficiency. The most important findings and conclusions of this study are as follows:

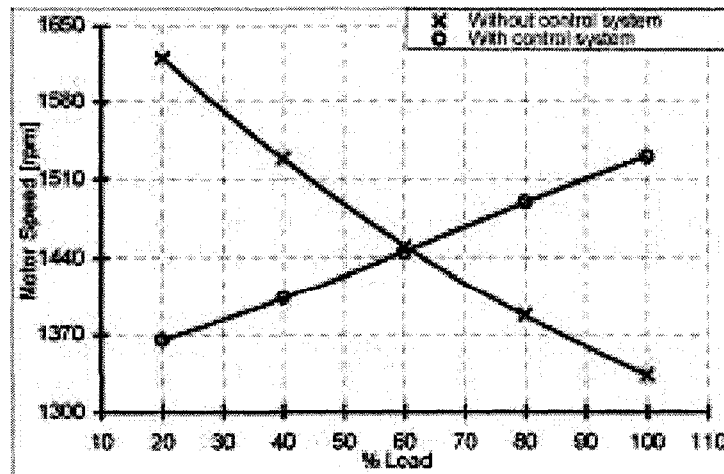


Figure 9. Variation in the measured motor speed as a function of load with and without the control system.

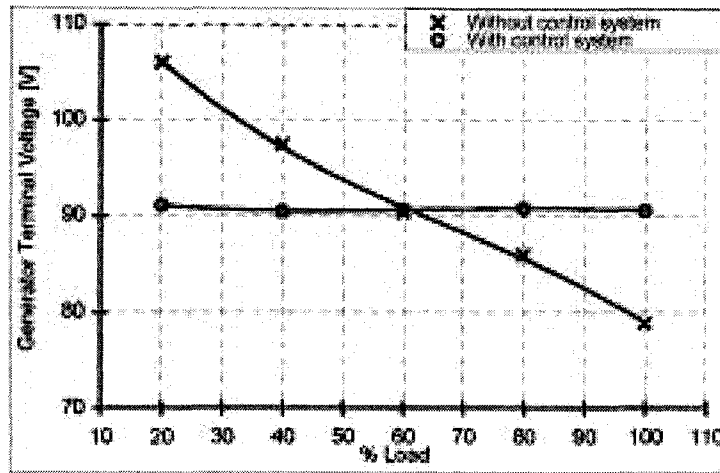


Figure 10. Variation in the measured generator terminal voltage as a function of load with and without the control system.

- 1) The APU system can be controlled to provide regulated power output depending on the load requirements.
- 2) The developed control system is able to regulate the output voltage of the APU under variable load conditions and, thus, the output voltage regulation has been found to be insignificant.

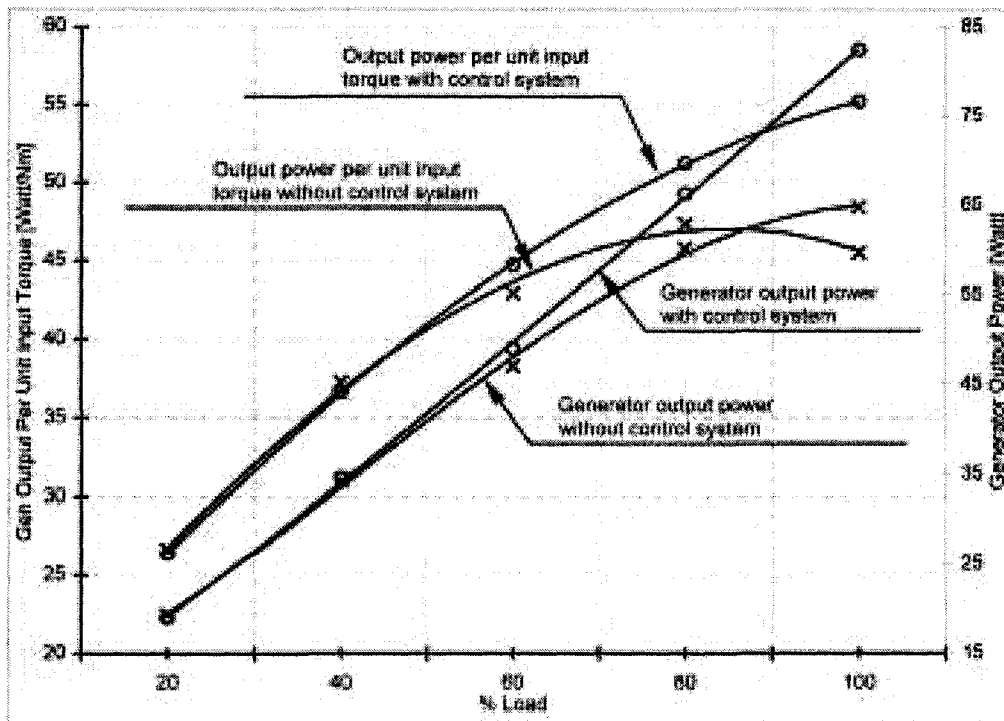


Figure 11. Measured generator output power and generator output power per unit motor input torque as a function of load with and without the control system.

- 3) The effect of the control system is to increase the generator output power per unit motor input torque especially in the high load region.
- 4) The APU system can significantly reduce the fuel consumption, cut the operating costs, enhance truck engine life and reduce pollution.

### Acknowledgement

The work reported in this paper was supported by the Natural Sciences and Engineering Research Council (NSERC) of Canada.

### References

- [1] Brodrick, C.-J., Lipman, T.E., Farshchi, M. and Lutsey, N.P., 2002, Evaluation of fuel cell auxiliary power units for heavy-duty diesel trucks. *Journal of Transportation Research*, **7-D**, 303–315.
- [2] US Federal Motor Carrier Safety Administration website. Available online at: <http://www.fmcsa.dot.gov/> (accessed 10 August 2006).
- [3] Ontario Ministry of Environment, 2004, Air Quality in Ontario –Report, ISBN 0-7794-9921-2.
- [4] Huai, T., Shah, S.D., Miller, J.W., Younglove, T., Chernich, D.J. and Ayala, A., 2006, Analysis of heavy-duty diesel truck activity and emissions data. *Journal of Atmospheric Environment*, **40**, 2333–2344.
- [5] Argonne National Laboratory website. Available online at: <http://www.ead.anl.gov/> (accessed 10 August 2006).
- [6] Costlow, T., 2004, Long-haul truckers: idle no more. *IEEE-USA Today's Engineer On Line*, January.
- [7] Bumby, J.R. and Brown, N., 2000, Auxiliary power units: a role for the torus generator? IEE Seminar on Electric, Hybrid and Fuel Cell Vehicles, 1–4 April.
- [8] Naidu, M., Nehl, T.W., Gopalakrishnan, S. and Wurth, L., 2005, Keeping cool while saving space and money: a semi-integrated, sensorless PM brushless drive for a 42-V automotive HVAC compressor. *IEEE Industry Applications Magazine*, **11**, 20–28.
- [9] Koot, M., Kessels, J.T.B.A., de Jager, B., Heemels, W.P.M.H., van den Bosch, P.P.J. and Steinbuch, M., 2005, Energy management strategies for vehicular electric power systems. *IEEE Transactions on Vehicular Technology*, **54**, 771–782.
- [10] Algrain, M.C., 2005, Efficient idle – on the electrification of class-8 trucks. *IEEE Industrial Applications Magazine*, **8**, 34–43.
- [11] Koot, M., de Jager, B., Kessels, J.T.B.A., Heemels, W.P.M.H. and van den Bosch, P.P.J., 2004, Energy management strategies for vehicle power nets, in: *Proceedings of the IEEE American Control Conference*, pp. 4072–4077.
- [12] Kassakian, J.G., Wolf, H.-C., Miller, J.M. and Hurton, C.J., 1996, Automotive electrical systems circa 2005. *IEEE Spectrum*, 22–27 August.
- [13] Kassakian, J.G., Wolf, H.-C., Miller, J.M. and Hurton, C.J., 1996, The future of automotive electrical systems. *IEEE Power Electronics in Transportation*, pp. 3–12.
- [14] Emadi, A., Rajashekara, K., Williamson, S.S. and Lukic, S.M., 2005, Topological overview of hybrid electrical and fuel cell vehicular power system architectures and configurations. *IEEE Transactions on Vehicular Technology*, **54**, 763–770.
- [15] Perreault, D.J. and Caliskan, V., 2004, Automotive power generation and control. *IEEE Transactions on Power Electronics*, **19**, 618–630.
- [16] Stodolsky, F., Gaines, L. and Vyas, A., 2001, Technology options to reduce truck idling. Center for Transportation Research, Argonne National Laboratory Publication, March.
- [17] Hawelti, D., 2003, Proposal to reduce idling from new 2007+ heavy-duty diesel trucks. California Environment Protection Agency, Air Resources Board, Public Workshop, 4 June.
- [18] The American Transportation Research Institute Publication, 2006, Idle reduction technology: fleet preferences survey, February.
- [19] Pony Pack website. Available online at: <http://www.ponypack.com/> (accessed 15 August 2006).
- [20] Perrot, T.L., Tario, J.D., Kim, J.C. and Hagan, C., 2006, Installation and economics of a shore power facility for long-haul trucks. New York State Energy Research and Development Authority Publications, August.

## VITA AUCTORIS

NAME: Khurshid bin Hafiz

PLACE OF BIRTH: Dhaka, Bangladesh

YEAR OF BIRTH: 1955

EDUCATION: St. Joseph's High School, Dhaka, Bangladesh  
1963-1965

St. Gregory's High School, Dhaka, Bangladesh  
1966-1970, Secondary School Certificate

Notre Dame College, Dhaka, Bangladesh  
1970-1972, Higher Secondary Certificate

Bangladesh University of Engineering &  
Technology. Dhaka, Bangladesh  
1973-1977, B.Sc. Electrical Engineering

University of Windsor, Ontario, Canada  
2002-2005, BCS[G] Computer Science

University of Windsor, Ontario, Canada  
2005-2008, M.A.Sc. Electrical Engineering